Silver Nanocrystals Differing By Their Coating Agents : Unexpected Behaviors

Jingjing Wei

THÈSE

DE DOCTORAT DE L'UNIVERSITÉ PIERRE ET MARIE CURIE (PARIS VI)

ECOLE DOCTORALE DE CHIMIE-PHYSIQUE ET CHIMIE ANALYTIQUE DE PARIS CENTRE

SPÉCIALITÉ «CHIMIE-PHYSIQUE»

présentée par

JINGJING WEI

pour obtenir le diplôme de

DOCTEUR DE L'UNIVERSITÉ PIERRE ET MARIE CURIE

Sujet de la thèse

SILVER NANOCRYSTALS DIFFERING BY THEIR COATING AGENTS: UNEXPECTED BEHAVIORS

Thèse soutenue le 10 Juillet 2015 devant le jury composé de:

Pr. DIDIER ASTRUC	Examinateur
Pr. PIERO BAGLIONI	Rapporteur
Pr. GIORGIO BENEDEK	Examinateur
Pr. GIULIO CERULLO	Rapporteur
Pr. HELENE GERARD	Président du jury
Pr. MARIE-PAULE PILENI	Directrice de thèse
Dr. NICOLAS SCHAEFFER	Examinateur

Acknowledgements

Abstract

Over the last few decades, nanotechnology, which is the development of new methods for synthesizing and manipulating discrete nanoparticles and larger nanostructured assemblies, have made great progress. Nanoparticles provide a high surface-to-volume ratio (compared to the bulk phase), representing an important state of condensed matter, hence exhibiting novel physical and chemical properties that are not observed in their bulk state. Self-organization of spherical particles into two-dimensional (2D) and three-dimensional (3D) superlattices is commonly observed in nature, where nanoparticles having similar diameters and very narrow size distributions can self-organize into 2D or in 3D ordered structures, also called supracrystals. Furthermore, binary nanocrystal superlattices, which are co-assembled from two distinct series of nanoparticles, have also emerged. Compared to the limited phase structures formed in the single-component nanoparticle superlattices, a variety of phase structures of binary nanocrystal superlattices can be produced, and the prediction of these phase structures mainly relies on the space-filling principles. However, in addition to the well-known crystal structures formed with hard sphere model, such as AlB_2, $NaZn_{13}$, NaCl, and laves phases in binary superlattices, other phases such as CuAu-type, Cu_3Au-type, CaB_6-type as well as quasicrystalline ordering are also discovered in binary nanocrystal superlattices, where nanoparticle interactions must be considered.

In this manuscript, recent advances in the synthesis and optical properties of Ag nanocrystals and their assemblies into 2D/3D superlattices will be reviewed in **Chapter 1**. **Chapter 2** focuses on the SPR response from 2D self-assemblies of both Ag and Au spherical nanocrystals. The collective SPR bands observed in the measured absorption spectra are described and compared to those calculated using dipole approximation (DDA) method. The similar results provided by these two approaches show that the theoretical DDA methods are suitable for the simulation of linear optical response of 2D superlattices made of such ultrafine metal nanocrystals and can be used to model and predict their optical responses. The influence of the nanocrystals coating agent and its influence on the validity of DDA simulations is also discussed. **Chapter 3** describes the optical properties of silver nanocrytals when dispersed in a solvent. The SPR band of those nanocrystals is shown to be dependent

not only on the nanaocrystal diameter, but also on the nature of the coating agent. In **Chapter 4,** the fabrication of thin supracrystalline films made of Ag nanocrystals is explained, and the optical properties of the as-obtained films composed of nanocrystals with varying diameters and coating agents studied. By comparing the SPR spectra of dispersed Ag nanocrystals with their assemblies of supracrystalline films, marked changes are observed. The energy discrepancy (ΔE), determined from the difference in SPR band between dispersed nanocrystals and their corresponding assemblies is shown to be mainly dependent on both the nanocrystals size and the interparticle distances within the supercrystalline films. These results also show a good agreement between simulated optical properties of 2D superlattices with data acquired with 3D thin films assembled in fcc crystalline structure. Furthermore, it is shown that the interparticle distance of nanocrystals, modulated by the alkyl chain length of the coating agents, could effectively tune the SPR band position. **Chapter** 5 is related to the fabrication of binary nanocrystal superlattices. Colloidal binary nanocrystal mixtures containing two distinct nanocrystals with either the same surface coating agent, called single ligand system, or with two different surface coating agents, refered as multiple ligands system, are used to grow binary nanocrystal superlattices. The mechanism of formation of binary nanocrystal superlattices from Ag-Ag binary mixtures and the effect of surface capping agents on the formation of binary nanocrystal superlattices is discussed.

Résumé

Au cours des dernières décennies, les nanotechnologies, c'est à dire le développement de nouvelles méthodes de synthèse et la manipulation de nanoparticules et de leurs assemblage en nanostructures plus grandes, ont connu d'important progrès. Les nanoparticules offrent un grand ratio de surface sur volume (par rapport au solide), en faisant d'elles un état de la matière condensée important de par les nouvelles propriétés physiques et chimiques qu'elles offrent et qui n'existent pas dans le solide. L'auto-organisation de particules sphériques en deux dimensions (2D) et en trois dimensions (3D) des super-réseaux est couramment observée dans la nature, où les nanoparticules ayant des diamètres et des répartitions de tailles très fines peuvent s'auto-organiser en structures ordonnées en 2D ou en 3D, appelées supracristaux. En outre, les super-réseaux de nanocristaux binaires, qui sont des co-assemblages de deux séries distinctes de nanoparticules, ont également émergé. Par rapport aux structures formées de nanoparticules à une composante unique, une variété de structures de réseaux de phase binaires de nanocristaux ont été produites, et la prédiction de ces structures repose principalement sur le principes de remplissage d'espace. Cependant, en plus des structures cristallines connues formées avec le modèle de sphère dure, comme AlB2, NaZn13, NaCl en réseaux binaires, d'autres phases telles que les types CuAu, Cu_3Au et CaB_6, ainsi que des structures quasi cristallines ont également été découvertes, pour lesquelles les interactions entre nanoparticules doivent être prises en compte.

Dans ce manuscrit, les récents progrès faits dans les procédés de synthèse et l'étude des propriétés optiques des nanocristaux d'argent et leurs assemblages en réseaux 2D / 3D seront examinées dans le **Chapitre 1**. Le **Chapitre 2**, se concentre sur la réponse SPR des auto-assemblages 2D de nanocristaux sphériques d'argent et d'or. Les bandes SPR observées dans les spectres d'absorption mesurés sont décrites et comparées à celles calculées en utilisant la méthode d'approximation de dipôles discrets (DDA). Les résultats semblables fournies par ces deux approches montrent que les méthodes théoriques sont adaptées pour la simulation de réponse optique linéaire de réseaux 2D de nanocristaux métalliques ultrafins et peuvent être utilisés pour modéliser et prédire leurs réponses optiques. L'influence de l'agent stabilisant des nanocristaux et leur influence sur la validité des simulations DDA est également discutée. Le **Chapitre 3** décrit les propriétés optiques de nanocrytaux argent dispersés

dans un solvant. La bande SPR de ces nanocristaux dépend non seulement du diamètre des nanaocristaux, mais également de la nature de l'agent stabilisant. Dans le **Chapitre 4**, la fabrication de films minces de supracristaux d'Ag et les propriétés optiques des films obtenus avec des nanocristaux de différents diamètres et des agents de stabilisation differents sont discutées. En comparant les spectres SPR de nanocristaux d'Ag dispersés avec ceux des films supracrystallins correspondants, d'importantes variations sont observées. La différence d'énergie (ΔE), décrivant la différence entre les positions des bandes SPR entre des nanocristaux dispersés et les assemblages correspondants se révèle être principalement dépendante à la fois de la taille des nanocristaux, mais aussi des distances entre particules à l'intérieur des films supercristallins. Ces résultats montrent également un bon accord entre les propriétés optiques simulées de réseaux 2D avec des données acquises avec des films minces 3D assemblés en structures cristallines cfc. En outre, il est démontré que la distance interparticulaire de nanocristaux modulée par la longueur de chaîne alkyle de l'agent de stabilization peut aider à faire varier la position de la bande de SPR. Le **Chapitre 5** est lié à la fabrication de réseaux de nanocristaux binaires. Des mélanges binaires de nanocristaux colloïdaux contenant deux types distincts de nanocristaux, soit avec le même agent de stabilisation, appelé système de ligand unique, ou avec deux stabiliseurs différents, appelé système de ligands multiples, sont utilisés pour faire croître les réseaux de nanocristaux binaires. Le mécanisme de formation de réseaux de nanocristaux binaires Ag-Ag et l'effet de l'agent de surface sont discutés.

Abbreviations

2/3D	two/three dimension or dimensional
AFM	antiferromagnetic
a.u.	arbitrary units
BNSLs	binary nanoparticle superlattices
fcc	face centered cubic
FFT	Fast Fourier Transform
HRSEM	high-resolution scanning electron microscopy
HRTEM	high-resolution transmission electron microscopy
hcp	hexagonal close packed
bcc	body centered cubic
QC	quasicrystals/quasicrystalline ordering
UV-vis	ultraviolet visible spectroscopy
SPR	surface plasmon resonance
SAXS	small angle X-ray scattering
SEM	scanning electron microscopy
STEM	scanning transmission electron microscope/microscopy
TEM	transmission electron microscope/microscopy
VDW	Van der Waals

Contents

Introduction

Nanomaterials, in their natural or engineered states, surrounds us and are present in a variety of products and technologies with applications ranging from advanced magnetic recording media, light emitting devices, to solar cells amongst many others. In parallel to the development of various synthetic methods and analytical techniques to produce and characterize them, a fundamental understanding of the chemistry and physics of those nanomaterials has been reached over the last few decades. Nanomaterials are known to be a new generation of advanced materials exhibiting unusual chemical and physical properties due to the high surface-to-volume radio that differs from those of bulk phase materials. Besides, the considerable economical benefits are also a driving force in the number of studies in this field.

Recently, synthesis of high-quality metallic nanocrystals has been dramatically improved. Several breakthroughs have been made in view of the producion of well-defined nanoparticles via wet-chemistry methods, allowing furthter possibilities to study and understand those materials. The surface ligands used in the synthesis of high-quality nanocrystals are relatively important, they consist in most cases of a small anchoring group with strong affinity with the metal for bounding onto the surface of the nanocrystals, and a long hydrocarbon chain which provies steric and/or electrostatic repulsions to stabilize the nanocrystals in suspension and counterbalance Van der Waals attractive forces. Polymeric ligands or bulky bio-based molecules are also employed for the synthesis and stabilization of nanocrystals. Silver, which is very important coin metal, exhibits very specific optical properties at the nanometer scale, making it a very interesting candidate for various applications. Hence, Ag at the nanometer regime is widely investigated. Recently, silver nanocrystals with various shapes and sizes have been synthesized and the properties of those silver nanostructures are studied. However, silver nanocrystals with small diameters and rather narrow distribution withour further size selection remains technically challenging to produce, limiting the understanding of the physical properties, and possible new discoveries related to this type of materials.

The organization of monodisperse colloidal particles has been a topic of interest since the discovery of the iridescence of gem opals, which was attributed to

diffraction of light from regular packed silica spheres. Furthermore, it has also been found that silica spheres with two different sizes (Brazilian opal) can self-assemble into complex binary structures. The performance of these assemblies is dictated by the properties of individual nanocrystals as well as their mutual interactions. In the past two decades, the formation of supracrystals composed of metals, semiconductors, or magnetic nanoparticles have been investigated since the report of CdSe and Ag_2S superlattices in 1995 by Bawendi's group. Later, those studies were extended to the formation of binary nanocrystals superlattices made of two different types of nanoparticles in a single materials, as first reported by Murray et al. in 2003. The formation mechanism of single component nanocrystals is now relatively well understood and can be described by a relatively simple hard-sphere packing model. However, the formation of binary superlattices can yield to superlattices with different phase diagrams with multiple close-packed and non-close-packed periodic phases. Several thermodynamic forces can drive the formation of superlattices from suspensions: all entropic force and the energetic force from the interparticle interactions. It has also been shown that the type of solvent used during the evaporation process leading to the formation of the superlattices is critical to the self-assembly process. However, other parameters that affect the formation of binary superlattices, such as the coating agents and electrostatic interactions are rarely investigated.

The interesting colors of noble metal nanoparticles have attracted considerable interest since historical times, as shown by their use as decorative pigments in stained glasses and artworks for example. When the sizes of those materials are decreased to the nanoscale regime, the tunable optical properties and associated fuctions such as SERS response or fluorensence are dramatically changed, those properties have attracted considerable interest and become a very promising topic. As firstly demonstrated by Gustav Mie in 1908, the interaction of light with metal nanoparticles results in the collective oscillation of the free electrons with the light field. From those properties stems the apparition of a large light absorption, called Surface Plasmon Resonnance (SPR). Several experiments and simulation works have shown that the plasmon resonances are highly dependent on the nanocrystals size, shape, environment dielectric constant, and their organization. All those parameters have an influence on the position, profile and intensity of the SPR. Silver is partricularily interesting for plasmonic applications, due to its intrinsic optical and electronic

properties, and exhibit a relatively good quality factor with neglectable damping effect in a large spectral region of the UV-visible spectra (from 300 nm to 1200 nm). Moreover, silver is relatively cheaper than gold, making it a more suitable candidate for the preparation of plasmonic materials at larger scale. Finally, the ligands that are anchored on the nanoparticles' surface to stabilize them against aggregation can also modulate their SPR properties by modifying the dielectric constant of the silver surface.

By assemblying the nanocrystals into two-dimensional or three-dimensional superlattices, the coulpling of the electromagnetic fields between neighbouing nanocrystals provide a tool that can be used to tune the plasmon resonances of the assemblies. From previous simulation, it is known that 2D silver nanocrystal arrays show an anisotropy in their optical properties. In this case, two resonaces corresponding to transverse and longitudinal resonances can be obtained when the incident electromagnetic (EM) field is perpendicular to the substrate, and only one resonance is observed when the incident EM field is parallel to the substrate. These properties are intrinsic to silver assemblies and do not exist for gold. So investigating the collective optical properties of silver superlattices in order to gain an in-depth understanding of those phenomena is of great importance.

The first part of this thesis will focus on the preparation and optical properties of silver nanocrystals, their chemical and optical properties being significantly affected by their sizes, ligands and ordering. Furthermore, simulations and experimental works will be used to describe the optical properties of either silver or gold 2D assemblies at different incident angles, the optical response of those structures will be discussed in Chapter 2. In the third and fourth Chapters, monodisperse silver nanocrystals coated with different types of coating agents and exhibiting narrow size distributions will be used to show that the optical properties of those assemblies are highly dependent on the ligand type and the size of the nanocrystals. When the nanocrystals are assembled into thin 3D superlattices films, the optical properties are in opposition with those observed for nanocrystals dispersed in a solvent. In the last part of this thesis, report the role that the ligands play in the assembly of nanocrystals and their ability to tune the superlattices structures types and ultimately affect the optical properties of the final structure will be described.

Chapter 1

State of the Art

1.1 Nanotechnologies and Nanocrystals, Introduction

1.1.1 General Overview

Nanosciences and nanotechnologies have become a very important research field in the last few decades and an increasing number of scientists have shown interests in this relatively new topic. It can be said to have started on December 29th 1959, with Richard P. Feynman's lecture at the annual meeting of the American Physical Society, and his famous statment: "ultimately-in the great future-we can arrange the atoms the way we want; the very atoms, all the way down! What would happen if we could arrange the atoms one by one the way we want them?"[1] This now classic talk inspired the first research on new materials organized at the nanoscale. Although it is nowadays still challenging for researchers to arrange atoms exactly the way they intend in the solution phase, controlling the synthesis of nanomaterials with different sizes and morphologies has now become much easier and an important number of synthetic procedures, some of them being now used at industrial level, have been developed. Compared to bulk materials, nanomaterials exhibit unique physical and chemical properties due to their high surface-to-volume ratios. Hence, the detailed procedures enabling a precise control over nanomaterials withe uniform sizes and shapes is a significant question for researchers, and is still under investigation. [2-4]

1.1.2 Silver Nanomaterials

1.1.2.1 History and Prospect of Silver at Different Scales.

Bulk silver (Ag), which was discovered approximate 3000 BC, is a relatively soft and shiny metal. Its widest and well-known use is its utility as coinage metal. It is also known for its widespread use in photography development because of the black color associated with the large aggregates of Ag nanoparticles.[5] Recently, with the increasing understanding of the control of Ag at the atomic scale, applications of silver nanomaterials related to Ag in its

nanocrystalline form have also emerged. Like most materials when their size is decreased in the nanoscale, Ag exhibits a variety of unique properties that are drastically different from those of their bulk state. The optical properties of Ag in this size rergime are particularily interesting, thus, in an attempt to better understand and use those properties, preparation of size-tunable plasmonic Ag nanocrystals, with controlled crystal structure has been studied. Silver nanocrystals intrinsic properties are dependent on their size, shape, composition, crystallinity and structure. It is to be noted that, from a structural point of view, bulk metallic Ag and nanoscaled Ag materials both crystallize in *fcc* phase. [6]

1.1.2.2 Applications of Ag at Different Scales

Silver is one the most important material in plasmonics since it offers many advantages over Au, Cu, Li and Al for example, On a large spectral area and for spectra across ranging from 300 to 1200 nm.[7] The difficulties of manufacturing nanostructures and the costs inherent to their production are also factors that determines the usefulness of a metal for plasmonic application, especially for large-scale applications. Silver is cheaper than Au, and even though it tends to oxidate, some synthetic methods have been developed to overcome this issue.[7]

Furthermore, Ag materials are widely used for Surface Enhanced Raman Scattering (SERS) applications since nanostructured silver have been discovered.[8] Both theoretical calculation and experimental measurements have shown that SERS properties are strongly dependent on the exact morphology of silver nanostructures.[9, 10] For example, by changing the shape of silver nanoparticles from cubes to cube-octahedra to octahedral, the sensitivity of SERS will dramatically increase.[11]

Silver also has the highest electrical conductivity and thermal conductivity amongst all metals, resulting in the use of Ag as conductive fillers of conductive adhesives and thermal interfacial materials in electronics.[7] Ag nanowires are widely used in the electronics fields.[12]

Besides, silver nanomaterials also have potential applications in catalysis.[1, 13] For example, Linic et al. demonstrated that metallic silver nanostructures can release electrons when irradiated with continuous-wave low-intensity visible light, thus enabling further chemical reaction in the medium. These electrons can be used in tandem with thermal energy to drive commercially relevant catalytic chemical transformation at viable rates, through elementary reduced temperatures compared to those of pure thermal processes.[14]

1.2 Synthesis Strategies

1.2.1 General Synthesis Strategies of Nanocrystals

Generally, two distinct approaches can be considered to synthesize nanomaterials. The physical method of decreasing the size of an existing object (by laser ablation for example) is known as the "top-down" method, and focuses on subdividing bulk materials into nanomaterials. The second approach relies on chemical methods, and is known as the "bottom-up" method; in this case, particles are grown from metal atoms in which solution phase colloidal chemistry is often employed.[13, 15-18] The bottom-up approach generally leads to the production of finer materials with a better control over their sizes, size distributions and shapes.

Many reaction parameters can be tuned in the bottom-up approach to control the size, shape, and composition of the as-produced nanomaterials, such as selecting appropriate reagents and stabilizers, modifying the reaction time, reaction temperature and the precursor concentration, etc.[2, 13, 19, 20] Numerous theoretical and computational methods have been investigated to study the exact formation process of various nanomaterials. Based on these theoretical works and experimental experiments, two steps have been recognized within the formation of a nanomaterial: first, a nucleation step, followed by a growth process,[1, 21-23] as described in Figure 1.1. According to the nucleation and growth mechanism, a supersaturation regime is needed to produce highly crystalline nanoparticles.[24-26] Based on this theory, the size and shapes of nanomaterials can be well-controlled by tuning the thermodynamic and kinetic parameters of the synthesis system.[17, 18, 22] However, the detailed nucleation and growth mechanisms of nanocrystals are not yet completely understood, limiting the possibility of controlling the formation of some materials.[1]

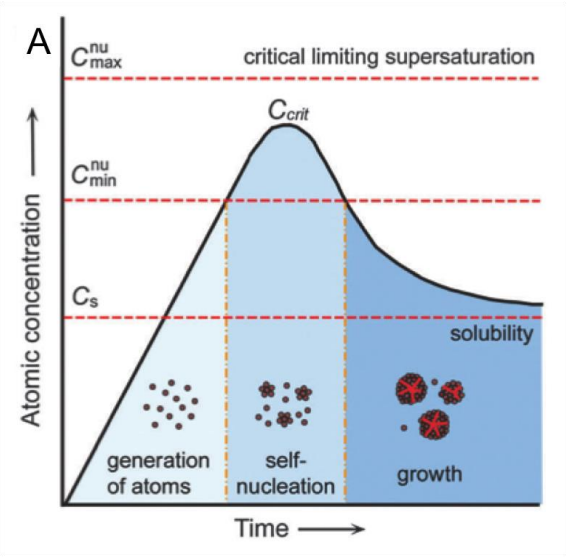

Figure 1.1. LaMer model describing the nucleation and growth of nanocrystals as a function of reaction time and concentration of precursor atoms. Reprinted from reference 23.

Despite a limited level of understanding of the growth process, several techniques have been developed to produce metallic nanocrystals according to the nucleation and growth mechanism over the last three decades. Those strategies mainly relies on two distinct techniques: chemical reduction of metal salt precursors, and controlled decomposition of organometallic compounds or metal-surfactant complexes.[19] In 1857, Faraday reported the fabrication of gold colloidal sol by reducing $HAuCl_4$ by phosphorous.[27, 28] Then Turkevich's group synthesized uniform 13-nm Au nanaoparticles by using sodium citrate as a reductant.[29, 30] In 1991, Pileni's group synthesized uniform silver nanocrystals from reverse micelles. In this method, metal atoms (Ag) were linked to a surfactant (AOT) to form a precursor (Ag(AOT)), and hydrazine was used as the reducing agent. After the nanocrystals formed within the micelles, dodecanethiol, capping agent, was used to extract and stabilize the as-formed nanocrystals from micellar solution.[31] Later, this method was further developed to produce Cu or Co nanoparticles.[32, 33] In 1994, Brust's group described a biphasic method of producing 3nm gold nanoparticles.[34] This method involves the phase tranfer of an organic solution in a two-phase liquid/liquid system, followed by reduction with sodium borohydride in the presence of the thiol stabilising ligand. In 2000, Alivisatos' group used decomposition methods, to produce either the CdSe quantum dots or CdSe nanorods by controlling the types of ligands as well as the concentration of monomer.[35] They also obtained Co nanocrystals by thermal-decomposition of $Co_2(CO)_8$.[36] Besides, this method can also be used to fabricate alloyed FePt nanocrystals[37] by using two precursor platinum bis(acetylacetonate) and $Fe(CO)_5$.

Regarding the synthesis of nanocrystals via thermal decomposition, two important heating methods should be mentioned here: hot injection method and heating-up method (one-pot). In 1993, Murray *et al*. used hot-injection methods to synthesize CdS or CdSe nanocrystals with Me_2Cd as precursor and trioctylphosphine oxide (TOPO) as solvent, which provides a new method to synthesize monodisperse nanocrystals.[13, 38] In the hot-injection method (Figure 1.2), the fast injection of the precursor induces a high degree of supersaturation, resulting in a short burst of nucleation.[16] During the nucleation process the precursor concentration in the solution decreases abruptly. The hot-injection method was widely used later and further modified by many groups. In the so-called "heating-up" method, the reaction solution is prepared at relatively low temperature. Subsequent heating initiates the crystallization process, finally leading to the formation of nanocrystals.[39] In 2005, Hyeon group obtained Fe_3O_4 nanocrystals by heating-up (one-pot) method.[40] By refluxing Fe crystal seeds and Iron oleate in organic solvent the nanocrystal size can be tuned from 6-nm to 15-nm.

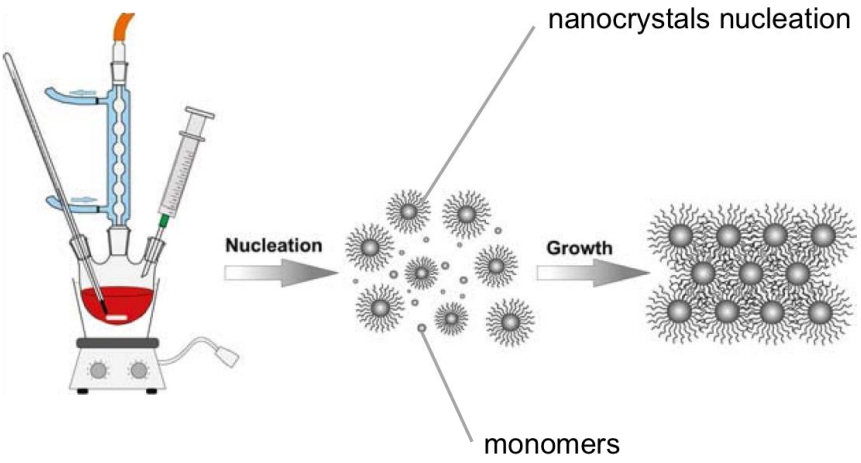

Figure 1.2. Experimental set-up and reaction scheme of the hot injection method. Reprinted from reference 38.

1.2.2 Synthesis Strategies of Silver Nanostructures

1.2.2.1 The need of Stabilization of Ag nanocrystals

Most synthesis methods described above mention the need of a coating agent or stabilizer, with different molecules being used for various types of materials. The first use of

those coatings is to protect the nanostructures from aggregation. These coating molecules introduce short-range steric repulsions and counterbalance the van der Waals attractive forces that exist between particles.[18] Therefore all synthetic approaches to stable metal colloids must include astabilizing agents, which is generally adsorbed at the material's surface.[19] The stabilizing agents are molecules of surfactant linked through covalent, coordinate, ionic bonds or physically adsorbed on the nanocrystal surface. Furthermore, the surfactant can also play a role in controlling the size of the nanocrystals.[41] During nanocrystal growth in solution, the surfactant can adsorb to the specific surface of the nanocrystal, decreasing the rate of materials addition to the nanocrystal, resulting in smaller nanocrystal sizes. The stabilizers most commonly used are electron-donor ligands, polymers and surfactant molecules. [16]

For Ag nanocrystals, capping agents also play a very important role either for the stabilization of the nanoparticles or for the shape control of Ag nanocrystals. The most common capping agents used in polar solvent for the synthesis of Ag are PVP (polyvinyl pyrrolidone), PEG (polyethylene glycol) and CTAB.[7] In non-polar solvents, the most common capping agents are dodecanethiol[28, 42] and oleylamine.[43, 44] These capping agents have long hydrocarbon chains protecting the nanocrystals from aggregation. Dodecanethoil is commonly used to protect noble metal (Au or Ag) nanostructures because the bonds between sulfer head group is strong, making the nanoparticles stable.[45, 46, 47]

1.2.2.2 Synthesis Methods

According to the crystal nucleation and growth mechanism and the need for a coating agent decribed above, the most common ways to prepare silver nanomaterials rely on the reduction of a silver precursor using a suitable reducing agent, in the presence of a coating agents that will stabilize the as-formed particles in appropriate conditions. During the reducing process, zero-valence Ag is continuously provided to maintain a sustainable growth of Ag nanoparticles. As long as more zero-valence Ag are produced, zero-valence Ag reach a critical value of concentration and the zero-valence Ag can condense to form nuclei.[23] $AgNO_3$ is the most commonly used precursor. Chemical reducing agents, such as sodium borohydride, alcohols, and sodium citrate, are typically used to reduce the dissolved Ag^+ ions to Ag atoms, which finally assemble into nanostructures.[7]

The synthesis of quasi-spherical Ag nanoparticles, such as icosahedral silver nanocrystals, which has the lowest surface energy compared to other shapes is the most

studied. Several methods are available to make this kind of nanomaterials in different size ranges. The most common method in water solution is the reduction of $AgNO_3$ by $NaBH_4$, which finally yields to Ag particles with a relatively narrow size distribution.[7] Besides, Ag colloids can also obtained via the reduction of citrate in an aqueous solution.[48] Two other relatively common methods to produce Ag nanocrystals rely on the reduction of $AgNO_3$ with hot oleylamine or ethylene glycol (EG). In these two methods, oleylamine and EG are used as reducers, solvent to dissolve $AgNO_3$ and the oleylamine is also used as capping agent.[23, 49] For instance, Peng *et al*. synthesized icosahedral Ag nanocrystals with very large-scale size ranging from 2 nm to around 17 nm by reducing the $AgNO_3$ in hot oleylamine (Figure 1.3-a).[43] Lim *et al*. synthesized silver nanospheres particles in EG by electrochemically-assisted polyol process. In this method, PVP is electrochemically stable and facilitates the formation of well-defined nanospheres of sizes around -11 nm (Figure 1.3-b).[50] Besides, Pileni's group also prepared Ag nanoparticles around 5 nm in diameter by reverse micelles method with dodecanethiol as capping agents (Figure 1.3-c).[51]

Recently, seeding growth approaches have become increasingly popular; they consist in using preformed nanocrystals and smoothing them to subsequent growth.[52, 53] This method is highly versatile and can be used to manipulate the size, aspect ratio, and shape of the resulting nanostructures. [54, 55]

Ag nanostructures of different shapes have also been studied.[56] There are many factors that can be controlled to obtained Ag nanomaterials with varying structures, such as controlling the concentration of silver precursor and the types of solvent; inducing the presence of a soft or hard template, inducing a guest ions to adsorb to a particular crystal plane.[56] For example, Varma *et al*. fabricated silver nanorods (Figure 1.4-a) in PEG (polyethylene glycol) using microwave irradiation and Ag nanoparticles can also be obtained by modifying the ratio between PEG and Ag precursor.[57] Sun *et al*. also fabricated nanocubes in binary organic solvent mediated with DDAC (dimethyldistear-ammonium chloride) that was used as a source to provide free Cl^- ions (Figure 1.4-b).[58] Carrol *et al.* fabricated silver truncated, triangular nanoplates and circular nanodisks in the presence of CTAB (Figure 1.4-c) [7, 59] and Pileni *et al.* synthesized nanodisks by sonicating $AgNO_3$ and hydrazine in the presence of reverse micelles self-assembled from an AOT/isooctane/water system (Figure 1.4-d)[60] . Sun *et al*. synthesized Ag nanowires as well as other 1D nanostructures derived from Ag nanowires (Figure 1.4-e). [12]

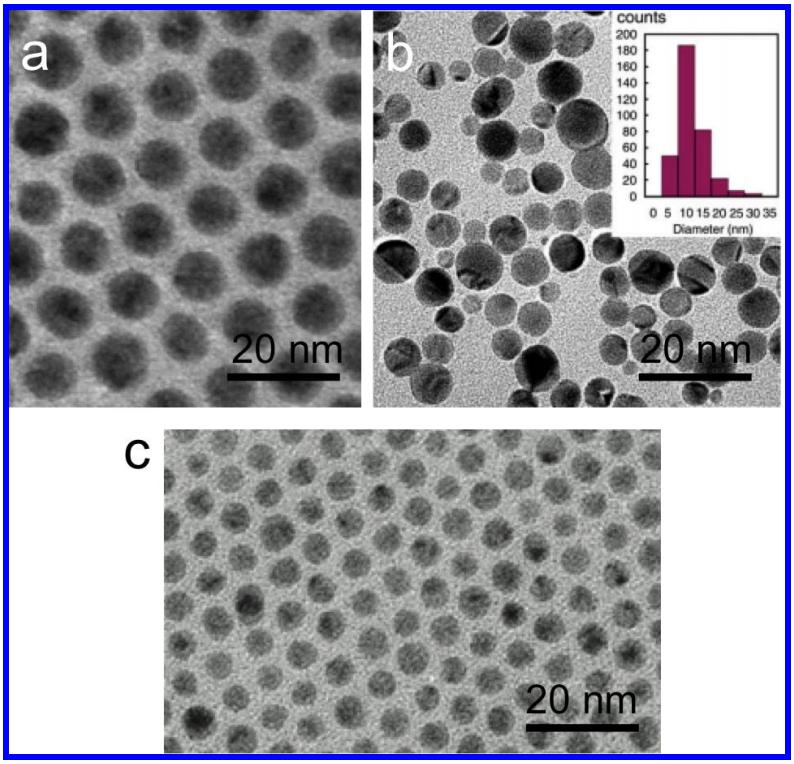

Figure 1.3. Ag nanoparticles synthesized by different methods: (a) reduction of $AgNO_3$ with hot oleylamine; (b) electrochemical-assisted polyol process; (c) Ag nanoparticles prepared in reverse micelles. Reprinted from references 43, 50 and 51, respectively.

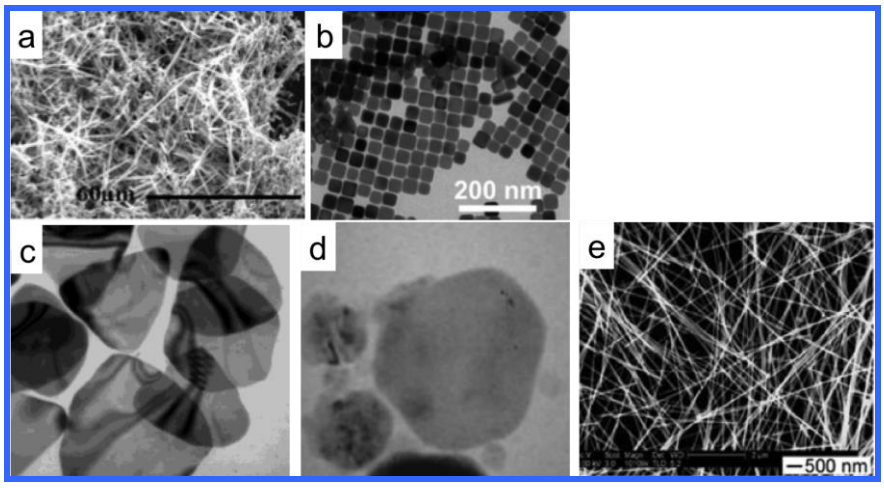

Figure 1.4. Ag nanomaterials with different shapes: (a) nanorods; (b) nanocubes; (c) nanoplates; (d) nanodisks; (e) nanowires. Reprinted from references 57, 58, 59, 60 and 12 respectively.

1.3 Optical Properties of Colloidal Nanocrystals

When irradiated by an electromagnetic wave, metallic nanocrystals exhibit a very large absorption band that stem from the free electrons at the metal surface resonatibng with the incident photons. This effect is known as a Surface Plasmon Resonnance (SPR).

Plasmonics is related to the localization, guiding, and manipulation of electromagnetic waves down to the nanometer-length scale.[6, 7, 61, 62] Metals are key component in plasmonics because they supports surface plasmon polariton modes. [63-65]

Surface plasmons have been known for more than 160 years since Micheal Faraday demonstrated their existence for the first time in 1857.[27] Two types of plasmons can be differenciated, that are two common types of plasmonic modes: localized surface plasmons (LSPs) and propagating surface plasmons (PSPs).[7] When metal nanoparticles are irradiated by light at wavelengths much larger than the size of the metal nanoparticles, the surface electron cloud is displaced with respect to the metal nuclei, generating a restoring force arising from Coulomb attractions between electrons and nuclei. This kind of attraction leads to the oscillation of the surface electron. At a special frequency the surface electrons are oscillating coherently with the incident light, resulting in the plasmonic resonance, which is commonly known as a localized surface plasmon resonance (LSPR) mode.[66] (Figure 1.5-a) There are several factors influencing the oscillation frequency: (1) the density of surface electrons; (2) the effective electron mass (3) the shape and size of the charge distribution.[64]

In contrast, PSPs are supported by structures that have at least one dimension that approaches the excitation wavelength, such as nanowires, as shown in Figure 1.5-b.[6] In this case, the electron field is not uniform across the structure and other effects must be considered.

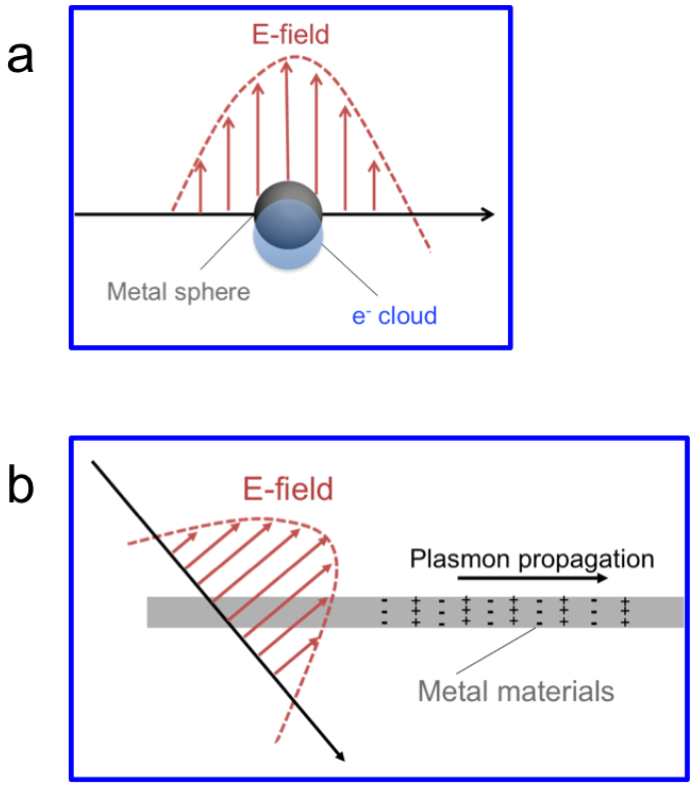

Figure 1.5. Schematic illustration of the two types of plamonic nanostructures: (a) Schematic of plasmon oscillation for a sphere, showing the displacement of the conduction electron charge cloud relative to the nuclei; (in this case, the nanostructure is smaller than the wavelength of light) (b) the nanowire has one dimension much larger than the wavelength of light. Reprinted from reference 66 and 7, respectively.

Since the plasmonic properties of a material are dependent on its size and shape, nanostructures can be used as active components to guide and manipulate light. Compared to other properties, plasmonic is a unique property of metal nanomaterials because plasmon relies on light matter interactions. Therefore plasmoncis is a new subfield of nanoscale science and technology that aims to understand the control light and metal nanostructures in novel ways.[67-70]

There are several simulation works on the plasmonic properties of metal nanoparticles.[63, 64, 71, 72] As early as 1908, Gustave Mie developed an analytical solution to Maxwell's equation[73] that described the extinction spectra (extinction = scattering + absorption)[74] of spherical particles of arbitrary sizes. Since then, many research groups contributed to this pioneering work on simulation works of metal nanomaterials plasmon. For example, Schatz's group used efficient CG/FFT (Conjugate Gradient Solution with Fast Fourier Trans- forms) methods for calculating coupled dipole optical response to the coupled

nanosphere problem. They determined aspects of the structural basis for the UV-vis extinction properties of DNA-linked nanoparticle aggregates.[63] Guyot-Sionnest's group synthesized Au/Ag core/shell nanorods and subjected those to optical measurements. The longitudinal plasmon resonance of core/shell nanorods was found to be blue shifted as the Ag layer became thicker. They also used new energy-loss model to evaluate the extra damping of a conduction electron in an arbitrary-shaped metal particle to explain the plasmonic results observed.[75]

1.3.1 SPR of silver nanoparticles

As mentioned above, noble metallic nanoparticles, especially silver nanoparticles are a very important material in plasmonics. Ag has the largest quality factor across most of the spectrum from 300 to 1200 nm.[76] In physical and engineering the quality factor is a dimensional parameter that describes how under-damped an oscillation or resonators, are as well as characterized a resonators' bandwith relative to its center frequency. Compared to Au and Cu that exhibit a rather broad and anisomerous plasmonic resonance due to damping effect, the interband transitions of silver, that is the special area where electrons are excited from the conduction band to higher energy levels, take place at much higher frequencies than that of the LSPRs. That is why silver plasmon spectra show very narrow resonance band and the shape of the band is much more symmetrical compared to other methods.[76]

It is worth noting that the most traditional approaches used to characterize the plasmonic response of metal nanostructures is to measure their extinction spectrum using UV-vis-NIR spectroscopies.[77] Several calculations and experimental works reported that various factors affect the plasmonic properties of silver nanostructures. First of all, the morphology of Ag nanocrystals is an important factor. For example, Xia's group showed UV-visible extinction spectra of three Ag nanostructures in aqueous media and containing silver spheres, cubes, and triangular thin plates with almost the same sizes. (Figure 1.6) The silver nanospheres exhibit one symmetric extinction peak centered at 430 nm due to the isotropic symmetry of sphetical structures. However, cubic nanoparticles displayed three SPR peaks located at 350, 400, and 470 nm, respectively. The spectra of triangular nanoplates displayed three peaks at around 335, 470 and 690 nm. This phenomenon can be explained by theoretical calculation carried out by Schatz's group: these peaks correspond to the out-of-plane

quadrupole, in-plane quadrupole, and in-plane dipolar plasmon resonance modes, respectively.[78]

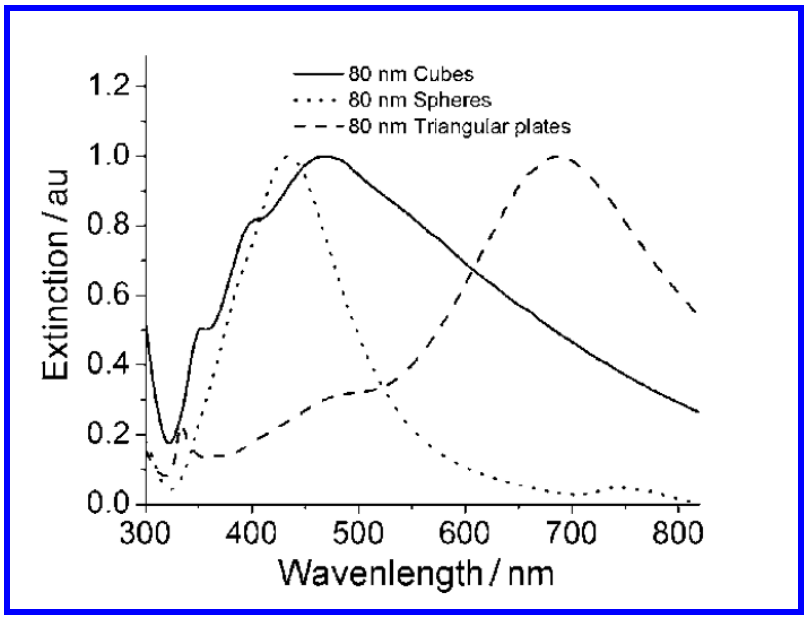

Figure 1.6. UV-visible/near-infrared spectra recorded on aqueous dispersions containing quasi-spheres, cubes, and triangular thin plates of silver. The spectra have been normalized against the intensities of their strongest peaks. Reprinted from reference 78.

Secondly, modifying the dimensions of Ag nanostructures can also be used to tune their plasmonic properties. The size of a nanoparticle determines plasmonic features including the ratio of absorption to scattering, the number of LSPR modes, the peak position of an LSPR mode.[77, 79-81] Sun's group synthesized silver nanoparticles, their sizes ranging from about 2 nm to 17 nm and measured the UV-visible absorption spectra when dispersed in various organic solvents. They observed that, when the nanoparticles size increases, the SPR is blue shifted for relatively small particles, and then red shifted for larger sizes. In their research, the solvent of the colloidal solution was also found to play a very important role on the plasmonic properties. (Figure 1.7) [43] Xia's group also found that plamonic spectra exhibit considerable differences for Ag nanocubes with different edge length ranging from 36 to 172 nm. The major dipole peak of Ag nanocubes shows a continuous red-shift along with an increase of their edge length. The relationship between the LSPR peak position and the edge length of nanocubes is almost linear.[53]

Other factors are also affecting the Ag plasmonic properties, including their coating agents and the intrinsic composition of the nanoparticles. By changing the coating agents, the

dielectric constant of the nanocrystals is varied. This phenomenon has also been proved by many theoretical simulations.[43, 63, 64, 82] Besides, several groups produced Ag/Au alloyed nanoparticles, such as Ag/Au core-shell structures or Au/Ag hollow structures to manipulate the optical properties.

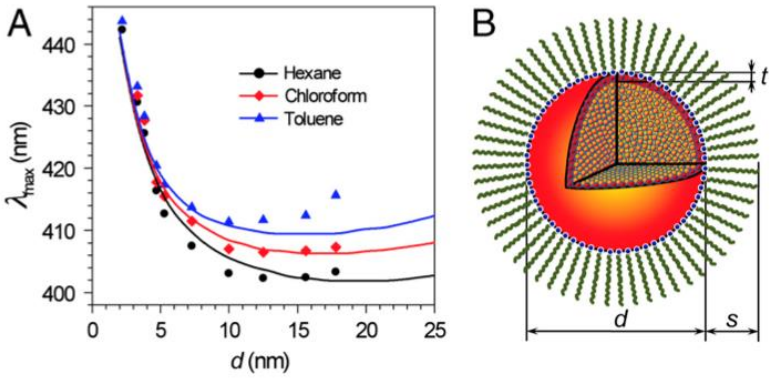

Figure 1.7. Comparison of experimental and theoretically calculated absorption spectra. (A) Experimental (dots) and theoretically predicted (lines) SPR peaks positions for Ag nanoparitlces of various size dispersed in hexane (black), chloroform (red), and toluene (blue). (B) Schematic illustration of the theoretical model: d represents the diameter of a Ag nanoparticles, t is the thickness of the outermost atomic Ag layer with lowered conductivity, and s is denoted as the thickness of the surfactant layer. Blue dots represent N atoms bonded to the surface of the NP. This figure is reprinted from reference 43.

1.4 Self-assemblies of Nanocrystals

In nature, living systems often tend to self-organize in order to build larger and more complex structures; this is nature's preferred way of building and creating at various scales. Self-assembly is the process in which isolated components organize autonomously and spontaneously into ordered and functional structures in static and dynamic states.[26] As we know, the properties of colloidal inorganic nanoparticles are significantly dependent on the nanoparticle's sizes and morphologies. Fabricate more complicated structures made of nanocrystals with different sizes and morphologies is highly necessary, which are expected to lead to superstructures with a range of practical applications.[83-85]

1.4.1 Application of Superlattices

To date, a large number of groups have succeeded in preparing various self-organized superlattices. This growing interest is due to the fact that, compared to dispersed nanocrystals, these superlattices show considerable changes in the physical properties of the whole structures they form, due to that nanocrystals are all in close vicinity one form each other. [25, 26, 86, 87]

For superlattices composed of metallic nanocrystals, such as silver, gold, and cobalt, collective properties are attributed to dipole-dipole interactions. For example, Pileni's group measured by STM the electronic properties of very thick gold nanocrystals assembled into superlattices. In this case, for a given nanocrystal, the conductance exhibits a slight additional modulation superimposed on the collective conductance background that mimics the Coulomb staircase structure normally associated with an isolated nanocrystal.[88]

Binary nanocrystal superlattices also showed outstanding collective physical properties compared to either isolated nanocrystals or their corresponding single component superlattices. For example, the collective plasmonic response of binary superlattieces assembled with Au and Fe_2O_3 nanocrystals. In this system, the strength of near-field couplings between adjacent plasmonic nanocrystals can be systematically engineered by varying the NC size, composition and the lattice symmetry, leading to broadband spectral tenability of the collective plasmonic response of superlattices across the entire visible spectrum.[89] In 2007, Murray's group also presented for the first time that the electronic measurements of multicomponent nanocrystal solid composed of PbTe and Ag_2Te, demonstrating synergistic effects leading to enhenced p-type conductivity.[90]

1.4.2 Two-dimensional (2D) nanocrystal superlattices

Over the last 20 years, a number of groups have succeeded in fabricating self-ordered nanocrystals in two-dimensional closed-packed superlattices with a small number of defects and at very large scale. These 2D superlattices self-assembled by inorganic nanoparticles provide new possibilities of fabricating new solid-state materials and devices with novel physical properties because the interactions between nanopariticles can generate new collective phenomenon. [91-94]

There are several dominating strategies to produce 2D self-assembled superlattices: (1) Langmuir-Blodgett methods are well known procedures to generate 2D hexagonal closed-

packed superlattices.[95] This type of strategies was developped in the early 20th century by Irving Langmuir and Katherine Blodgett. In this method, a Langmuir monolayer is held at constant surface pressure while transferring it onto a solid substrate. Currently, this approach has already been explored to fabricate closed-packed 2D films composed of nanomaterials with different shapes. Tao *et al*. used Langmuire-Blodgett methods to fabricate 2D superlattices assembled of silver nanowires and then subjected the sample to SERS measurements.[96] (2) There is another convenient way to prepare 2D superlattices: one-drop colloidal solution of known concentration is deposited on the substrate and the evaporation process occurs at the substrate surface.[47] This method is easier and more flexible than LB based procedures, but the superlattices obtained only exhibit local ordering, with some areas containing multilayers. Other parameters that must also be considered are related to the material itself, the particle-particle and the particle-substrate interactions.[86, 91] For instance, Pileni's group successfully prepared 2D Cobalt self-assembled arrays with this method.[86] (3) Finally, liquid-air interfacial assembly approaches have become a popular method in recent years to produce 2D superlattices.[97] This method is a combination of modified LB and evaporating method. Murray *et al*. used this method to prepare 2D superlattices with different kind of nanocrystals. 2D superlattices films obtained in the centimeter-scale and transferable for example.[93]

1.4.3 Three-dimensional (3D) Nanocrystal Superlattices

Similarily to 2D superlattices, controlled assembly of long range three-dimensional (3D) superlattices with well-defined structures and desired types of NCs can lead to many unique properties and their subsequent use in different applicatiomns, hence their production has been a long-standing challenge.

The structures of 3D superlattices are similar to atoms in bulk phase metals and in nanocrystals such as body centered cubic (bcc), face centered cubic (fcc) and also the hexonganal close packed (hcp) structures. Amorphous structures of disordered nanoparticles also exist. (Figure 1.8)[25] When the fabrication conditions of these superlattices are well controlled, the structures can be varied between the different types.[51]

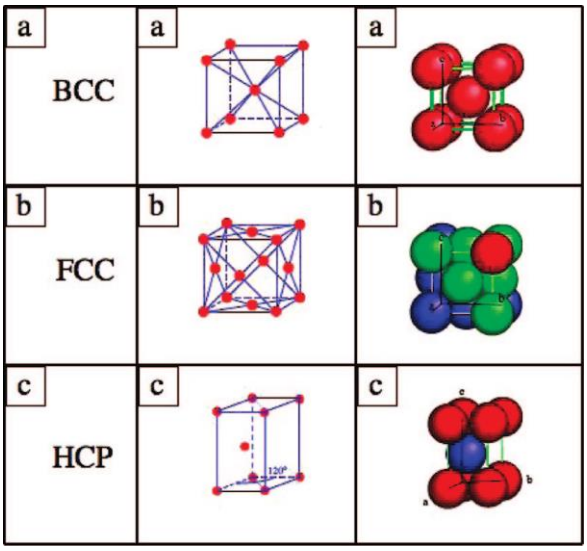

Figure 1.8. Schematic representation of sphere packing into (a) bcc, (b) fcc and (c) hcp. The figures reprinted from reference 25.

1.4.3.1 General View on Formation Mechanism of 3D Superlattices

During superlattices growth in a solvent, the nanoparticles crystallize from the suspension in order to achieve the thermodynamic equilibrium state, which results in the minimum Gibbs free energy [98, 99] of the system. The Gibbs free energy changes (ΔG) at a given temperature is as follows:

$$\Delta G = \Delta H - T\Delta S$$

where ΔH is the standard enthalpy of formation, ΔS is the standard entropy formation, and T is the temperature in K. The energetic contribution ΔH accounts for the various types of interactions (van der Walls force, Columbic force, dipolar interaction, *etc*) between nanoparticles in the suspension, while the entropy changes during the self-assembly processes are generally related to the sum of each nanoparticles' free volumes in the system.[22, 100, 101] Both entropy and isotropic van der Walls interactions should favor structures with high packing densities, fcc and hcp. In the hard-sphere system, fcc is favored over hcp due to its higher entropy, although the free energy difference is small. In addition, the solvent flow can direct nanocrystals toward the fcc lattice. [25, 102]

1.4.3.2 Growth Methods

As mentioned above the mechanism of superlattices self-assembly is driven primately by entropy, as well as a complex interplay of entropic and enthalpic components. Based on quantitative reported data, two principal methods, which are similar as the method used for 2D superlattices, are applied to grow nanocrystal 3D superlattices: crystallization induced by solvent evaporation and by adding a bad solvent.[98, 103-105] The most common method is the slow and controlled evaporation of the organic solvent, or even water, on a suitable surface. As early as 2003, Pileni *et al*. produced supracrystals composed of Cobalt nanocrystals with more than 1000 layers of organized nanocrystals (Figure 1.9-a).[106] In this approach, particle-substrate interaction plays an important role on the ordering of superlattices. When using HOPG (Highly Oriented Pyrolitic Graphite) as a substrate instead of silicon wafer, the ordering is improved. Later, the solvent-evaporating method was further modified by Talapin's group (Figure 1.9-c).[101] They prepared superlattices with 11-nm $Fe_xO/CoFe_2O_4$ nanocrystals. In this process, a beaker holding the substrate is tilted to an angle to avoid coffee ring effect during the drying process. Besides, the solutions were evaporated under vacuum controlled by a needle penetrating the cap of the closed beaker. By adjusting the needle type, the evaporating rate can be controlled. With this method, the solvent can be evaporated relatively fast under dynamic vacuum condition even when using a high boiling point solvent. In 2010, Murray's group applied a liquid-air interfacial method to make large-scale 3D superlattices (Figure 1.9-b), as described in Section 1.4.2 on 2D superlattices synthesis.[97] In 2001, Rogach *et al.* demonstrated a new method named non-solvent method to prepare 3D superlattices. They prepared supercrystals composed of CdSe nanocrystals by slow diffusion of a non-solvent into a concentrated solution of CdSe nanocrystals, either directly or through a buffer layer, resulting in nucleation of nanocrystals on the walls of tubes and in the bulk of the solution. The buffer layer used here is low, but its solubility is not negligible enough for nanocrystals. (Figure 1.9-d) [103, 107] This method can also be used to grow supracrsyals in polar suspensions and the as-obtained supracrystals are well-shaped crystals instead of films.

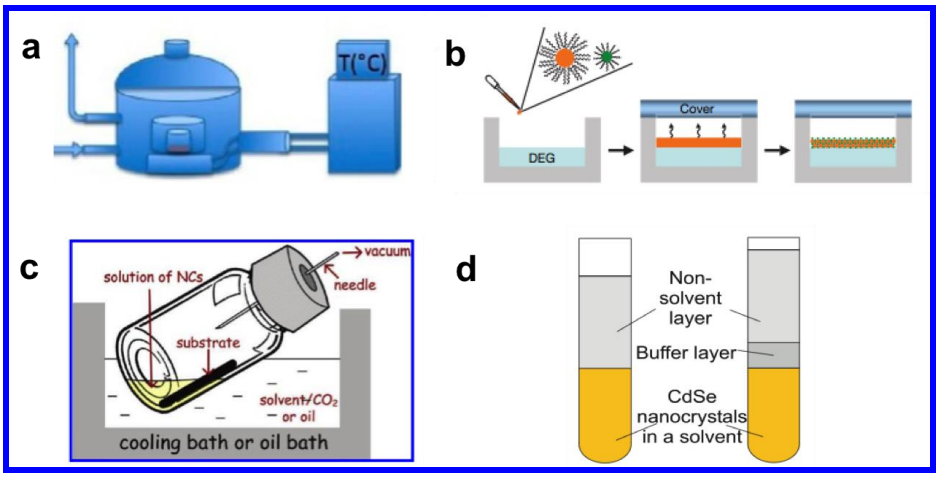

Figure 1.9. Schematic illustrations of the set-ups used for the 3D superlattices preparation: (a) slow evaporating solvent method;[108] (b) liquid-air interface method;[97] (c) modified solvent evaporating method;[101] (d) non-solvent method.[103] Reprinted from reference 108, 97, 101, and 103, respectively.

1.4.4 Binary Nanocrystal Superlattices

Superlattices composed of nanocrystals with single component and morphology have been extensively investigated. However, In recent years, the attentions have also been focused towards bimetallic materials, that are superlattices composed of multi-components materials. Those types of materials are known to exhibit novel properties that can be used in various applications, so superlattices made of different types of nanocrystals with properties arising from the controlled interaction of the different nanocrystals is a long standing challenge for scientists.[109-112] However, preparation of binary superlattices comes across many technical difficulties and limitations. Previous multi-component nanocrystal assemblies usually resulted in amorphous or short-rang-ordered structures.[83] Besides, it is difficult to obtain superlattices with only one structure.

Recently, a better understanding of the formation mechanism of superlattices has been reached allowing the production of high-quality nanocrystals with controlled sizes and shapes; those can now be routinely synthesized in a relatively large quantity, hence leading to the facilitation of binary nanocrystal superlattices co-crystallization from suspension of two nanocrystals with selected size ratios. Again, similarily to what is being observed for atoms, many different types of binary superlattices structures can be made. The arrangement types of superlattices and the interparticle distances, influencing the coupling effect between the superlattices, can be well controlled. Thus binary superlattices containing two distinct type of

nanocrystals provide new possibility to building materials with potentially novel chemical and physical properties. [109-111]

1.4.4.1 General View on Formation Mechanism

The formation mechanism of binary nanocrystal superlattices is a complex process, and is still not yet well understood. It is widely recognized that the driving force of formation of various binary structures can be explained by entropic considerations, similarly to single component superlattices formation mechanism mentioned above.[109, 113] However, other factors involving Coulomb interactions from particles charges, Van der Waals interaction forces or dipole-dipole interactions should also be taken into consideration. In the hard-sphere model, the formation of binary superlattices is correlated to the configurational entropy and free volume entropy, regardless of the energetic contribution. The system is expected to adopt the crystal structure corresponding to the most efficient space filling system to reach the maximization of packing density ρ for a given ratio of the sphere radii γ. Therefore, space filling curves plotting the packing density ρ versus ratio of the sphere radii γ provides a good estimate for entropic contribution.[114-116]

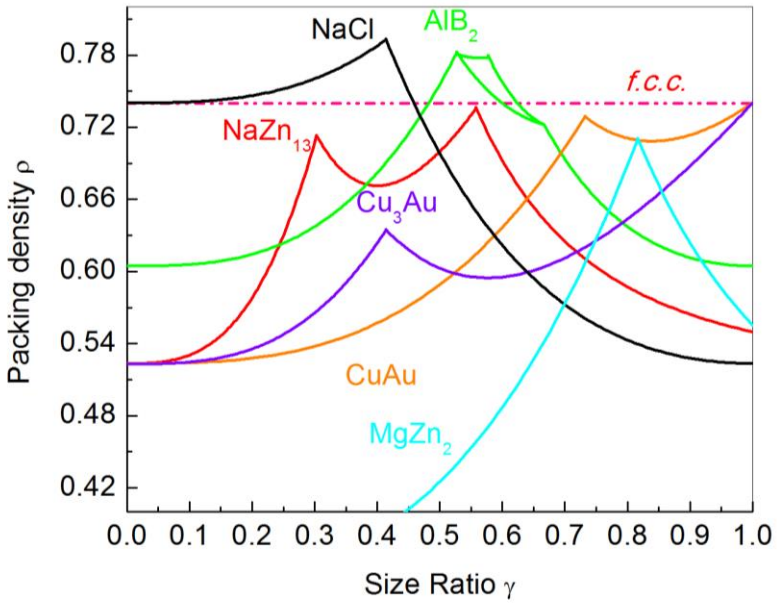

Figure 1.10. Space filling curves of various binary structures that have been observed in the literature.

1.4.4.2 Growth Methods

Based on series of data reported previously, it can be established that the growth of binary superlattices is almost identicaly to that of single component nanocrystal superlattices. Solvent evaporation method and liquid-air surface interface methods are the most used strategies. For example, in 2003, O'Brien *et al.* used solvent evaporation methods to produce 3D binary superlattices composed of PbSe and Fe_2O_3 nanocrystals.[83] In their system, the size ratio of two different nanocrystals is a key factor for the structure of superlattices. By modifying the size ratio between these two nanocrystals, various types of binary superlattices were obtained. After this report, many researchers demonstrated the synthesis of binary superlattices with different structure types by controlling the size ratio of composing nanocrystals.[85, 113, 117] It is worth noting that with this method, the nanocrystal concentrations ratios between the large and small nanocrystals should also be precisely controlled in order to get pure phase superlattices. For example, for a certain size ratio, an increase of smaller nanocrsyatl relative concentration will lead to the AB_{13} type superlattices instead of AB_2. Later, in 2010, Murray's group applied liqud-air interface method to co-crystallized multicomponent nanocrystals into binary superlattices; with this method large-scale membranes of long-range-ordered binary superlattices was achieved rapidly.[118]

As mentioned above, non-solvent method is efficient for single component systems to generate well-shaped supracrystals. However, those methods were found to be unsuitable for the growth of binary supracrystals. For example, when bad solvent was added into a suspension containing a mixture of large PbSe and smaller CdSe nanocrystal, the nanocrystals with different sizes crystallized separately, resulting in single component superlattices.[119] This phenomenon could be explained as follows: the nanoparticles' potential is increased by adding a bad solvent, thus the interactions between the nanoparticles are significantly increased, which drives the nanoparticles to crystalize into supracrystals. Because the nanoparticles potential increases with the ascending of particle diameter, the larger sized nanoparticles will crystallize first due to the stronger thermodynamic driving force when bad solvent was added. Until now, the growth of binary nanoparticle superlattice by adding bad solvent into the mixed suspensions for non-polar solvent system remains challenging. If the potential differences of two nanocrystals can be well controlled by adding bad solvent, it will be possible to produce binary superlattices with this method. For example, in the aqueous solvent, by adding a bad solvent, the Au and Ag nanocrystals can co-crystallize to get binary

diamond-shaped superlattices. In this experiment, the Au and Ag nanocrystals have the same sizes but with different charged ligands and the formation of this kind of supracrystals is the consequence of electrostatic effects specific to the nanoscale.[120]

1.5 Optical Properties of Assemblies

The plasmonic properties of 2D or 3D superlattices show major changes compared to isolated nanoparticles due to the collective dipolar interaction between the nanoparticles.[121] Gwo *et al.* prepared large-area, highly ordered 2D superlattices of alkanethiolate-stabilized gold nanoparticles onto quartz substrate with varying lattice constant, this can be controlled by the alkyl chain lengths of their coating agents ranging from C_{12}, C_{14}, C_{16} to C_{18}. These 2D nanoparticle superlattices show strong collective surface plasmon extinction bands and pronounced chain-length-dependent red shifts have been confirmed for synthesized superlattices.[122] Murray *et al.* studied the collective plasmonic response of self-assembled binary nanocrystals superlattices using correlated optical microspectrophotometry and electron microscopy over individual superlattices domains, which represent a versatile platform for the rational design of microscopic 3D plasmonic metamaterials exhibiting emergy optical chatateristics. There are also some simulation works focusing on the 2D or 3D superlattices. For example, Pileni *et al.* worked on the DDA simulations of the optical absorption of 5 nm spherical silver and gold nanoparticles arranged in hexagonally closed-packed planar array; Ag showed two absorption bands of in increasing order of energy while Au only show one absorption band.[123] However, the study of plasmonic properties on 3D silver superlattices and 3D silver binary superlattices are still rare, making it challenging to understand the relationship between plasmonic properties and self-assembled nanoparticles.

Chapter 2

Collective Surface Plasmon Resonances in Two-Dimensional Assemblies of Metal Nanocrystals: experiments and simulations

2.1 Abstract

In this Chapter, the plasmonic responses of two-dimensional (2D) assemblies of Ag or Au nanocrystals coated with dodecanethiol are studied by measuring their UV-visible absorption spectra in transmission at variable incidence angle, for three different NP diameters (7 nm, 5 nm and 4 nm). The silver nanocrystals are synthesizd from reverse micelles and the gold nanocrystals are obtained from modified Stuky's method. The measured spectra are compared to the results calculated using the discrete dipole approximation (DDA) method. The anisotropy observed in the optical response is inherent to the planar geometry of the close-packed arrangements and originates from the near-field coupling between nanocrystals. In 2D assemblies of Ag nanocrystals, this coupling induces the splitting of the collective surface plasmon resonance (SPR) absorption band into two components, namely, the transverse and longitudinal modes. A good agreement between experiments and DDA calculation can be obtained with only slight divergency that is probably due to the substrate effect or the strong bonding between ligands and silver nanocrystals.

At variance, by replacing Ag by Au nanocrystals assemblies with average diameter, coating agent and differing by the procedure used to produce them, no splitting is observed. As already observed by DDA simulation this was attributed to the different intrinsic dielectric properties of Au and Ag. Nevertheless disagreements are also obtained concerning the longitudinal modes. This is attributed to the large amount present of the dodecanthiol adsorbed both at the Au surface atoms and on the alkyl chains used as coating agent which are origined from the synthesis method. This induces a significant increase of the damping effect at the surface of the nanoparticle.

2.2 Article: Collective Surface Plasmon Resonances in Two-Dimensional Assemblies of metal Nanocrystals: experiments and simulations

Collective surface plasmon resonances in two-dimensional assemblies of Au and Ag nanocrystals: Experiments and DDA simulation

J. J. Wei[1,2], P. Yang[1,2,$], H. Portalès[1,2] and M.P Pileni[1,2,3,*]

[1] UPMC - Sorbonne Universités, UMR 8233, MONARIS, 75005, Paris, France
[2] CNRS, UMR 8233, MONARIS, 75005, Paris, France
[3] CEA/IRAMIS, CEA Saclay, 91191, Gif-sur-Yvette, France
[$] Present address: School of Advanced Materials and Nanoscience, Xidian University, Xi'an, 710071, P. R. China

INTRODUCTION

Superstructures composed of nanosized particles ordered in close-packed arrangements with programmable design are attracting many interests,[1-4] especially by using noble metal nanocrystals as building blocks in view of promoting tunable plasmonic properties. As clearly established in previous studies, the characteristics of the localized surface plasmon resonances (LSPRs) of such nanocrystals (NCs) depend on their composition, shape, size and size distribution, local dielectric environment as well as their potential electromagnetic coupling to other vicinal nanocrystals. In two-dimensional (2D) NC arrangements, the near-field coupling between neighboring NCs was demonstrated to allow for the coherent response of the nanocrystals and the emergence of collective optical properties.[5, 6] In this way, the 3D superstructures may exhibit neither the same properties as that of the bulk phase materials, nor those of individual NCs, which enables the NC superstructures to act as photonic crystals. These novel properties are promising for their use in functional devices, thus motivating many efforts on their controllable, bottom-up fabrication on large scale.[7, 8]

During this last decade, both experimental and theoretical studies were devoted to the collective SPR in 2D assemblies of metal NCs. On the basis of reflectivity spectra of Ag NCs self-assembled in 2D superstructures onto a graphite substrate exposed to *p*-polarized light (polarization parallel to the incidence plane), collective optical properties were found from the emergence of additional plasmonic features in their spectra compared to those of similar NCs dispersed in solution.[5, 9] Besides, the substrate effect on the reflectivity spectra of 2D self-assemblies of Ag NCs was also investigated by using various substrates, namely, highly oriented pyrolytic graphite (HOPG), gold, silicon, and $Al_{0.7}Ga_{0.3}As$. [10]

Recently, using the discrete dipole approximation (DDA) method, the absorption spectra of well-ordered 2D assemblies of ultrafine Ag and Au nanospheres were simulated for different interparticle distances and incidence angles.[11, 12] From these last calculations, optical anisotropy of thin films of Ag nanospheres was distinctly observed through the emergence of transverse and longitudinal modes for incidence angle larger than 30° and interparticle distance not exceeding one nanosphere radius typically. Conversely, for identical nanostructured films composed of Au nanospheres, only a shift without any splitting of the SPR band was observed in the DDA calculated absorption spectra. Chen *et al.*[6] reported on the evolution of the optical response of highly ordered 2D superlattices of alkanethiolate-stabilized Au NCs onto quartz substrate. By finely varying the lattice constant through the change in alkyl chain length while keeping the metal core size unchanged, they demonstrated their ability to tune the collective SPR extinction band via near-field coupling between adjacent NCs. The extinction measurements performed on the 2D assemblies exhibited the progressive blueshift of the SPR peak for increasing interparticle distance.[6]

Here, on the basis of both spectrophotometry measurements and computational simulations of the absorption spectra, we conjointly study the plasmonic response from 2D self-assemblies of either Ag or Au spherical NCs. The samples under investigation are prepared by depositing dodecanethiolate-stabilized Ag or Au NCs with different diameters ranging from 4-nm to 7-nm, onto a glass substrate where they self-assemble and form close-packed planar arrangements. Through both experimental and numerical approaches, one points out the tunability of the collective SPR in these Ag NC assemblies, as induced by the near-field coupling between nanocrystals. The collective SPR bands observed in the measured absorption spectra are described and compared to those calculated using the DDA method.

EXPERIMENTAL AND SIMULATION METHODS

a. Synthesis of Ag and Au NCs and their 2D assemblies

The reverse micelle technique[13] was used to synthesize Ag NCs with average diameters of 7.0 nm, 5.0 nm, and 3.9 nm. The nanocrystals were extracted with dodecanethiol from the micellar solution and then were subjected to the ethanol-hexane wash cycles.[14] Finally, the Ag NCs were dispersed in hexane for use. Au NCs were synthesized by revisiting the Stucky's method.[15]

2D assemblies of Ag or Au NCs are produced as follows: 30 μL of toluene was deposited on a glass substrate, followed by the deposition of 20 μL of metallic colloidal solution (Ag or Au) onto the toluene surface. After the evaporation of the solvent, 2D assemblies of NCs were formed on the glass substrate. In parallel, a drop of the colloidal solution is deposited on a TEM grid to determine the nanocrystal size distribution. Typical transmission electron microscopy (TEM) images of the synthesized NPs along with the size distribution and interparticle distance histograms are shown in Figure 1 and Figure 2 for Ag and Au NCs, respectively. Table 1 summarizes the average diameters and interparticle distances determined by TEM analysis over a population of around 500 NCs. Simultaneously, to the TEM experiments, the same amount of colloidal solution is deposited onto a glass wafer to measure the optical properties of such assemblies.

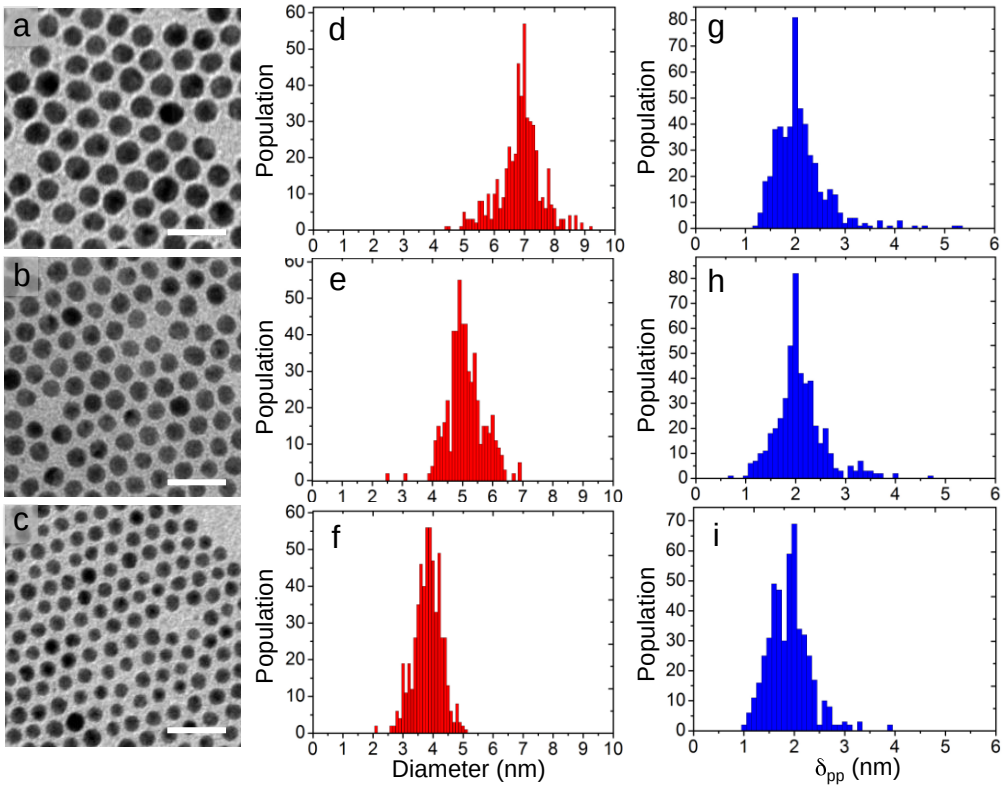

Figure 1. (a-c) TEM images and (d-f) size distribution histograms of Ag NCs issued from samples Ag-7, Ag-5 and Ag-4, from top to bottom. (g-i) Histograms of the border-to-border interparticle distance, δ_{pp}. Each histogram was determined by TEM analysis over a population of around 500 NCs. The scale bar is 20 nm.

Table 1. Average diameter, $\langle D \rangle$, of Ag and Au NCs and border-to-border interparticle distance, δ_{pp}, determined by TEM analysis. The relative interparticle distance, $\gamma = \delta_{pp}/\langle D \rangle$, is also indicated.

Sample	$\langle D \rangle$ (nm)	δ_{pp}	$\gamma = \delta_{pp} / \langle D \rangle$
Ag-7	7.0 ± 0.6	2.0 ± 0.4	0.286 ± 0.063
Ag-5	5.0 ± 0.5	2.0 ± 0.3	0.400 ± 0.073
Ag-4	3.9 ± 0.4	1.9 ± 0.4	0.49 ± 0.12
Au-7	7.4 ± 0.5	2.3 ± 0.3	0.311 ± 0.046
Au-5	5.4 ± 0.4	1.7 ± 0.4	0.315 ± 0.078
Au-4	3.8 ± 0.3	1.6 ± 0.4	0.42 ± 0.12

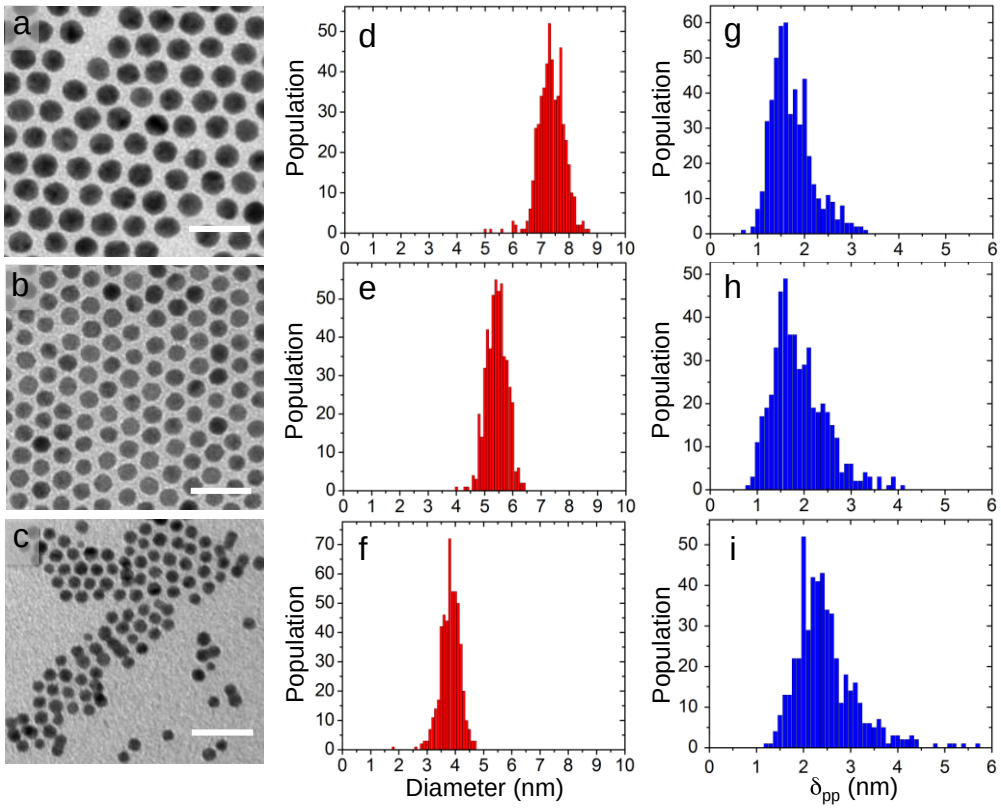

Figure 2. (a-c) TEM images and (d-f) size distribution histograms of Au NCs issued from samples Au-7, Au-5 and Au-4, from top to bottom. (g-i) Histograms of the border-to-border interparticle distance, δ_{pp}, determined by TEM analysis. The scale bar is 20 nm.

b. UV-visible absorption measurements

The UV-visible absorption measurements presented here were performed using a Varian Cary 5000 double monochromator recording spectrophotometer. To perform measurements in transmission geometry at various angles of incidence, the spectrophotometer was equipped with a Harrick Scientific (Pleasantville, NY) variable angle transmission accessory (VATA), which has been specially designed for transmission studies of samples up to 3 mm thick. The VATA allows a given sample and a blank, which should match the former in both thickness and refractive index, to be placed in the light beam at the same angle of incidence, but in the opposite orientation, in order to avoid any misalignment of the detected beam that could affect the measured transmittance. A Glan-Taylor polarizer was also used in all our

measurements to polarize the light parallel to the plane of incidence. Under such a configuration, information on the optical anisotropy of the sample can interestingly be achieved by considering the fact that the electric field is then projected in both perpendicular and parallel directions to the 2D assembly of nanocrystals.

c. Discrete dipole approximation method

The discrete dipole approximation (DDA) method[16, 17] is used to simulate the optical response of the NP assemblies. The DDA is a flexible and powerful method widely used to simulate the scattering and absorption by nanometer-sized targets of chosen geometry and dielectric properties.[17-28] The principle and accuracy of the DDA method are described elsewhere.[29] In this work, the free software 'DDSCAT 7.0' is used to carry out the DDA calculations.[30] As illustrated in the inset of Figure 3, the 2D nanocrystal assembly is modeled as a planar hexagonal arrangement of 91 regularly spaced and equally sized spheres. The relevance of using this DDA target was already discussed in previous works.[11, 12] For these calculations, the refractive index of the surrounding medium is set to be that of dodecanethiol (n = 1.46) which is used as coating agent to passivate the Ag and Au nanospheres. To account for the finite size effects, the bulk dielectric functions of Ag and Au, as taken from Palik's handbook,[31] are size-corrected following the procedure described elsewhere.[32, 33] The DDA absorption spectra of Ag and Au nanospheres films are calculated for various incidence angles ranging from 0° to 60°.

RESULTS AND DISCUSSION

Experiments and calculated optical properties are compared for three different NC sizes (7 nm, 5 nm and 4 nm). The use of dodecanethiol molecules as coating agent makes the interparticle distance in the assembly to be around 2 nm. The absorption spectra of the 2D assemblies of nanocrystals, deposited on glass wafer substrate, were recorded at various incidence angles ranging from 0^o to 60^o. Graphs in Figure 3a-c show the SPR absorption spectra of 2D assemblies composed of Ag NCs issued from samples Ag-7, Ag-5 and Ag-4. For sample Ag-7 (Figure 3a), the absorption spectra exhibit an intense absorption band around 478 nm (2.59 eV) corresponding to the in-plane (longitudinal) SPR mode. On increasing the incidence angle, the maximum wavelength of the SPR band remains unchanged while a shoulder grows up from its low-wavelength side, at around 376 nm (3.30 eV). The presence of an isosbestic point at 388 nm (3.20 eV) underlies the mutual contributions of the transverse and longitudinal SPR modes in the measured absorption band. Graphs in Figure 3d-f show the DDA absorption spectra calculated to simulate the 2D ordered assembly of Ag spheres at various incidence angles and for different diameters, while fixing the border-to-border interparticle distance to $\delta_{pp} = 2$ nm, for coherence with the experimental data. In the assembly of 7 nm spheres, the longitudinal SPR peak is centered at 460 nm (2.70 eV) and one still distinctly observes an isosbestic point on increasing the incidence angle, at 400 nm (3.10 eV). The transverse SPR mode is centered at 364 nm (3.41 eV) and progressively grows up by increasing the incidence angle. Experimental and simulated SPR spectra exhibit similar features and are therefore in good qualitative agreement. Note that a broadening of the SPR band is observed in the experimental spectra compared to the calculated ones. This broadening mostly originates from the size and interparticle distributions of the nanocrystals used to produce the 2D assemblies (Table 1).

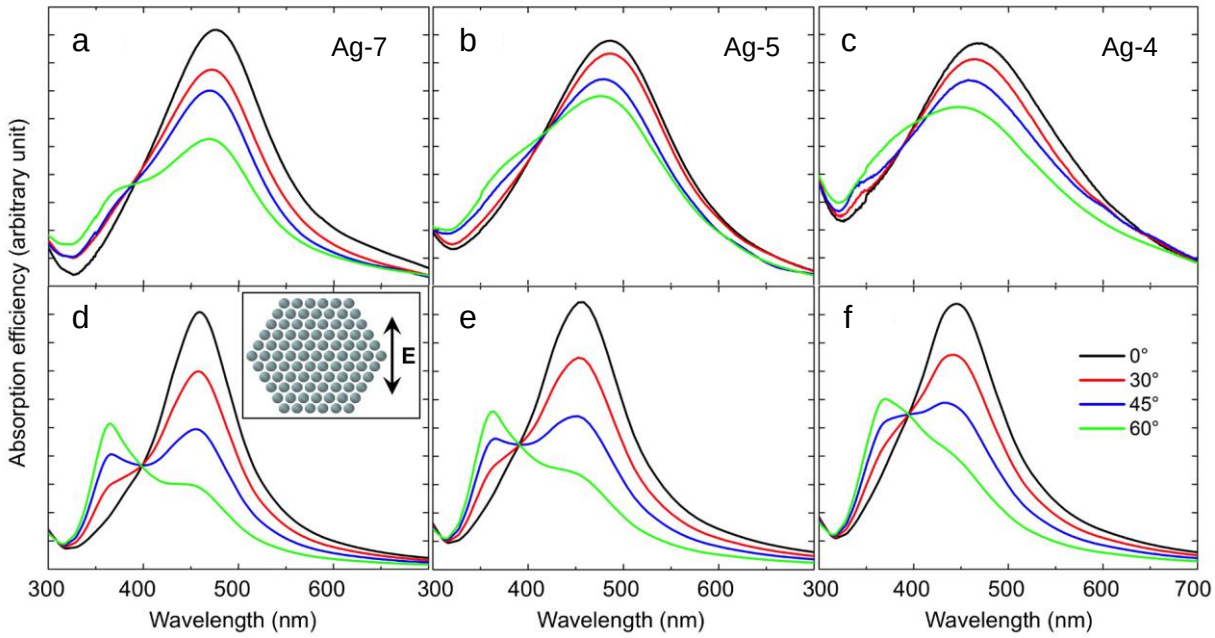

Figure 3. Measured absorption spectra of 2D assemblies composed of Ag NCs issued from samples (a) Ag-7, (b) Ag-5, (c) Ag-4, for different incidence angles (black-0°, red-30°, blue-45°, and green-60°). DDA absorption spectra simulating the optical response of a 2D assembly of Ag nanospheres with different diameters: (d) D = 7 nm, (e) D = 5 nm, and (f) D = 4 nm. The interparticle distance is set to the experimental value ($_{pp}$ = 2 nm) and the refractive index of the host dielectric medium is fixed to that of dodecanethiol (n = 1.46). Inset: Schematic representation at normal incidence (0°) of the DDA target designed as a 2D hexagonal system of N = 91 equally sized nanospheres.

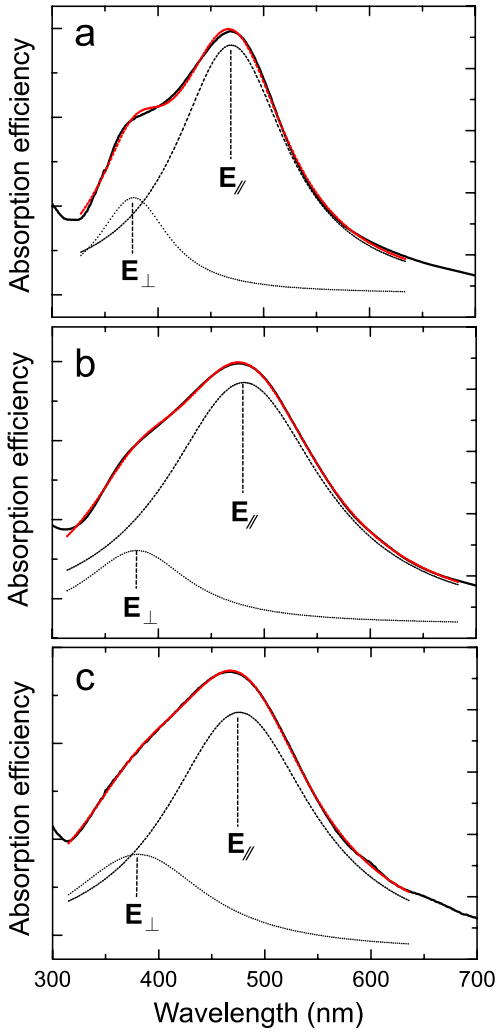

Figure 4. Deconvolution of the longitudinal and transverse SPR modes (dotted curves) achieved for three different samples: (a) Ag-7, (b) Ag-5, and (c) Ag-4. The experimental absorption spectra (red curve) were recorded fixing the incidence angle to 60°.

To go further in the examination of the spectra and taking advantage from the presence of the aforementioned isosbestic point, we quantitatively assessed the longitudinal and transverse energy modes. In this aim, we fitted the structured SPR absorption band using two component bands with a lorentzian profile. Figure 4 shows the deconvolution of the longitudinal and transverse SPR contributions in the absorption spectra of three different samples recorded using an incidence angle of 60°. In parallel, Table 2 compares for all samples the longitudinal and transverse SPR mode energies as deduced from such a deconvolution of the structured band in both experimental and measured absorption spectra. Concerning the sample Ag-7, the mismatch $\Delta E_{//}$ between the measured and calculated

longitudinal SPR mode energies does not exceed 0.06 eV and $\Delta E_{\perp}$ = 0.10 eV for the transverse mode. It should also be noticed that the SPR bands in the calculated spectrum exhibit a slight but systematic blue-shift as compared to the experimental ones. This behavior primarily originates from the discrepancy between the dielectric constants of the real system (metal NCs + host medium) and those used in the DDA calculations where, in particular, the substrate was not taken into account. Moreover, in the samples, the structural parameters such as the interparticle spacing and the NC size are dispersed (see uncertainties in Table 1) around average values that were considered in the simulations.

Table 2. Comparison of the experimental longitudinal ($E_{//}$) and transverse ($E_{\perp}$) SPR mode energies to those issued from the DDA calculated spectra.

SPR energy	**Ag-7**	**Ag-5**	**Ag-4**	**Au-7**	**Au-5**	**Au-4**
$E_{//}^{exp}$ (eV)	2.64	2.59	2.61	2.20	2.20	2.25
$E_{//}^{DDA}$ (eV)	2.70	2.73	2.77	2.38	2.36	2.38
$E_{\perp}^{exp}$ (eV)	3.31	3.30	3.27	NA	NA	NA
$E_{\perp}^{DDA}$ (eV)	3.41	3.40	3.35	NA	NA	NA

Note: "NA" means "not available"

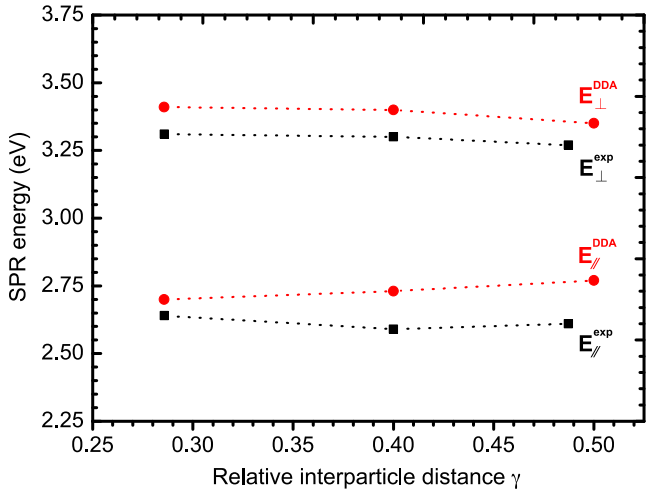

Figure 5. Experimental (black squares) and calculated (red dots) energies of the longitudinal ($E_{//}$) and transverse ($E_{\perp}$) SPR modes in 2D assemblies of Ag NCs plotted *versus* the relative interparticle distance, $\gamma = \delta_{pp} / \langle D \rangle$ characterizing the samples Ag-7, Ag-5 and Ag-4. For clarity, error bars are not shown on the graph.

On decreasing the NC size, one observes the broadening of the SPR absorption band in both experimental and simulated spectra. This effect related to the well-known 1/*D*-size dependence of the SPR damping time[32] appears to be more pronounced in the experimental spectra. This behavior probably results from the decrease in the van der Waals interactions between NCs for decreasing the NC size and, consequently, the worst capacity of nanocrystals to closely self-assemble. The distributions in both NC size and interparticle distance may also contribute to the broadening of the SPR bands, thus favoring the convolution of the two SPR modes. Figure 5 illustrates the variation on the relative interparticle distance of the longitudinal and transverse SPR mode energies as deduced for 2D assemblies of Ag NCs from both experimental and DDA absorption spectra. The overestimation of around 0.10 eV of the calculated energies with respect to the experimental ones is likely to arise from not taking into account the substrate when designing the DDA target used in our calculations. Moreover, the SPR characteristics of dodecanethiol molecules capped Ag NCs are also sensitive to the coating agent. The ligands-metal chemical interactions affect the coherent oscillation of conduction electrons within the nanocrystals[33-35] by inducing an additional "interface" damping of the electron oscillations, thus modifying the effective refractive index at the near-field of the nanocrystals. As a matter of fact, due to these chemical interactions, a lowered electron conductivity in the outermost atomic Ag layer was invoked to explain the red-shift of the SPR band observed for decreasing the Ag NC diameter from 12 to 2 nm.[36] Such lowering of the electron conductivity originating from the interactions of the NCs with the capping molecules was not taken into account in the DDA simulations presented in this work. In spite of these approximations, as seen from the values reported in Table 2 and their plots in Figure 5, our experimental assessment of the SPR energies reasonably agrees with the DDA results.

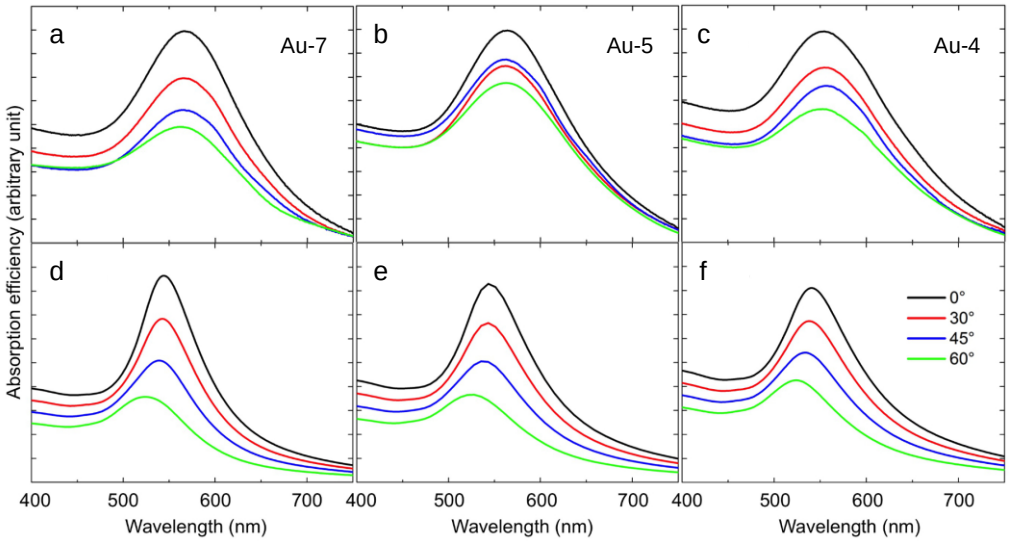

Figure 6. Measured absorption spectra of 2D assemblies composed of Au NCs issued from samples (a) Au-7, (b) Au-5, (c) Au-4. The absorption spectra were recorded using the following incidence angles (from top to bottom in each graph): black-0°, red-30°, blue-45°, and green-60°. Calculated absorption spectra of a 2D assembly of Au nanospheres of different diameters: (e) D = 7 nm, (f) D = 5 nm, and (g) D = 4 nm. The border-to-border interparticle spacing is set to the constant value δ_{pp} = 2 nm, and the refractive index of the dielectric medium surrounding the nanospheres is fixed to that of dodecane (n = 1.46).

Let us go further in this study looking at the optical response of 2D assemblies of Au NCs. Graphs in Figure 6a-c show the SPR absorption spectra of such Au NCs assemblies on a glass wafer. These absorption spectra are dominated in the visible domain by an intense band corresponding to the collective SPR of the system. Conversely to the observations described above for Ag NCs, the longitudinal SPR peak remains unchanged for any NC sizes and no residual peak is observed on increasing the incidence angle of the irradiation light. No splitting between the longitudinal and transverse collective SPR modes is detectable. Even though the size distributions of Au NCs are narrower than those of Ag NCs, the SPR band in the experimental spectra is much broadened than the calculated ones presented in Figure 6d-f. The spectra calculated for nanosphere diameters of 4-nm, 5-nm and 7-nm, while still setting the interparticle distance to 2-nm, show a blue-shift of the SPR band on increasing the incidence angle. In a previous work,[12] the SPR band profile (amplitude and position) of a 2D assembly of 5-nm Au NCs was observed to change on varying the interparticle distance. This change in the SPR band profile was attributed to the increasing contribution in the absorption

spectrum of the transverse SPR mode on progressively rotating the planar array from in-plane to out-of-plane configuration. Probable reasons for not observing similar change in the recorded SPR band profile of 2D assemblies of Au NCs relate, as mentioned above, to the significant SPR broadening as well as to the technical limitation in varying the incidence angle, knowing that this latter cannot exceed 60° with our setup. Due to this lack in completely reproducing the same configuration in the experiments as compared to the simulated one, measured and calculated absorption spectra of 2D assemblies of Au NCs do not exhibit the same trends on increasing the incidence angle. In particular, the slight blue-shift of the SPR band observed in the simulation for increasing the incidence angle is not detectable in the recorded absorption spectra.

CONCLUSION

Two different chemical routes have been applied to synthesize colloidal Ag and Au NCs whose average size ranges between 4 and 7 nm. After deposition onto a glass wafer, these nanocrystals self-organize in thin layer films where interparticle spacing is short enough to promote near-field coupling between nanocrystals and the emergence of collective optical properties. The UV-visible absorption spectra of 2D assemblies of Ag and Au NCs are recorded at various incidence angles. In 2D assemblies of Ag NCs, due to the optical anisotropy of the system, the SPR absorption band splits in two contributions, namely, the longitudinal and transverse SPR modes. For Ag NCs, these features are satisfactorily reproduced in the absorption spectra calculated using the DDA method. At variance, in similar assemblies of Au NCs, only one SPR band is observed whatever the incidence angle and NC size. The transverse SPR mode is difficult to observe experimentally, partially due to the strong ligands-metal interactions that lower the electron conductivity in the outermost metal atomic layer of the nanocrystals. These findings allow further using the DDA method to simulate more complex systems, especially binary and/or bimetallic NP superlattices that are made of building blocks of two different compositions and/or sizes.

ACKNOWLEDGEMENTS

Thanks to N. Goubet for providing the colloidal solutions used to prepare the 2D assemblies of Au nanocrystals and for fruitful discussion. This research has been supported

by the advanced grant of the European Research Council under n° 267129. J. J. W. thanks the China Scholarship Council for financial support.

REFERENCES

(1) Mirkin, C. A.; Letsinger, R. L.; Mucic, R. C.; Storhoff, J. J. *Nature* **1996**, 382, 607-609.

(2) Korgel, B. A.; Fullam, S.; Connolly, S.; Fitzmaurice, D. *J. Phys. Chem. B* **1998**, 102, 8379-8388.

(3) Song, R. -Q.; Cölfen, H. *Adv. Mater***. 2010**, 22,1301-1330.

(4) Liao, C.-W.; Lin, Y.-S.; Chanda, K.; Song, Y.-F.; Huang, M. H. *J. Am. Chem. Soc.* **2013**, 135, 2684-2693.

(5) Taleb, A.; Russier, V.; Courty, A.; Pileni, M. P. *Phys. Rev. B* **1999**, 59, 13350.

(6) Chen, C. F.; Tzeng, S. D.; Chen, H. Y.; Lin, K. J.; Gwo, S. *J. Am. Chem. Soc*. **2008**, 130, 824-826.

(7) Park, S. Y.; Lytton-Jean, A. K. R.; Lee, B.; Weigand, S.; Schatz, G. C.; Mirkin, C. A. *Nature* **2008**, 451, 553-556.

(8) Corricelli, M.; Depalo, N.; Fanizza, E.; Altamura, D.; Giannini, C.; Siliqi, D.; Di Mundo, R.; Palumbo, F.; Kravets, V. G.; Grigorenko, A. N.; Agostiano, A.; Striccoli, M.; Curri, M. L. *J. Phys. Chem. C* **2014**, 118, 7579-7590.

(9) Liu, Y.; Begin-Colin, S.; Pichon, B. P.; Leuvrey, C.; Ihiawakrim, D.; Rastei, M.; Schmerber, G.; Vomir, M.; Bigot, J. Y. *Nanoscale* **2014,** 6, 12080-12088.

(10) Pinna, N.; Maillard, M.; Courty, A.; Russier, V.; Pileni, M. P. *Phys. Rev. B* **2002**, 66, 045415.

(11) Portalès, H.; Pinna, N.; Pileni, M. P. *J. Phys. Chem. A***. 2009**, 113, 4094-4099.

(12) Yang, P.; Portalès, H.; Pileni, M. P. *Phys. Rev. B* **2010**, 81, 205405.

(13) Pileni, M. P. *J. Phys. Chem*. **1993**, 97, 6961-6973.

(14) Taleb, A.; Petit, C.; Pileni, M. P. *Chem. Mater*. **1997**, 9, 950-959.

(15) Goubet, N.; Richardi, J.; Albouy, P.-A.; Pileni, M. P. *Adv. Funct. Mater*. **2011**, 21, 2693-2704.

(16) Purcell, E. M.; Pennypacker, C. R. *Astrophys. J.* **1973**, 186, 705-714.

(17) Draine, B. T.; Flatau, P. J. *J. Opt. Soc. Am. A*. **1994**, 11, 1491-1499.

(18) Zhao, J.; Pinchuk, A. O.; McMahon, J. M.; Li, S. Z.; Alisman, L. K.; Atkinson, A. L.; Schatz, G. C. *Acc. Chem. Res.* **2008**, 41, 1710-1720.

(19) Yang, P.; Portalès, H.; Pileni, M. P. *J. Phys. Chem. C* **2009**, 113, 11597-11604.

(20) Zhu, J.; Li, F. K. *Eur. Phys. J. B* **2011**, 80, 83-87.

(21) D'Agostino, S.; Sala, F. D. *J. Phys. Chem. C* **2011**, 115, 11934-11940.

(22) Yang, P.; Portalès, H.; Pileni, M. P. *J. Chem. Phys*. **2011**, 134, 024507.

(23) Alsawafta, M.; Wahbeh, M.; Truong, V. V. *J. Nanomater*. **2012,** Vol. 2012, 283230.

(24) Blaber, M. G.; Henry, A. I.; Bingham, J. M.; Schatz, G. C.; Van Duyne, R. P. *J. Phys. Chem. C* **2012**, 116, 393-403.

(25) Xu, X. B.; Yi, Z.; Li, X. B.; Wang, Y. Y.; Geng, X.; Luo, J. S.; Luo, B. C.; Yi, Y. G.; Tang, Y. *J. J. Phys. Chem. C* **2012**, 116, 24046-24053.

(26) Xu, X.-B.; Yi, Z.; Li, X.-B.; Wang, Y.-Y.; Liu, J.-P.; Luo, J.-S.; Luo, B.-C.; Yi, Y.-G.; Tang, Y.-J. *J. Phys. Chem. C* **2013**, 117, 17748-17756.

(27) Lermé, J.; Bonnet, C.; Broyer, M.; Cottancin, E.; Manchon, D.; Pellarin, M. *J. Phys. Chem. C* **2013**, 117, 6383-6398.

(28) Lyamkina, A. A.; Moshchenko, S. P. *J. Phys. Chem. C* **2013**, 117, 16564-16570.

(29) Yurkin, M. A.; De Kanter, D.; Hoekstra, A. G. *J. Nanophotonics* **2010**, 4, 041585.

(30) Draine, B. T.; Flatau, P. J., User Guide for the Discrete Dipole Approximation Code 'DDSCAT 7.0'. In **2008**.

(31) Palik, E. D., Handbook of Optical Constants of Solids. Academic Press: New York, 1985.

(32) Hövel, H.; Fritz, S.; Hilger, A.; Kreibig, U.; Vollmer, M. *Phys. Rev. B* **1993**, 48, 18178-18188.

(33) Coronado, E. A.; Schatz, G. C. *J. Chem. Phys*. **2003**, 119, 3926-3934.

(34) Kelly, K. L.; Coronado, E.; Zhao, L. L.; Schatz, G. C. *J. Phys. Chem. B* **2003**, 107, 668-677.

(35) Peng, S.; McMahon, J. M.; Schatz, G. C.; Gray, S. K.; Sun, Y. *Proc. Natl. Acad. Sci.* USA **2010**, 107, 14530-14534.

Chapter 3

Ag Nanocrystals : Effect of Ligands on Plasmonic Properties

3.1 Abstract

In this part, silver nanocrystals (NCs) stabilized using amine terminated coating agents (oleylamines), their size ranging between 2 and 12 nm in diameter, are synthesized by hot injection methods and one-pot method. Their dispersion in size is relatively low (typically below 10%) without the need of post-synthesis size segregation process. Here 2.2-nm nanocrystals are synthesized by adding two coating agents: oleylamine and oleic acid, and then wash away the oleic acid by toluene-ethanol washing cycle with additional oleylamine. Similarly, by using dodecylamine instead of oleylamine, 3 – 7 nm nanocrystals coated with dodecylamine can also obtained with a rather narrow distribution (< 10%). The amine terminated coating agents is replaced by thiol terminated molecules (dodecanethiol or hexadecanethiol) by ligand exchange, allowing the formation of alkanethiols coated Ag colloids. All NCs with various surface coatings are dispersed in toluene.

Regardless of the nature of the coating agent, the surface plasmon resonance (SPR) is red-shifted and the bandwidth is increased with decreasing the NC size. For a given size, the SPR peak of thiol-stabilized NCs is shifted to lower energies compared to that of amine-stabilized NCs. Core-shell theory in this study are used to explain the plasmon divergencies of these nanocrystals with different coating agents and sizes. Furthermore, with thiol-stabilized Ag NCs, the position of the SPR peak was found to be sensitive to the length of the alkyl chains of the coating agent, whereas minor differences is detected for Ag NCs coated with amine-terminated with differing alkyl chain lengths.

3.2 Articles: Ag Nanocrystals : Effect of Ligands on Plasmonic Properties

Ag Nanocrystals: 1. Effect of Ligands on Plasmonic Properties

Jingjing Wei [1,2], Nicolas Schaeffer [1,2], Marie-Paule Pileni[1,2,3] *

1- Sorbonne Universités, UPMC Univ Paris 06, UMR 8233, MONARIS, F-75005, Paris, France

2- CNRS, UMR 8233, MONARIS, F-75005, Paris, France

3- CEA/IRAMIS, CEA Saclay, 91191, Gif-sur-Yvette, France

* Corresponding author: marie-paule.pileni@upmc.fr

Keywords: Ag nanocrystals; SPR; ligand; nanocrystal size

INTRODUCTION

Metallic nanocrystals (NCs) stabilized by a monolayer of organic coating agent have attracted growing interest during the last few decades due to their size- and shape-dependent physical properties, making them potential candidates for the design of new functional materials.[1-3] The main role of the organic layer anchored to metallic core is to avoid coalescence between the NCs in solution and counterbalance the Van der Waals attractive forces. This layer also governs the physical properties of the NCs surface.[1] The coating agent is usually a relatively large organic molecule or polymer bearing one or more anchoring group for bonding onto the surface of the NCs.[4, 5] Functional groups such as thiols, amines, or silanes are routinely used to prepare stable metallic NCs and a handful of efficient synthetic procedures have been developed for the production of NCs. In some cases, the NC size and shape can be controlled through changes in the nature or amount of coating agent. Thus, optimization of the NCs properties in view of specific applications requires careful considerations when choosing the nature of the coating agent.[6]

The optical properties of noble-metal NCs have fascinated scientists because they exhibit a strong surface plasmon resonance (SPR) effect that is characteristic of the size regime at the nanoscale, hence making them potentially interesting units for designing optical devices,[7] or for optical energy transport applications,[8, 9] and surface-enhanced Raman scattering (SERS) spectroscopy.[10-14] This SPR results from the collective resonance oscillation of conduction electrons upon light irradiation.[15-17] As reported previously, the oscillation frequency is dependent on several factors, such as the density of electrons and the shape and size of the charge distribution.[16, 18, 19] Thus, in order to fully understand the optical properties of noble-metal NCs, different parameters must be considered: the type of material, the size and shape of the NCs, the dielectric properties of the solvent, the nature of the stabilizing agent, and the possible inter-particle coupling interactions.[20-23] For example, extinction spectra of gold nanorods exhibit two plasmon bands that correspond to longitudinal and transverse SPR respectively.[21, 24] In the case of spherical NCs, size-dependent surface plasmon resonances have been studied; Peng *et al.* [25] reported a gradual blue-shift of the SPR absorption band when decreasing Ag NCs size down to 12 nm, followed by a strong red-shift when decreasing the size further. In the case of Ag NCs, various reports describe their size- or shape- dependent optical properties. However, only a handful of investigations have included an in-depth study of the influence of the coating agent on these optical properties. [26-29]

Here, we report the synthesis of Ag NCs of various sizes using different coating agents, all the specimens being characterized by a low size distribution (<10%) without the need of size selection process. The optical properties of these Ag NCs dispersed in toluene differing by their sizes or coating agents is studied. For a given coating agent, a size-dependent shift in the SPR occurs. Furthermore, for a given NCs size, the SPR shift is observed to be dependent on the type of coating agent. For NCs coated with alkyl amines (oleylamine or dodecylamine) the alkyl chain length does not affect the position of the SPR peak. However, the chain length has a marked effect on the SPR peak position in the case of alkanethiol coated NCs (dodecanethiol or hexadecanethiol).

MATERIALS AND METHODS

Silver nitrate (99.9%) was purchased from VWR, toluene (98%) from Riedel de Haen, ethanol (99%) from Prolabo, o-dichlorobenzene (99%) from Sigma, oleylamine (70%) from Sigma, and dodecanediol (99%) from Sigma. All reagents were used as received without further purification. The detailed synthesis of Ag NCs can be found in the results part.

Transmission electron microscopy (TEM) images were recorded on a JEOL JEM 1011 (acceleration voltage: 100 kV). Optical absorption measurements were carried out on a Varian Cary 5000 spectrophotometer using 1-mm cuvettes.

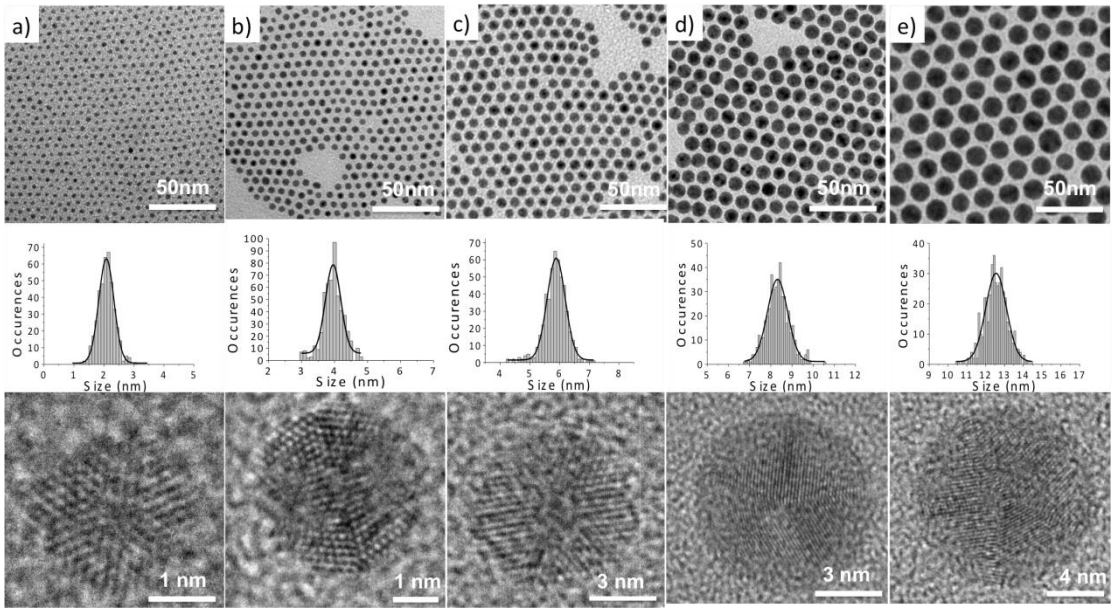

Figure 1. TEM images, size distribution histograms and high-resolution TEM of oleylamine coated silver NCs: a) 2.2 nm b) 4.1 nm c) 5.9 nm d) 8.7 nm e) 12.9 nm.

RESULTS AND DISCUSSION

The synthetic procedure for the preparation of Ag NCs coated with oleylamine (C18-NH_2) and dodecylamine (C12-NH_2) are based on hot-injection method. Briefly, an $AgNO_3$ *o*-dichlorobenzene (DCB) solution mixed with oleylamine or dodecylamine is rapidly injected into a hot dodecanediol DCB solution (180^{o}C) and the mixture was allowed to react for 3 minutes; the solution was then cooled down to room temperature. With oleyamine (C18-NH_2), this procedure produces the size of the Ag NCs can be controlled from 2.2 to 7 nm by

controlling the relative ratio of $AgNO_3$ and oleyamine (Table S1). For larger NC size (8.7nm and 12.9nm) oleylamine coated NCs were prepared following a modified one-pot method as described elsewhere.[30] Hence this procedure permits to control the NC size from 2.2nm to 12.9nm. The TEM images in Figure 1 clearly show that all the NCs, regardless of their size, are well arranged in a two-dimensional hexagonal closed packed array, this is typical of NCs with low size distribution (typically below 10%).[31] Note that these NCs were obtained without any post-synthesis size selection process or size-focusing ripening process. This is, from the best of our knowledge, a new platform of size-controllable synthesis of Ag NCs without a size-focusing process.[32] High-resolution TEM images of the NCs reveal that all NCs are multiply twined particles (MTPs), probably holding icosahedral morphologies, and the same icosahedral crystals were reported by Peng *et al.*[25] When the oleyamine (C18-NH_2) is replaced by dodecylamine (C12-NH_2), which is a similar -NH_2 terminated coating agent with a shorter alkyl chain, stable monodisperse Ag NCs coated by dodecylamine is produced, as shown in Figure 2a and S2. In this case, the size of the Ag NCs can be controlled from 3.0 to 6.3 nm. Again, the size distribution of these dodecylamine coated NCs are kept below 10% without the need of size segregation procedures.

This hot injection process cannot be used for the preparation of alkanethiol coated Ag NCs since $AgNO_3$ cannot be dissolved in DCB in the presence of –SH terminated coating agent. When a mixture of $AgNO_3$ and dodecanethiol is injected into hot solutions containing polyols, only polydisperse small NCs are produced. Hence, in order to obtain Ag NCs of similar sizes and coated with alkanethiol, a ligand exchange procedure is carried out. Thiol coated Ag NCs are prepared from the pre-formed oleylamine coated NCs described above and a ligand exchange procedure. A small amount of dodecanethiol (20μl dodecanethiol per 10mg Ag NCs) is added to the suspension of Ag NCs and the mixture is kept under vigorous stirring for 1 hour. Then, ethanol is added to the solution, inducing flocculation. The excess dodecanethiol is removed from the supernatant and the NCs are re-dispersed in toluene. The sizes and size distributions of the various NCs prepared throughout this study are listed in Table S1(Supporting Information). The efficiency of the ligand exchange procedure was assessed by tracking by ICP-AES the relative amounts of Ag, N, and S in the preparation before and after exchanging the ligands. The results shown in Table 1 show that only traces of N could be detected after this procedure, inferring than at least 80% of the amine-terminated ligand was exchanged for the thiol-containing compound. Figure 2b and S3 show TEM images of the Ag NCs coated with dodecanethiol, and their size can be controlled from 2.2

nm to 6.0 nm. Figure 2c and S4 show TEM images of Ag NCs coated with hexadecanethiol prepared in a similar manner. It is worth noting here that the size distribution of all the NCs after ligand exchange is below 10% except in the case of 2.2 nm NCs coated with dodecanethiol (see Table S1 and Figure S3, Supporting information). Thus 2D hexagonal structures can be observed in most TEM images.

Table 1. 6-nm Ag Nanocrystals Coated with Oleylamine Were Analyzed by ICP-AES (Inductively Coupled Plasma-Atomic Emission Spectroscopy) before and after Ligand Exchange.

Elements	N(w/w)	S(w/w)	Ag (w/w)
Before ligand exchange	0.44%	NA[a]	70.96%
After ligand exchange	<0.10%	2.7%	90.09%

NA_a refers to not available

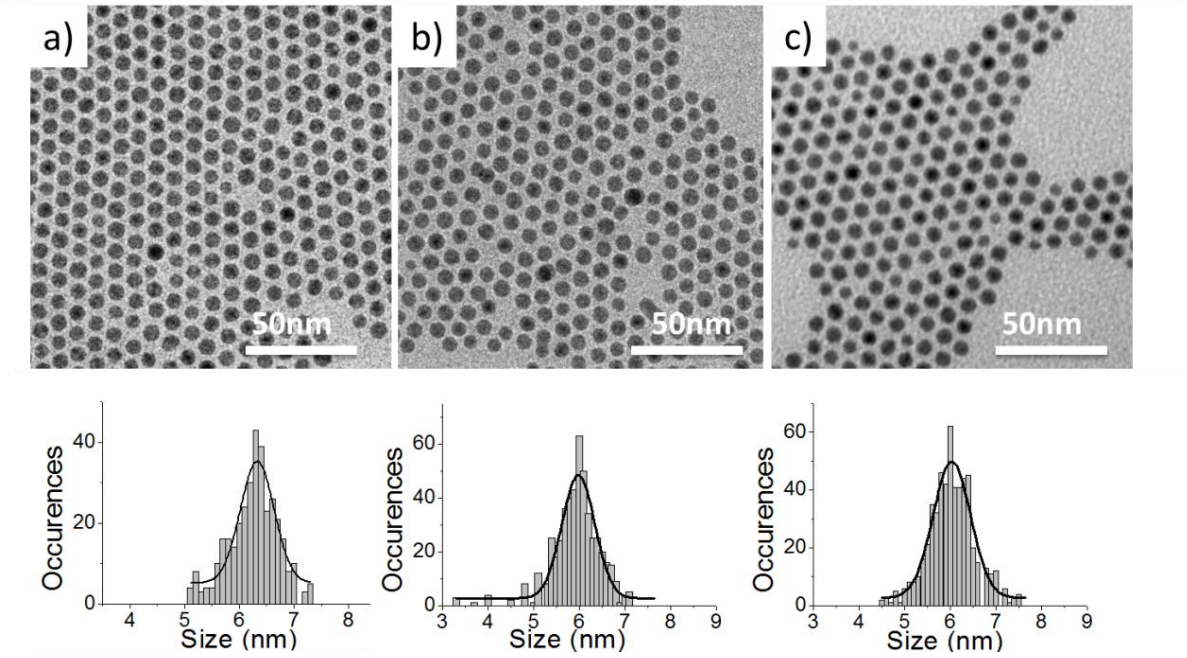

Figure 2. TEM images of silver NCs (a) 6.3 nm NCs coated with dodecylamine (b) 6.0 nm NCs coated with dodecanethiol (c) 6.0 nm NCs coated with hexadeanethiol.

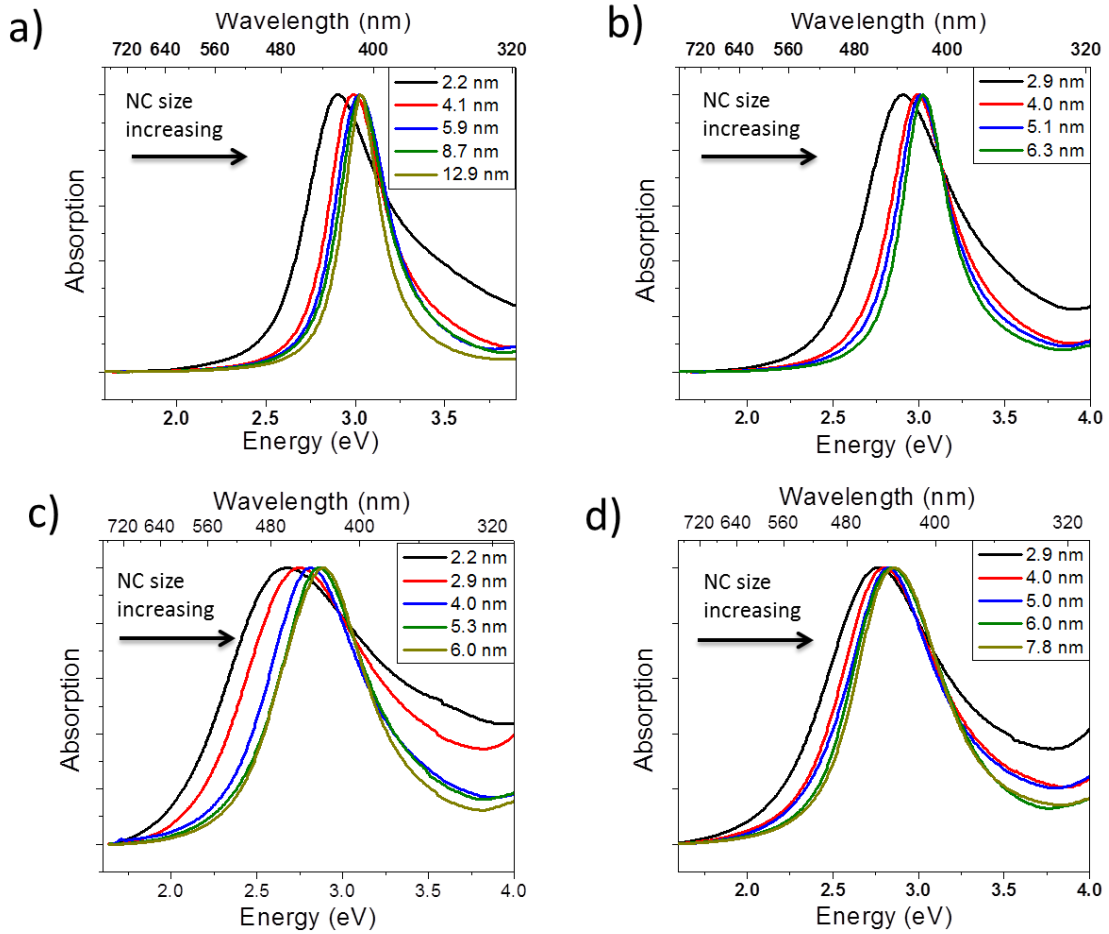

Figure 3. Absorption spectra (normalized) of NCs of varying sizes coated with a) oleylamine, b) dodecylamine, c) dodecanethiol and d) hexadecanethiol.

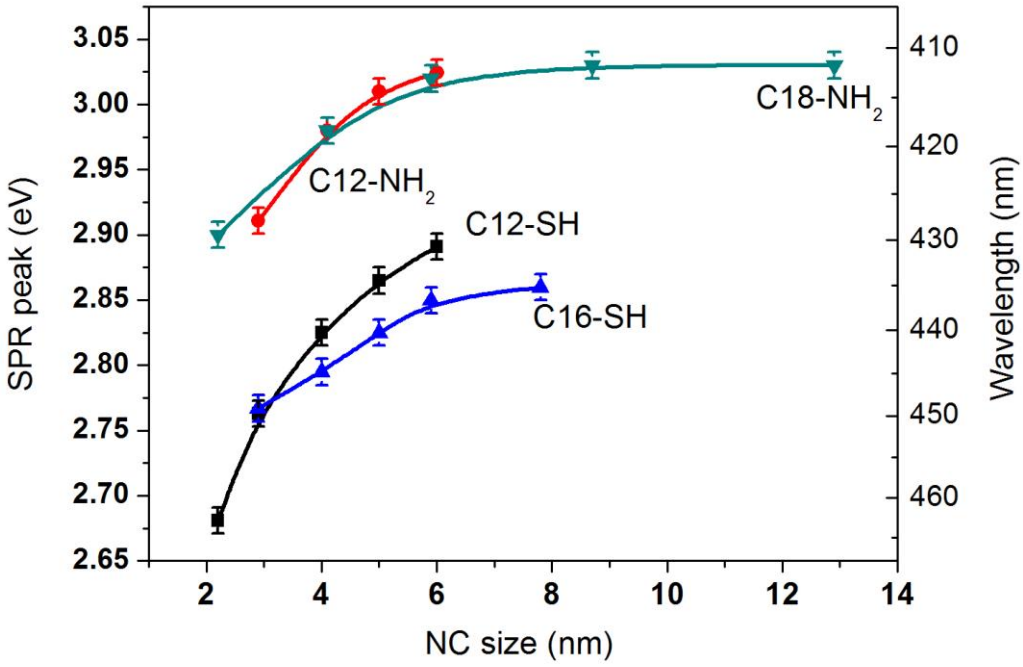

Figure 4. Maximum SPR peak value as a function of the diameter of the NCs size for the dodecanethiol coated (black), dodecylamine coated (red), hexadeanethiol coated (blue) and oleylamine (green) coated Ag NCs. The error bars in the measurements are ±0.02 eV.

The Ag NCs described above are dispersed in toluene and their UV-visible absorption spectra are depicted in Figure 3. A well-defined SPR band as shown in Figure 3a characterizes the normalized optical responses of colloidal Ag NCs coated with oleylamine. With the increase of the NC size, the SPR band shifts to smaller wavelength and higher energies. The same measurements are carried out on colloidal solutions of Ag NCs coated with the other three types of ligands (in Figure 3b - 3d) and dispersed in toluene. A similar trend is observed for these specimens: The SPR band is blue-shifted when increasing the NCs size. This is observed for any coating agents used. Figure 4 depicts a plot of the SPR peak position as a function of the NC size for the four types of coating agents used. For NCs coated with oleylamine (C18-NH_2), the SPR band position increases rapidly when the size of the NCs increases from 2.2 nm to 5.9 nm, and this trend is more profound within smaller sized nanocrystals. This result is in agreement with the previous report on the size-dependent optical properties of Ag NCs, and can be explained by the plasmonic "core/shell" theory.[25] Since the NCs are coated with organic molecules, the electron conductivity becomes lower in the outer Ag layer chemically bound to the coating agents than in the inner core. With the

increase of the nanocrystal size, the relative influence of the outer Ag surface decreases and the global conductivity of the nanocrystal increases, eventually inducing a blue-shift of the SPR band.

In a similar manner, the NCs coated with other ligands (dodecylamine, dodecanethiol and hexadecanethiol) show the same size-dependent SPR band shift trend, within the size range of the nanocrystals that are being studied in this work.

The SPR band is located at much lower energies for alkanethiols (Cx-SH) coated NCs (black and blue curves in Figure 4) than for NCs coated with alkylamine (Cx-NH_2), (red and green curves). The thiols head groups (-SH) are known to bond stronger than amine-terminated ligands onto metallic surfaces.[33] This also explains the possibility of efficient ligand exchange from amines to thiols, and not the other way around.[34] A combined coating agent nature and length dependence on the SPR band is also observed. For example, for 6-nm alkylamine (Cx-NH_2) coated NCs, the SPR band shows no significant shift when changing the alkyl chain length from C12 to C18 (3.02eV and 3.01eV, respectively). However, the SPR band position differs significantly between alkanethiol (Cx-SH) coated NCs of different alkyl chain lengths (2.89eV for C12 and 2.85 eV for C16). This shows that when the chemical bond between the NCs and the ligand is relatively weak, as it is for amine-terminated ligands, variations in the ligand chain length do not affect the SPR band position. However, the energy of the SPR band is clearly dependent on the alkyl chain length in the case of thiol terminated ligands. This is probably due to the stronger bonding between ligand and Ag NC surface.

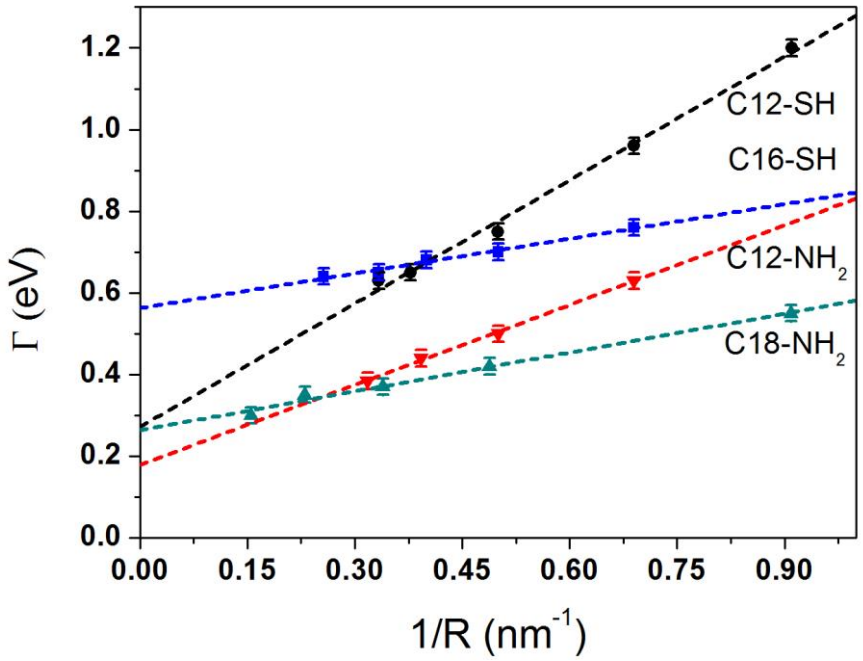

Figure 5. Full width at half-maximum (eV) of SPR band with various NC sizes as a function of the reciprocal effective radius of oleylamine (green), dodecylamine (red), dodecanethiol (black) and hexadecanethiol (blue) coated NCs.

Table 2. Γ_0 values and slopes (gv_F) extracted from Figure 5

Coating agent	C18-NH_2	C12-NH_2	C12-SH	C16-SH
Γ_0 (eV)	0.26	0.18	0.27	0.56
t (fs)	15.9	23.0	15.3	7.3
gv_F (eV nm)	0.32	0.65	1.0	0.28

In addition to this variable dependency of the SPR band energy, it is worth noticing that the shape of the SPR band is affected by many factors, such as the above-mentioned NC size, the local variation of the composition and structure of the NCs, and the modification of their electronic properties due to interaction with the surrounding matrix, known as chemical damping.[23] In this work, we focus on the effect of NC size and the coating agent, while giving a similar size distribution. Within a given NC size, after ligand exchange by alkanethiols, the SPR bands become broader compared to the sharp bands observed for alkylamine coated NCs. Note that no aggregation is observed either before or after the ligand exchange process. These

variations in the profile of the SPR bands are thought to stem from the strong interactions between the metal surface and the alkanethiol, as evident from the dampening effect observed on the SPR bands. Figure 3c (C12-SH coated NCs) shows that when increasing the NC size, the SPR bandwidth decreases. The same trend is also observed for the SPR bands of the NCs coated with other ligands (in Figure 3a, 3b and 3d). Quantitative interpretation of these data requires precise quantum mechanical calculation of the surface-induced broadening effects going beyond the quantum-box model.[35-37] Hence, the bulk-like Drude-type expression with an additional surface contribution to the electronic scattering rate, are used to express the data.[38-40] The bandwidth variations with the size can be described as follows: [38, 41, 42]

$$\Gamma = \Gamma_0 + g\frac{v_F}{R} \qquad (1)$$

where Γ_0 the contribution due to the intrinsic electron scattering in the particle, $g(\upsilon_F/R)$ a consequence of electron-surface interaction in spherical particles, g the surface factor in the range of 0 to 1, υ_F the Fermi velocity and, R to the particle radius determined from the TEM images. Note that this linear trend is a rough approximation. In fact, Γ_0 is size dependent through electron-electron, electron-phonon couplings and dielectric function. However Figure 5 shows the measured spectra fitted using equation (1) and indicates that, in such size range (2 nm – 12 nm), Γ_0 can be considered to be constant. A linear fit of the data presented in Figure 5 yields a varied Γ_0 values (shown in Table 1), which implies that the intrinsic electronic dephasing time of Ag NCs, $t = h/\Gamma_0$, (h being the Planck's constant), is particularly dependent on their surface coating agent. In the case of alkylamine coated NCs, namely C_{18}-NH_2 and C_{12}-NH_2, the intrinsic electronic dephasing times are 15.9 and 23.0 fs, respectively, indicating that a shorter chain length (C_{12}) give rise to a longer dephasing time. In addition, this trend is also observed in Ag NCs anchored with alkanethiols (Figure 5 and Table 1). Furthermore, the C_{12}-SH coated NCs gives much shorter dephasing time than the C_{12}-NH_2 coated ones, confirming that the surface-ligand interactions can play a role in determining the dephasing time of the small Ag NCs. However, previous report [40,41] show that Γ_0 has a range from 0.06 eV (69 fs) to 0.23 eV (18 fs) for silver, which was estimated from the refractive index measurements in bulk silver. Indeed, the Γ_0 deduced from Ag NCs with size larger than 10 nm in diameter is consistent with value from bulk Ag. Here, Γ_0 varied, and is particularly dependent on the coating agent, probably because the NCs used in our work are all smaller than 12 nm in diameter. For small NCs, the specific area is considerably larger and the

interplay between the surface atoms and the ligand is more pronounced, which is confirmed by the reversed size-dependence in SPR band peak, as discussed above. According to the "core/shell" plasmonic model,[25] the "core" part atoms are commonly considered as in bulk state, whereas the "shell" part constituted with the surface atoms and the bonded ligands. Here, we found that in the case of weak surface coating with amine-terminated ligands, namely C_{18}-NH_2 and C_{12}-NH_2, the Γ_0 values are 0.26 and 0.18 eV, respectively, falling in or approaching the range estimated from the bulk silver (0.06-0.23eV). While for Ag NCs with strong thiol-terminated ligand, the Γ_0 values are typically higher than the upper limit of bulk silver (0.23 eV). This unusual Γ_0 value is probably due to the presence of strong interactions between surface atoms and ligands, and is much more pronounced in longer chain length ligand, C_{16}-SH.

As shown in Table 1 and Figure 5, the slope of the linear fittings, which is correlated with the surface factor g, shows various values for the different surface coatings of Ag NCs. In the case of C_{12}-SH and C_{12}-NH_2 the g values are larger than that of C_{18}-NH_2 and C_{16}-SH, suggesting additional contribution of ligand-surface interaction takes place in this size range (2-12 nm). However, it is still an open question on how to predict the g value, and it should be noted that due to the different approximations used for obtaining an analytical g expression, different theoretical values were reported. [38, 39]

CONCLUSIONS

Here we describe synthetic procedures based on hot injection methods for the production Ag with very low size distribution, in the 2 – 12 nm size range coated with amine-containing organic molecules. Their size distribution is kept below 10% without the need of size selection process. The coating layer of these NCs is replaced by thiol-terminated coating agent via ligand exchange procedures. The optical properties of these different specimens reveal that the SPR band position is not only dependent on the NCs size, but also on the nature of the coating agent; would it be through the influence of the head-group (amine or thiol) or the chain length.

ACKNOWLEDGMENTS

The authors would like to thank Dr. L.Douillard and Dr J.Romann for fruitful discussions. An Advanced Grant of the European Research Council under Grant 267129 supports the research leading to these results. J. J. W. thanks the China Scholarship Council for financial support.

REFERENCES

1. Yin, Y.; Alivisatos, A. P., Colloidal nanocrystal synthesis and the organic-inorganic interface. *Nature* **2005**, *437* (7059), 664-670.
2. Alivisatos, A. P., NCs: Building blocks for modern materials design. *Endeavour* **1997**, *21* (2), 56-60.
3. El-Sayed, M. A., Small Is Different: Shape-, Size-, and Composition-Dependent Properties of Some Colloidal Semiconductor NCs. *Accounts of Chemical Research* **2004**, *37* (5), 326-333.
4. Pradhan, N.; Reifsnyder, D.; Xie, R.; Aldana, J.; Peng, X., Surface Ligand Dynamics in Growth of NCs. *Journal of the American Chemical Society* **2007**, *129* (30), 9500-9509.
5. Murray, C. B.; Kagan, C. R.; Bawendi, M. G., Synthesis and characterization of monodisperse NCs and close-packed nanocrystal assemblies. *Annual Review of Materials Science* **2000**, *30*, 545-610.
6. Ong, W.-L.; Rupich, S. M.; Talapin, D. V.; McGaughey, A. J. H.; Malen, J. A., Surface chemistry mediates thermal transport in three-dimensional nanocrystal arrays. *Nat Mater* **2013**, *12* (5), 410-415.
7. Dirix, Y.; Bastiaansen, C.; Caseri, W.; Smith, P., Oriented Pearl-Necklace Arrays of Metallic Nanoparticles in Polymers: A New Route Toward Polarization-Dependent Color Filters. *Adv. Mater.* **1999**, *11* (3), 223-227.
8. Krenn, J. R.; Dereux, A.; Weeber, J. C.; Bourillot, E.; Lacroute, Y.; Goudonnet, J. P.; Schider, G.; Gotschy, W.; Leitner, A.; Aussenegg, F. R.; Girard, C., Squeezing the Optical Near-Field Zone by Plasmon Coupling of Metallic Nanoparticles. *Physical Review Letters* **1999**, *82* (12), 2590-2593.
9. Pendry, J., Playing Tricks with Light. *Science* **1999**, *285* (5434), 1687-1688.
10. Shalaev, V. M., Transforming light. *Science* **2008**,*322* (5900), 384-386.

11. Wertime, T. A., BEGINNINGS OF METALLURGY - NEW LOOK. *Science* **1973**,*182* (4115), 875-887.
12. Rycenga, M.; Cobley, C. M.; Zeng, J.; Li, W.; Moran, C. H.; Zhang, Q.; Qin, D.; Xia, Y., Controlling the Synthesis and Assembly of Silver Nanostructures for Plasmonic Applications. *Chemical Reviews* **2011**,*111* (6), 3669-3712.
13. Lal, S.; Link, S.; Halas, N. J., Nano-optics from sensing to waveguiding. *Nature Photonics* **2007**,*1* (11), 641-648.
14. Jain, P. K.; Lee, K. S.; El-Sayed, I. H.; El-Sayed, M. A., Calculated absorption and scattering properties of gold nanoparticles of different size, shape, and composition: Applications in biological imaging and biomedicine. *J. Phys. Chem. B* **2006**,*110* (14), 7238-7248.
15. Mie, G., Articles on the optical characteristics of turbid tubes, especially colloidal metal solutions. *Annalen Der Physik* **1908**,*25* (3), 377-445.
16. Kelly, K. L.; Coronado, E.; Zhao, L. L.; Schatz, G. C., The optical properties of metal nanoparticles: The influence of size, shape, and dielectric environment. *J. Phys. Chem. B* **2003**,107 (3), 668-677.
17. Salzemann, C.; Brioude, A.; Pileni, M. P., Tuning of copper NCs optical properties with their shapes. J. Phys. Chem. B 2006,110 (14), 7208-7212.
18. Yang, P.; Portalès, H.; Pileni, M.-P., Dependence of the localized surface plasmon resonance of noble metal quasispherical nanoparticles on their crystallinity-related morphologies. The Journal of Chemical Physics 2011, 134 (2), 024507-1.
19. Amendola, V.; Bakr, O. M.; Stellacci, F., A Study of the Surface Plasmon Resonance of Silver Nanoparticles by the Discrete Dipole Approximation Method: Effect of Shape, Size, Structure, and Assembly. Plasmonics 2010, 5 (1), 85-97.
20. Link, S.; El-Sayed, M. A., Spectral properties and relaxation dynamics of surface plasmon electronic oscillations in gold and silver nanodots and nanorods. J. Phys. Chem. B 1999, 103 (40), 8410-8426.
21. Nehl, C. L.; Hafner, J. H., Shape-dependent plasmon resonances of gold nanoparticles. Journal of Materials Chemistry 2008, 18 (21), 2415-2419.
22. Ghosh, S. K.; Nath, S.; Kundu, S.; Esumi, K.; Pal, T., Solvent and Ligand Effects on the Localized Surface Plasmon Resonance (LSPR) of Gold Colloids. The Journal of Physical Chemistry B 2004, 108 (37), 13963-13971.

23. Wei, T.; Liu, Y.; Dong, W.; Zhang, Y.; Huang, C.; Sun, Y.; Chen, X.; Dai, N., Surface-Dependent Localized Surface Plasmon Resonances in CuS Nanodisks. ACS Applied Materials & Interfaces 2013, 5 (21), 10473-10477.
24. Murphy, C. J.; San, T. K.; Gole, A. M.; Orendorff, C. J.; Gao, J. X.; Gou, L.; Hunyadi, S. E.; Li, T., Anisotropic metal nanoparticles: Synthesis, assembly, and optical applications. J. Phys. Chem. B 2005, 109 (29), 13857-13870
25. Peng, S.; McMahon, J. M.; Schatz, G. C.; Gray, S. K.; Sun, Y., Reversing the size-dependence of surface plasmon resonances. Proceedings of the National Academy of Sciences of the United States of America 2010, 107 (33), 14530-14534.
26. Haes, A. J.; Van Duyne, R. P., A nanoscale optical blosensor: Sensitivity and selectivity of an approach based on the localized surface plasmon resonance spectroscopy of triangular silver nanoparticles. Journal of the American Chemical Society 2002, 124 (35), 10596-10604.
27. Malinsky, M. D.; Kelly, K. L.; Schatz, G. C.; Van Duyne, R. P., Chain length dependence and sensing capabilities of the localized surface plasmon resonance of silver nanoparticles chemically modified with alkanethiol self-assembled monolayers. Journal of the American Chemical Society 2001, 123 (7), 1471-1482.
28. Mock, J. J.; Barbic, M.; Smith, D. R.; Schultz, D. A.; Schultz, S., Shape effects in plasmon resonance of individual colloidal silver nanoparticles. Journal of Chemical Physics 2002, 116 (15), 6755-6759.
29. Hao, E.; Schatz, G. C., Electromagnetic fields around silver nanoparticles and dimers. Journal of Chemical Physics 2004, 120 (1), 357-366.
30. Wang, C.; Yin, H.; Chan, R.; Peng, S.; Dai, S.; Sun, S., One-Pot Synthesis of Oleylamine Coated AuAg Alloy NPs and Their Catalysis for CO Oxidation. Chemistry of Materials 2009, 21 (3), 433-435.
31. Pileni, M. P., Self-Assembly of inorganic NCs: Fabrication and Collective Intrisic Properties. Acc. Chem. Res 2007, 40 (8), 685-693.
32. Shankar, R.; Wu B. B.; Bigioni, T. P. Wet Chemical Synthesis of Monodisperse Colloidal Silver Nanocrystals Using Digetive Ripening. J. Phys. Chem. C 2010, 114, 15916-15923.
33. Hiramatsu H.; Osterloh F. E., A Simple Large-scale Synthesis of nearly Monodisperse Gold and Silver Nanoparticles with Adjustable Sizes and with Exchangeable Surfactants. Chemistry of Materials 2004, 16 (13), 2509-2511.

34. Linnert T.; Mulvaney P.; Henglein A., Surface Chemstry of Colloidal Silver: Surface Plasmon Damping by Chemisorbed I-, SH-, and C6H5S-, 1993, 97(3), 679-682.
35. Kawabata, A.; Kubo, R. Electronic Properties of Fine Metallic Particles. II. Plasma Resonance Absorption. J. Phys. Soc. Jpn.1966, 21 (9), 1765-1772.
36. Ruppin, R.; Yatom, Y. Size and Shape Effects on the Broadening of the Plasma Resonance Absorption in Metals. Phys. Status Solidi 1976, 74, 647-654.
37. Barma, M.; Subrahmanyam, V. Optical Absorpiton in Small Metal Particles. J. Phys.: Condens. Matter 1989, 1, 7681.
38. Lerme, J.; Baida, H.; Bonnet, C.; Broyer, M.; Cottancin, E.; Crut, A.; Maioli, P.; Fatti Del, N.; Vallee, F.; Pellarin, M. Size Dependence of the Surface Plasmon Resonance Damping in Metal Nanospheres. J. Phys. Chem. Lett. 2010, 1, 2922-2928.
39. Baida, H.; Billaud, P.; Marhaba, S.; Chistofilos, D.; Cottaicin, E.; Crut, A.; Lerme, J.; Maioli, P.; Pellarin, M.; Broyer, M.; Del Fatti, N.; Vallee, F. Quantitative Determination of the Size Dependence of Surface Plasmon Resonance Damping in Single Ag@SiO_2 Nanoparticles. Nano lett. 2009, 9 (10), 3463-3469.
40. Del Fatti, N.; Vallee, F.; Flytzanis, C.; Hamanaka, Y.; Nakamura, A. Electron dynamics and surface plasmon resonance nonlinearities in metal nanoparticles. Chem. Phys. 2000, 251, 215-226
41. Hodak, J. H.; Henglein, A.; Hartland, G. V., Photophysics of Nanometer Sized Metal Particles: Electron−Phonon Coupling and Coherent Excitation of Breathing Vibrational Modes. The Journal of Physical Chemistry B 2000, 104 (43), 9954-9965.
42. Kreibig, U.; Vollmer, M. Optical Properties of Metal Clusters; Springer: Berlin, 1995.

3.3 Supporting Information

NC size (nm)	NC size distribution	SPR eV
oleylamine coated		
2.2	9%	2.90
4.1	8%	2.98
5.9	8%	3.02
8.7	8%	3.03
12.9	8%	3.03
dodecylamine		
2.9	9%	2.91
4.0	9%	2.98
5.1	8%	3.01
6.3	8%	3.02
dodecanethiol coated (LE)		
2.2	13%	2.68
2.9	10%	2.76
4.0	9%	2.83
5.3	9%	2.86
6.0	9%	2.89
hexadecanethiol (LE)		
2.9	10%	2.77
4.0	9%	2.80
5.0	9%	2.83
6.0	9%	2.85
7.8	9%	2.85

Table S1: Sizes, size distributions and SPR position of the various Ag nanocrystals prepared in this study.

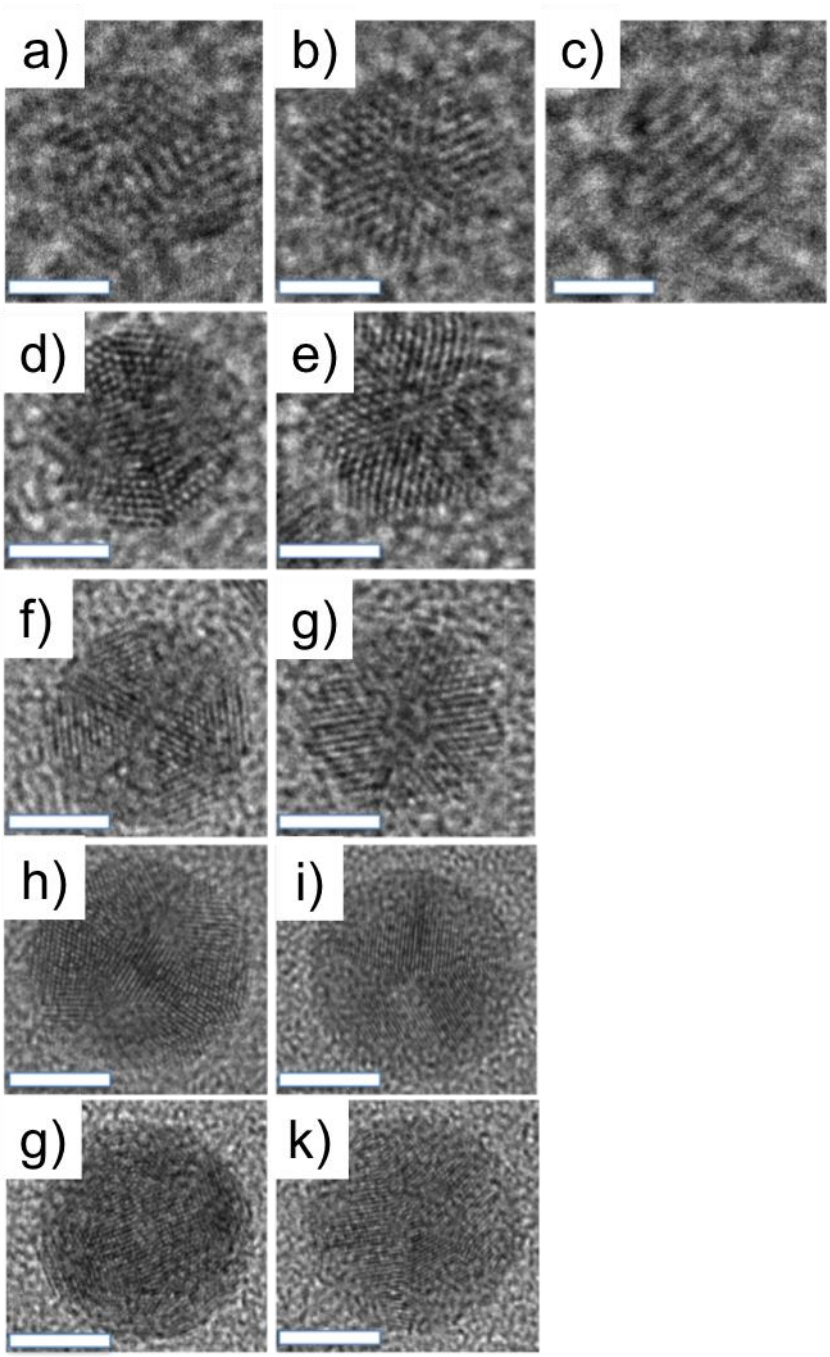

Figure S1: HRTEM pictures of the NCs coated with oleylamine:

- a)-c) : 2.2 nm Ag NPs (scalebar: 1nm)
- d), e) : 4.1 nm Ag NPs (scalebar: 2.5nm)
- f), g) : 5.9 nm Ag NPs (scalebar: 3nm)
- h), i): 8.7 nm Ag NPs (scalebar: 4nm)
- g), k): 12.9 nm Ag NPs (scalebar: 6nm)

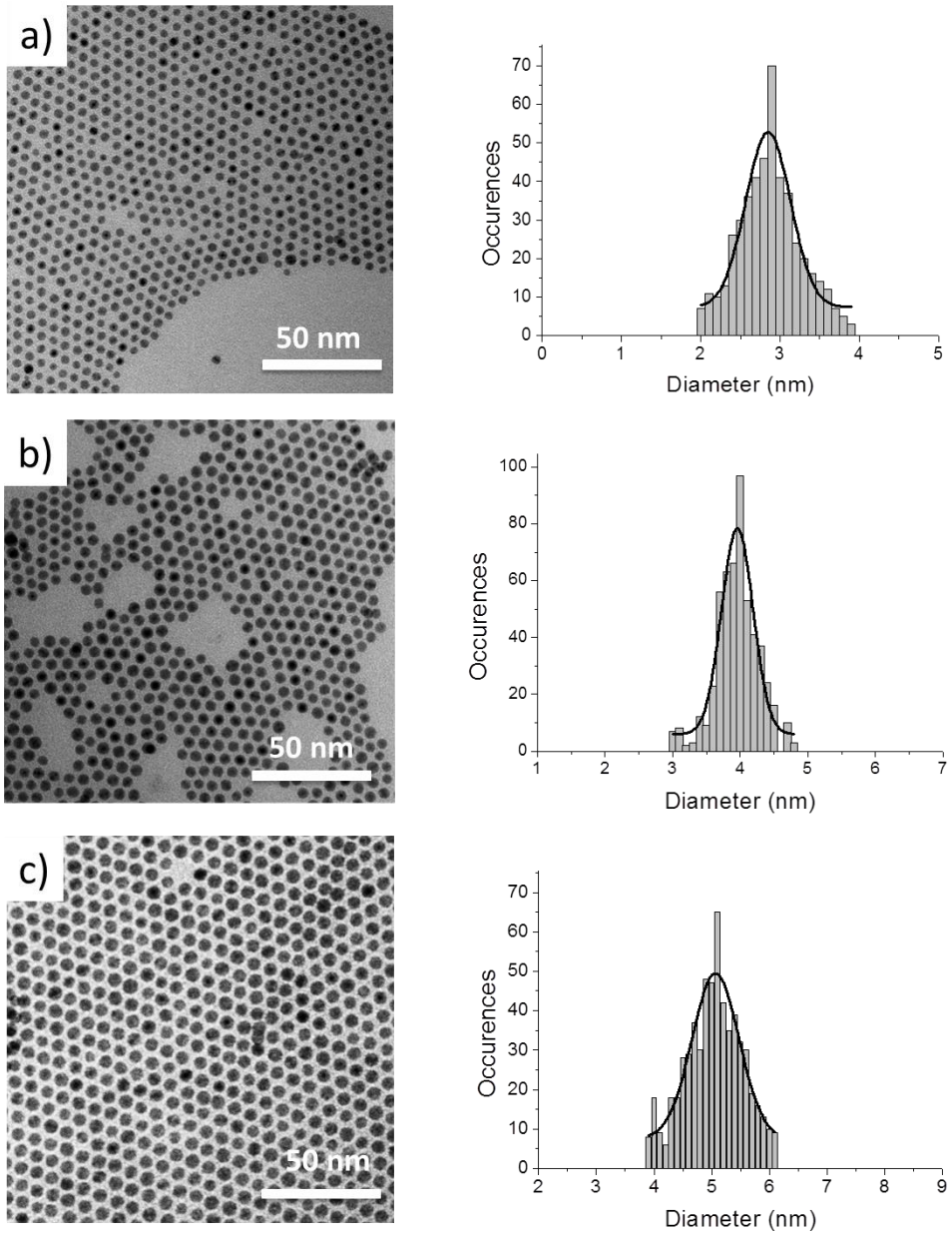

Figure S2. TEM images of colloidal silver nanocrystals coated with dodecylamine: a) 2.9 nm; b) 4.0 nm; c) 5.1 nm.

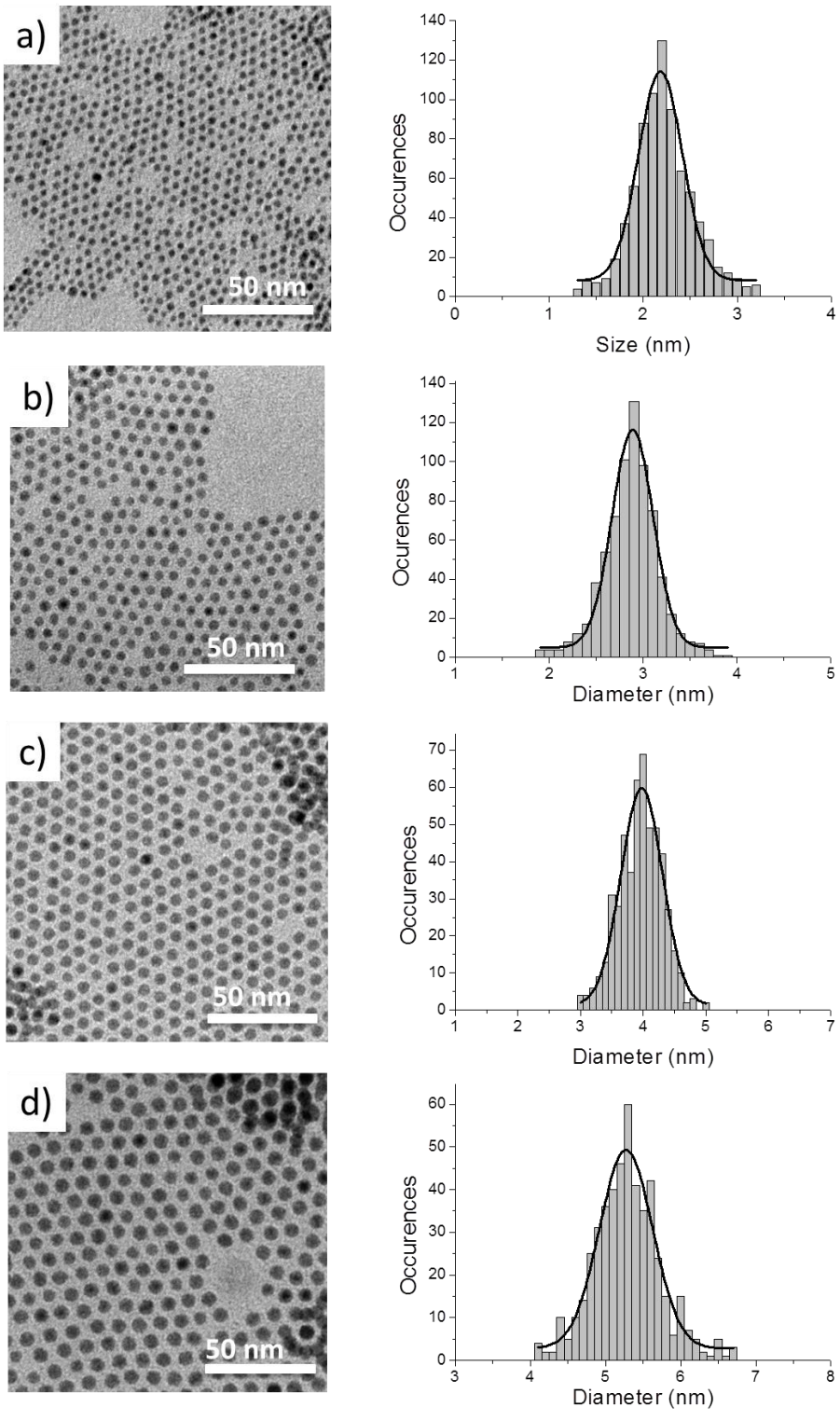

Figure S3. TEM images of colloidal silver nanocrystals coated with dodecanethiol: a) 2.2 nm; b) 2.9 nm; c) 4.0 nm; d) 5.3 nm.

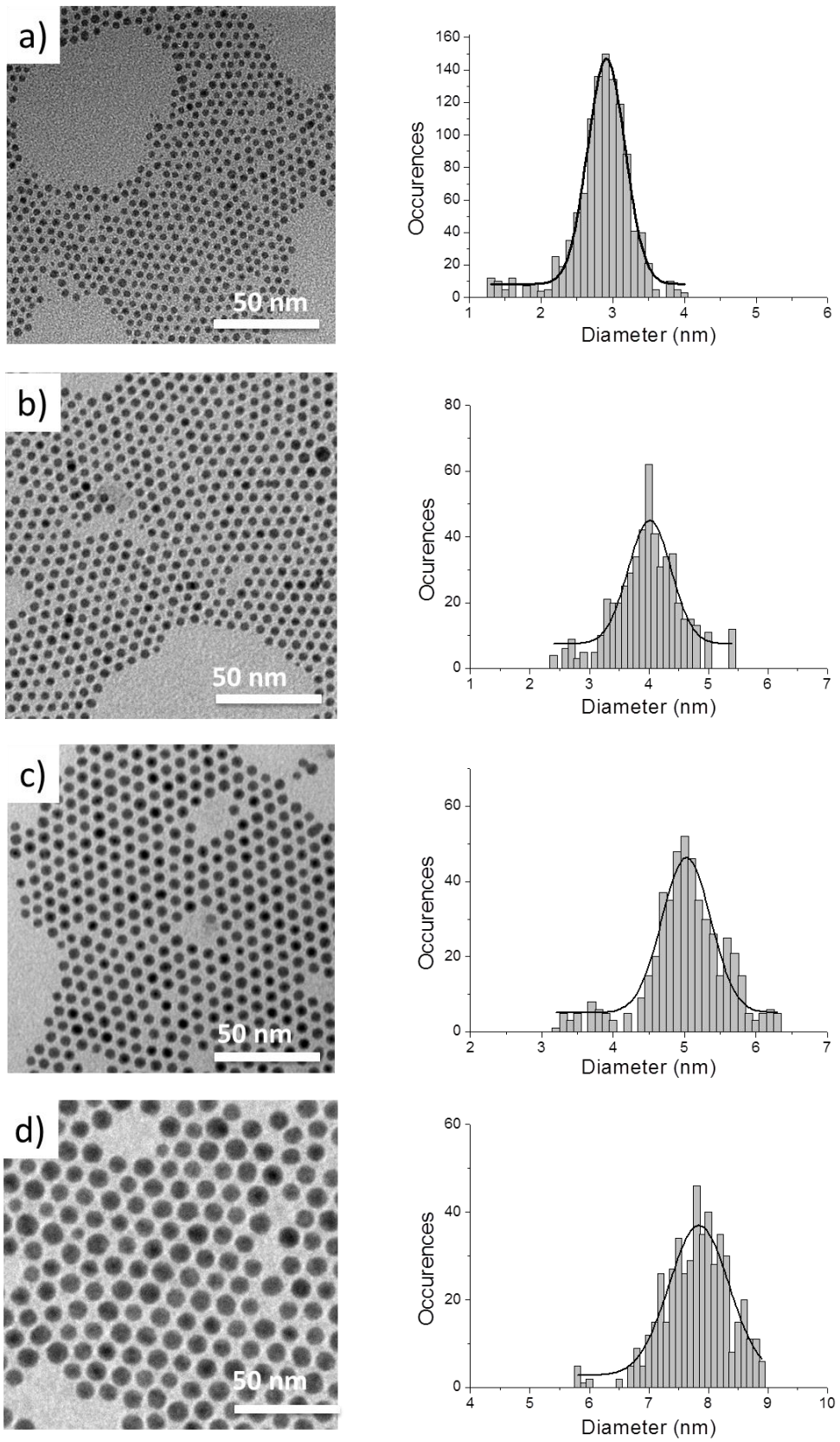

Figure S4. TEM images of the colloidal silver nanocrystals coated with hexadeanethiol : a) 2.9 nm; b) 4.0 nm; c) 5.0 nm; d) 7.8 nm.

Chapter 4
Surface Plasmon Resonance of Silver Nanocrystals Differing by Sizes and Coating Agents Ordered In 3D Supracrystals

4.1 Abstract

In this part, silver nanocrystals coated with oleylamine or dodecylamine with rather narrow distribution are synthesized by hot injection and one-pot method. Then ligand exchange strategy is used to prepare nanocrystals coated with dodecanethiols. Silver nanocrystals differing by their coating agents and sizes are self-assembled in thin supracrystalline films. The surface plasmon resonance (SPR) properties of such assemblies are presented. Nanocrystal size, interparticle distance and coating agent play key roles in the plasmonic coupling of Ag nanocrystals within supracrystals. By either increasing the diameter of nanocrystals or shortening the interparticle distance, the SPR band shifts to lower energy due to stronger coupling effect. Then, we demonstrate experimentally the predictions for 2D self-assemblies remains valid for thin 3D superlattices. The absorption spectra in the visible range are markedly dependent on the incidence of the light source and confirm the apparition of a splitting of the dipolar surface band into two components, namely longitudinal band and transverse band, upon increasing the incidence angle. The major parameter inducing the splitting of the SPR band is the relative ratio between the average distance of nanocrystals and their diameters. The nature of the coating agent is also of particular importance; it is hereby shown that theoretical predictions and experimental data are in agreement for alkylamine coating agents, whereas they differ for thiol-coated nanocrystals.

4.2 Article: Surface Plasmon Resonance of Silver Nanocrystals Differing by Sizes and Coating Agents Ordered In 3D Supracrystals

Surface Plasmon Resonance of Silver Nanocrystals Differing by Sizes and Coating Agents Ordered In 3D Supracrystals

Jingjing Wei,[a,b] *Nicolas Schaeffer,*[a,b] *Pierre-Antoine Albouy,*[c] *Marie-Paule Pileni**[a,b,d]

[a] Sorbonne Universités, UPMC Univ Paris 06, UMR 8233, MONARIS, F-75005, Paris, France

[b] CNRS, UMR 8233, MONARIS, F-75005, Paris, France

[c] Laboratoire de Physique des Solides, Université Paris-Sud, 91405 Orsay, France

[d] CEA/IRAMIS, CEA Saclay, 91191, Gif-sur-Yvette, France

INTRODUCTION

Inorganic nanocrystals self-assembled in two-dimensional (2D) or three-dimensional (3D), referred to as supracrystals, have received great interest over the last two decades.[1-5] Hence, long-range ordered assemblies of nanocrystals can in some cases exhibit novel optical, electronic, mechanical or magnetic properties, thus providing a route to the manufacture of metamaterials with unique chemical and physical properties.[6-9] For example, vibrational coherence in supracrystals was first discovered by Low-Frequency Raman Spectroscopy (LFRS) measurements for *fcc* supracrystals of 5-nm Ag nanocrystals, and is in good agreement with theoretical calculations carried out on similar system.[10] This vibrational coherence was demonstrated by a decrease in the quadrupolar mode bandwidth. Propagative vibrations in supracrystals have also been evidenced by time-resolved pump probe measurement (phonons are associated to long-range order: they can be evidenced not demonstrated). Long-time scale differential reflectivity dynamics reveal large oscillations for the ordered systems, whereas a monotonous decay was observed in the disordered system. Furthermore, it was shown that the electron transport properties can be controlled by the degree of ordering in the nanocrystal assemblies. [11- 14]

The bright and fascinating colors of noble-metal nanocrystals (*i.e.* Au, Ag…) have attracted considerable interest since historical times for their use as decorative pigments in stained glasses and artworks.[15-17] Nowadays, the attention is focused on applications ranging from photonics to biomedicine.[18, 19] Noble-metal nanocrystals, when dispersed in solvent, exhibit a strong localized surface plasmon resonance (SPR) peaks resulting from the collective resonance oscillation of conduction electrons under the irradiation light.[20, 21] The SPR frequency depends not only on the type of nanomaterials, but also on its size and shape,[20, 22] and on the dielectric properties of the carrier solvent.[23, 24] Colloidal Ag nanocrystals are attractive candidates as nanoscale plasmonic building blocks because of their sharper resonance, greater electromagnetic field enhancement and lower loss, compared to that of Au or Cu for instance.[25] Recent studies on the size-dependence SPR absorption band show a strong blue-shift when increasing the nanocrystal size from 2 to 12 nm, which is in opposition with observations made for this type of materials in the size range of tens of nanometers.[21,24]

When 5-nm Ag nanocrystals are self-assembled in 2D superlattices, it has been demonstrated by reflectivity, [26] photo-induced STM, [27] ellipsometry that splitting of the SPR band takes place. More recently it was also shown that this splitting was due to inter-particle coupling interactions,[13] and consequently the optical properties of noble-metal nanocrystals can be modulated efficiently through tailor-made design. The sensitivity of the SPR to the inter-particle interactions has been explored.[26,28,29] The discrete dipolar approximation (DDA) method pioneered by Purcell and Pennypacker [30] has been applied to simulate the absorption spectra of metal nanoparticles assembled in a 2D hexagonal network. However, the experimental demonstration of collective SPR of 3D supracrystals made of noble-metal nanocrystals remains to be demonstrated. Near-field-coupled noble-metal nanocrystals have been studied, revealing the coupled SPR in plasmonic dimers composed of octahedral gold nanocrystals within the near-field range.[31] Long-range periodic assemblies of noble-metal nanocrystals, are frequently studied through theoretical approaches, but rarely experimentally.[13, 23, 32]

Here we demonstrate that the SPR bands of nanocrystals with various sizes and coating agents self-assembled in thin supra-crystalline films are strongly red-shifted with increasing of the nanocrystal size and behave oppositely when the same nanocrystals are dispersed in a solvent. The size-dependent and ligand-dependent collective SPR properties of Ag nanocrystal supracrystals are demonstrated. Finally, the influence of the angle of incidence of the light onto the optical measurement reveals a size-dependent splitting within the SPR at

large enough angles; no SPR variation was observed when the coating agent and the interparticle distance remains constant.

METHODS

A. Materials. Silver nitrate (99.9%) was purchased from Sigma, toluene (98%) from Riedel de Haen, ethanol (99.8%) from Prolabo, *o*-dichlorobenzene (99%) from Sigma, oleylamine (70%) from Sigma, and dodecanediol (99%) from Sigma. All reagents were used as received without further purification.

B. Equipment. Transmission electron microscopy (TEM) images were obtained with a JEOL JEM 1011(100 kV). The UV-visible absorption measurements presented here were performed using a Varian Cary 5000 double monochromator recording spectrophotometer. To perform measurements in transmission geometry at various angles of incidence, the spectrophotometer was equipped with a Harrick Scientific (Pleasantville, NY) variable angle transmission accessory (VATA), which has been specially designed for transmission studies of samples up to 3 mm thick. The VATA allows a given sample and a blank (which should match the former in both thickness and refractive index) to be placed in the light beam at the same angle of incidence, but in the opposite orientation, in order to avoid any misalignment of the detected beam that could affect the measured transmittance. A Glan-Taylor polarizer was also used in all our measurements to polarize the light parallel to the plane of incidence. Under such a configuration, information on the optical anisotropy of the sample can interestingly be achieved by considering the fact that the electric field is then projected in both perpendicular and parallel directions to the nanocrystal 2D assembly. For particles in solution, absorption spectra were recorded in 1-mm cuvettes. Small-angle X-ray Scattering measurements were performed with a homemade system mounted on a rotating copper anode generator (focus size: 0.1×0.1 mm^2; 40 kV, 20 mA).

C. Synthesis of Ag nanocrystals. Nanocrystals with diameter of 2.2 nm, 4.1 nm, 5.9 nm are synthesized by the hot injection method and the coating agent used is oleylamine except 2.2 nm with both oleylamine and Oleic acid as coating agents.[21] The 8.7 nm and 12.9 nm nanocrystals were synthesized with a one-pot method and the coating agent is also oleyl amine.[24] Nanocrystals using dodecylamine as coating agent were similarly prepared by hot injection methods. [24] The nanocrystals coated with dodecanethiol were prepared by ligand exchange with the nanocrystals coated with oleylamine obtained above. Thiol coated Ag nanocrystals were prepared from the pre-formed oleylamine coated nanocrystals described

above and a ligand exchange procedure. The ligand exchange procedure was as follows: small amount of dodecanethiol (20 L dodecanethiol per 10 mg Ag nanocrystals) was added to the suspension of Ag nanocrystals and the mixture was kept under vigorous stirring for 1 hour. Then, ethanol was added to the solution, inducing flocculation. The excess dodecanethiol was removed with the supernatant and the nanocrystals was re-dispersed in toluene. Ultimately, all the nanocrystals were dispersed in toluene and exhibited a size distribution below 10% (Figure S1 and Figure S2, Supporting Information).

D. Preparation of the three-dimensional supracrystals. Preparation of the supracrystals is as follows: Ag nanocrystals differing by their diameters and their coating agents were synthesized and dispersed in toluene to obtain colloidal solution ($c_{Ag} \approx 1.0$ mg/mL). Two specimens were prepared simultaneously: two glass wafers were deposited on paper sheet. On one of the wafer an amorphous carbon coated copper mesh TEM grid was deposited. The same amount of colloidal solution (50 μL) was deposited on the two glass wafers. In order to slow down the evaporation rate the substrate was covered by watch glass. At the end of evaporation (≈ 30 min), a thin film is deposited either on TEM grid or on the glass wafer.

RESULTS AND DISCUSSION

Colloidal solution of Ag nanocrystals differing by their diameters and their coating agents are synthesized as described in the experimental section and dispersed in toluene ($c_{Ag} \approx$ 1.0 mg/mL). The so-formed supracrystalline films made of oleylamine (C_{18}-NH_2) coated Ag nanocrystals of varying sizes and recovered on the wafer carrying the TEM grid are presented in Figure 1. The Ag nanocrystals display long-range order (1-3 μm) as shown on Figure 1 and confirmed by the corresponding Fast Fourier Transform (FFT) pattern as shown in insets. The thickness of the films was evaluated to be 2-7 layers from those images. Note that insets (b), (c), (d) and (e) in Figure 1 show hexagonal patterns whereas inset in panel (a) shows only a rectangular one.

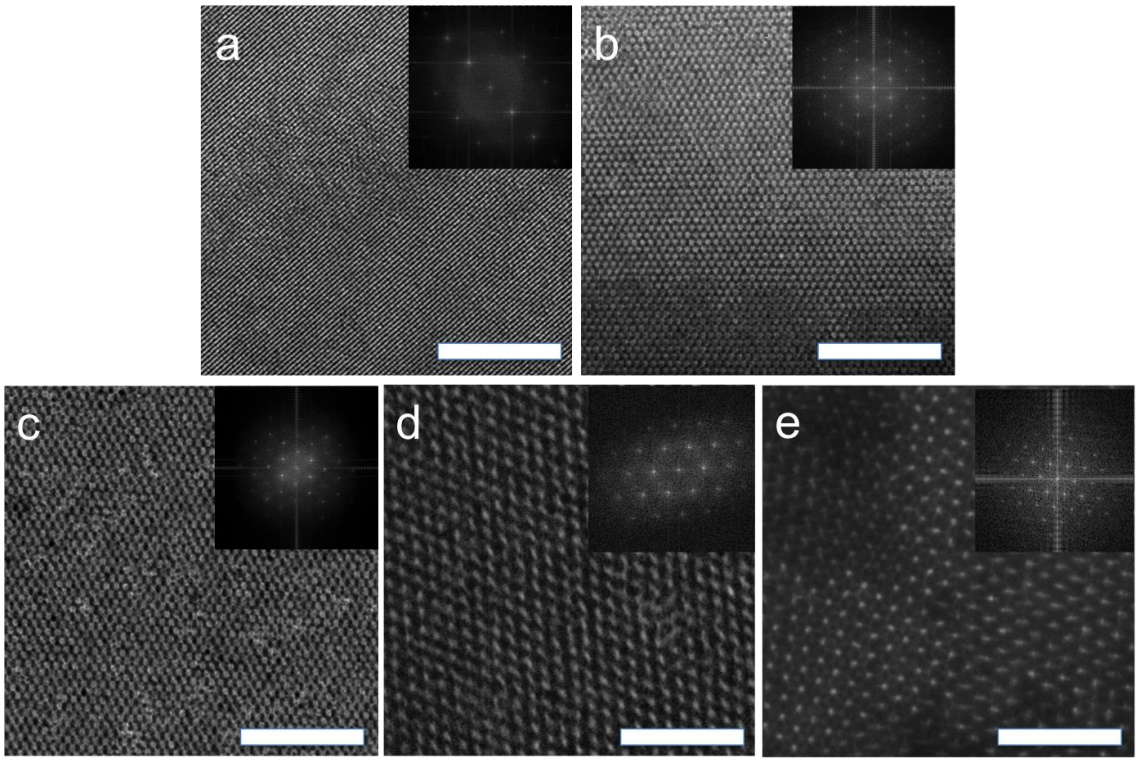

Figure 1. TEM images of thin supracrystalline films of Ag nanocrystals coated with oleyamine (C_{18}-NH_2) differing by their diameters: (a) 2.2 nm; (b) 4.1 nm; (c) 5.9 nm; (d) 8.7 nm; (e) 12.9 nm. The inserted scale bars are 100 nm.

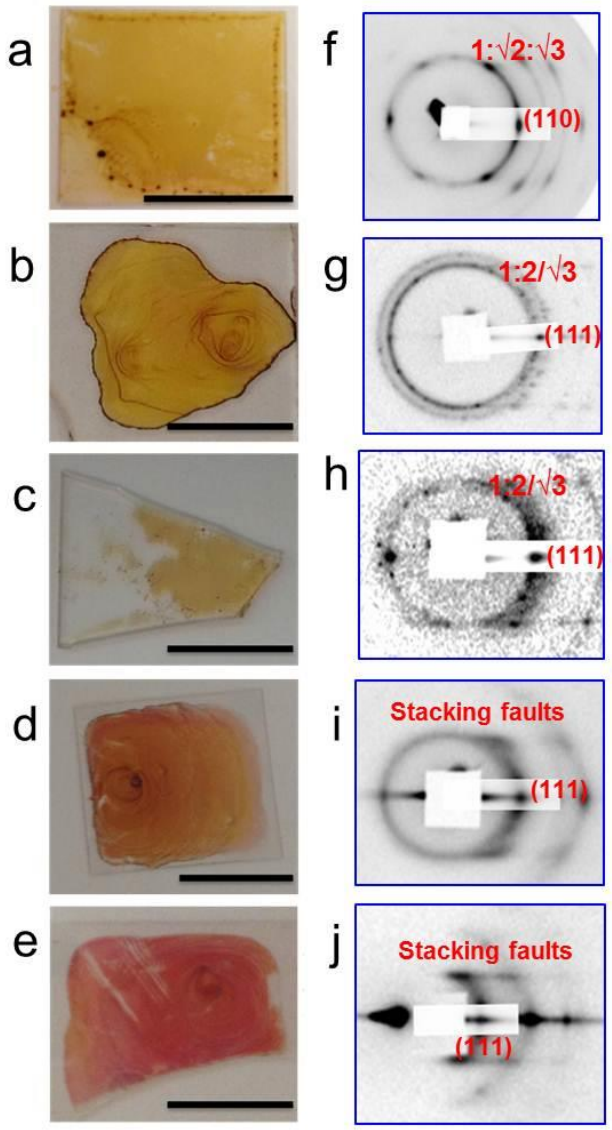

Figure 2. Optical images of the supracrystalline films on glass substrate and corresponding X-ray diffraction patterns for thin supracrystals of Ag nanocrystals coated with oleylamine (C_{18}-NH_2) and differed by their diameters: (a, f) 2.2 nm (b, g) 4.1 nm (c, h) 5.9 nm (d, i) 8.7 nm (e, j) 12.9 nm. The scale bars in the optical images all are 1cm. 1:√2:√3 (resp. 1:2/√3) positions for first diffraction lines are presently typical for bcc (resp. fcc) structures. Stacking faults in *fcc* result in streaks.

Specimens of 3D superlattices for UV-vis absorption spectroscopy were prepared by depositing the same amount of Ag nanocrystals on the glass wafer as the one used to record TEM images (wafer: 2x2 cm^2). Those colored films of nanocrystals differing by their sizes are

depicted in Figures 2a-2e and look rather inhomogeneous. However, the corresponding grazing incidence small angle X-ray scattering patterns confirm that the nanocrystals forming the films are well ordered in a supracrystalline structure (Figures 2f-2j). For 2.2-nm, as expected from the Landman theory,[34] the diffraction pattern corresponds to a body-centered cubic (bcc) structure (Figure 2f). On increasing the nanocrystals diameter, from 4.1 to 12.9 nm, the characteristic patterns of face-centered cubic (*fcc*) symmetry are produced (Fig. 2g-2j). The inter-particle distance, δ_{pp}, between nanocrystals deduced from SAXRS measurements remains in the same order of magnitude (Table 1).

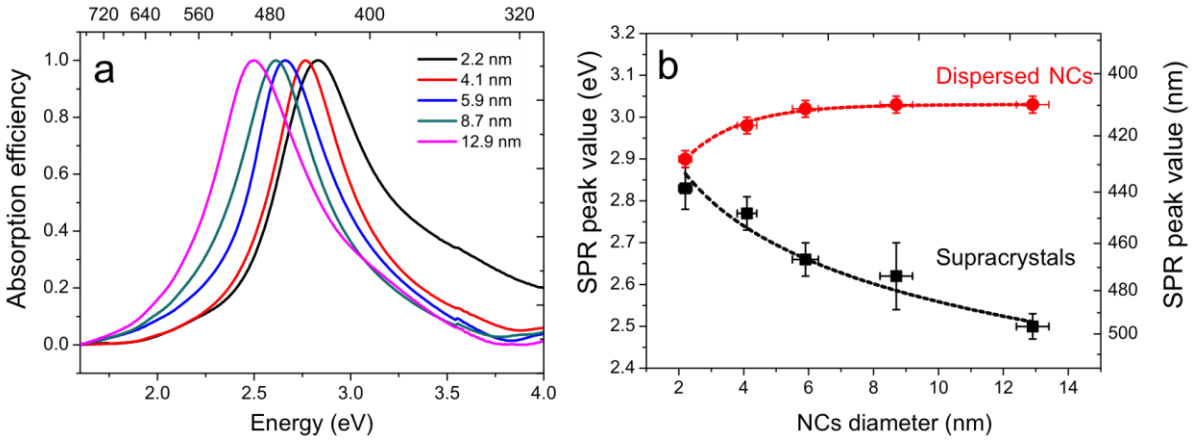

Figure 3. (a) Normalized UV-Vis absorption spectra recorded under normal incident light of thin supracrystalline films made of C_{18}-NH_2 coated Ag nanocrystals of various diameters (b) SPR peak position values of dispersed nanocrystals (red sphere) and corresponding supracrystalline films (black square) as a function of the nanocrystal diameter.

Table 1. Interparticle distance (δ_{pp}) between Ag nanocrystal coated with C_{18}-NH_2 within the supracrystals, deduced from small-angle X-ray scattering measurements. Maximum energy of the surface plasmon resonance (SPR) spectrum and the corresponding maximum wavelength (λ_{max}) of Ag nanocrystals either dispersed in toluene, E (dispersed nanocrystals/eV) or embedded within the supracrystals and measured at 0° angle, E (supracrystal films/eV). ΔE is the difference of E values between Ag nanocrystals dispersed in toluene and deposited on a glass substrate forming supracrystals.

Nanocrystal size/ nm	2.2	4.1	5.9	8.7	12.9
Size distribution	9%	8%	8%	8%	8%
δ_{pp} /nm	3.2	3.2	3.1	2.8	2.5
E (dispersed nanocrystals/eV)	2.90	2.98	3.02	3.03	3.04
E (supracrystal films/eV)	2.83	2.77	2.67	2.62	2.50
λ_{max} (supracrystal films/nm)	438	448	464	473	496
ΔE (dispersed supracrystal/eV)	0.07	0.21	0.35	0.41	0.54

The Surface Plasmon Resonance (SPR) spectra of the supracrystal films deposited on a glass wafer are recorded using a horizontally polarized light source and keeping the incident light parallel to the substrate. The SPR spectra of Ag nanocrystals, differing by their average diameters and coated with oleylamine (C_{18}-NH_2) are red-shifted (low energy shift) on increasing the nanocrystal diameters, as depicted in Figure 3a. This is in complete opposition with what has been observed with the same nanocrystals dispersed in toluene (and thus considered as isolated nanocrystals). As already described in our previous paper and by others [21, 24], a blue shift is observed on increasing the nanocrystal sizes in solution. This was explained by the lower conductivity of the outer layer in smaller nanocrystals. Figure 3b shows an increase in the maximum absorption wavelength (λ_{max}) of the SPR spectrum of nanocrystals dispersed in toluene when increasing the nanocrystal size, whereas a marked drop in the λ_{max} is observed when the same nanocrystals are assembled in thin supracrystals and deposited on a glass wafer. Table 1 and Figure S3 show the energy differences in the SPR band peak position between the dispersed nanocrystals and the corresponding thin supracrystalline films, ΔE. These non-negligible energy differences are attributed to the interactions between the Ag nanocrystals embedded in the supracrystals. In fact, due to an increase in the dipole moments led by an increase in the nanocrystals diameters, the

electromagnetic coupling between nanocrystals within the supracrystals increases and consequently induces a change in the optical properties of these assemblies.

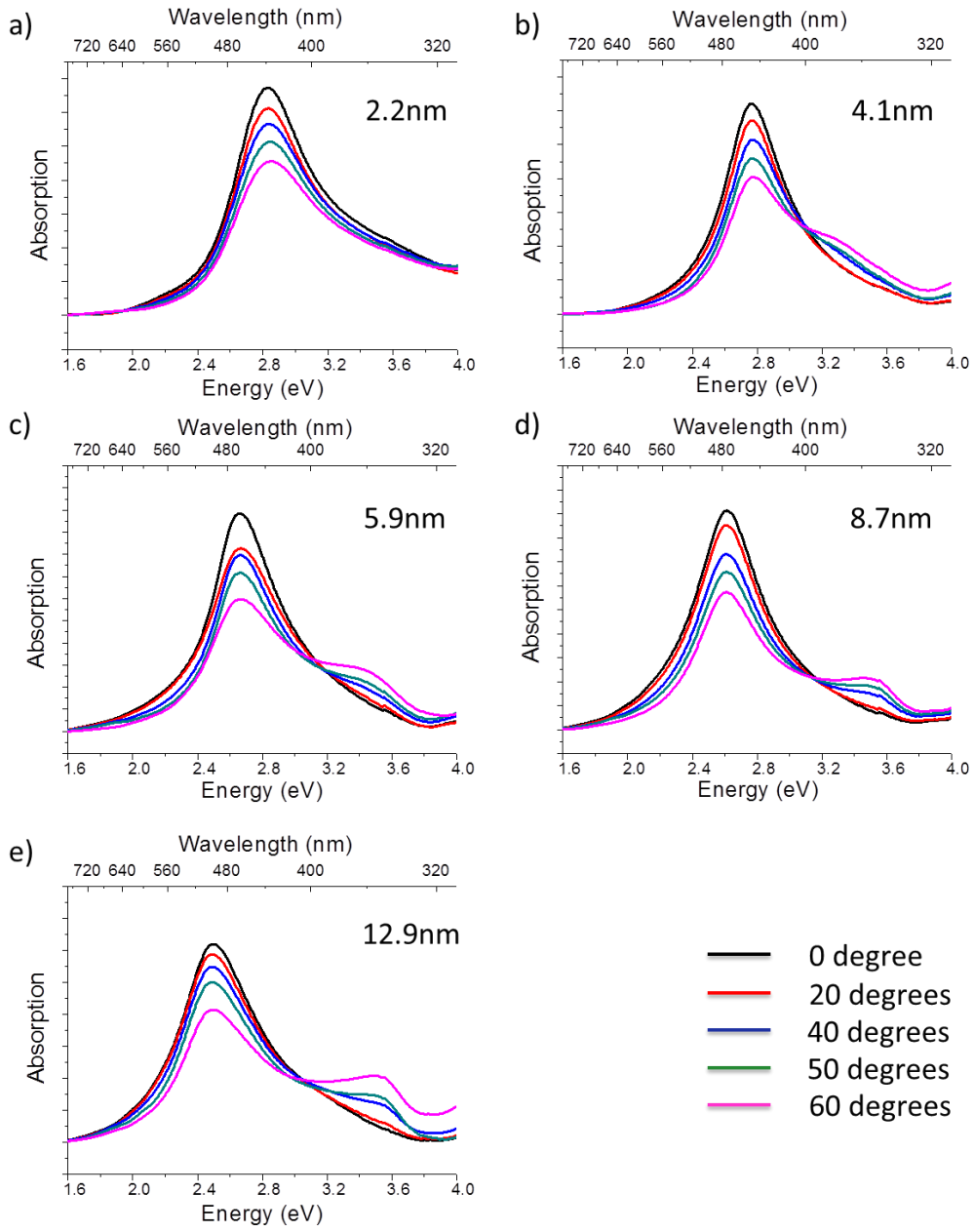

Figure 4. SPR spectra of the supracrystal films of nanocrystals differing by their diameters and coated with C_{18}-NH_2 at various incidence angles: (a) 2.2 nm; (b) 4.1 nm; (c) 5.9 nm; (d) 8.7 nm and (e) 12.9 nm.

By using polarized light parallel to the plane of incidence at various incident angles (θ), the absorption spectra of the ordered 3D assemblies show the appearance of a secondary peak, at higher energies (compared to that of the SPR) for relatively large incident angle above 40 °. Figure 4 and Table 2 show that the splitting of the SPR band is not well-defined for supracrystals of 2.2-nm nanocrystals whereas it is clearly discernible for larger Ag nanocrystals sizes and angles larger than 40 °. However, through deconvolution of SPR band under incidence angle of 60 °it is possible to detect a second peak for 2.2-nm Ag supracrystals. On increasing the nanocrystal diameters, the second peak at higher energy is becoming more pronounced. This reveals that the SPR spectra in the visible range are markedly dependent on the incidence of the light source. These data confirm those predicted by DDA simulation[13] and observed experimentally by reflectivity[26] for 5-nm Ag nanocrystals self-assembled in 2D superlattices. Appearance of a higher energy band is interpreted as follows: for incident angle $\theta \neq 0°$, the electric field of the incident radiation projects in both parallel and perpendicular direction to the nanocrystal arrays. The amplitudes of these two bands evolve in the opposite trends when varying the incident angle. The perpendicular component increases with θ, and the resonant excitation of both the longitudinal and transverse surface plasmon eigenmodes of the supracrystal films result in the appearance of two bands in the absorption spectra. This feature points out the optical anisotropy of the 3-D array of the nanocrystals. Such variations in the amplitude of both longitudinal and transverse SPR are well observed by plotting their correspondent energies with γ ($\gamma = \delta_{pp}/D$), where D and δ_{pp} are the nanocrystal diameter and the interparticle distance between nanocrystals within the supracrystals (Figure 5 and Table 2).

Table 2. SPR peak position of the longitudinal and transverse peaks with various Ag-nanocrystal sizes coated with oleylamine (C_{18}-NH_2) for an incident angle 60°.

Nanocrystal diameter/nm	2.2	4.1	5.9	8.7	12.9
E (longitudinal peak/eV)	2.84	2.78	2.67	2.62	2.50
λ_{max} (longitudinal/nm)	436	446	464	473	496
E (transverse peak/eV)	3.13	3.27	3.38	3.45	3.48
λ_{max} (transverse/nm)	396	379	367	359	356

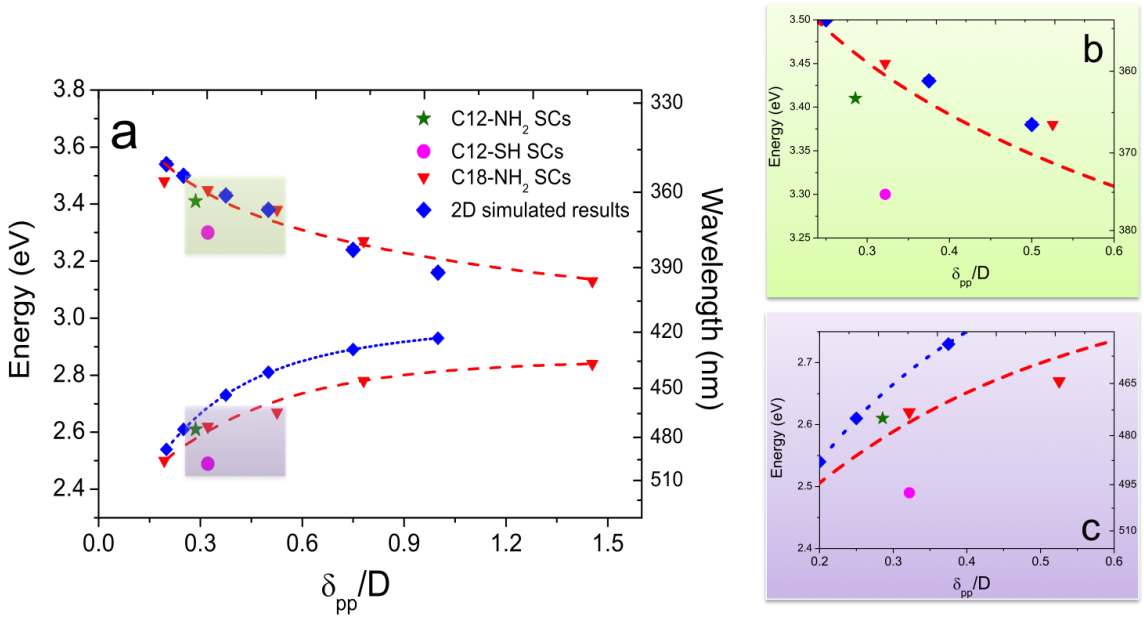

Figure 5. (a) Comparison of the experimental and simulated longitudinal and transversal SPR band position[13] values against $\gamma = \delta_{pp}/D$ of nanocrystals differing by their coating agents and sizes; (b-c) local magnifications of the Figure 5a.

The two SPR peaks tend, on increasing the γ value, to reach values close to their counterparts in supracrystals of 2.2-nm Ag nanocrystals. Such a feature, observed experimentally with nanocrystals differing by their sizes self-assembled in 3D superlattices with δ_{pp} rather constant (Table 2), was recently predicted by DDA simulation of 2D superlattices and is attributed to an increase in the dipolar interactions.[13]

Comparison between the data presented hereby and those deduced from simulations shows a good agreement for energy values of the transverse SPR energy band for C_{18}-NH_2 coated Ag-nanocrystals differing by their sizes, shown in Figure 5, whereas discrepancies are observed between experimental and theoretical energy values for the longitudinal SPR bands. This can be attributed to the fact that the longitudinal peak is more sensitive to the coating agent compared to the transverse one. In fact DDA simulations mentioned above did not take the surface coating agent into account, only assuming spheres surrounded by a continuous medium.[13] These data also show that the transversal SPR peak do not markedly depend on a weak coating agent as C_{18}-NH_2 whereas the longitudinal modes could be highly sensitive to this factor.

At this stage we raise a question on what is the influence of the coating agent on the SPR spectra of "thin 3D superlattices". To answer this question let us replace oleylamine (C_{18}-NH_2) by dodecylamine (C_{12}-NH_2) or by dodecanthiol (C_{12}-SH) keeping a similar average

diameter (*ca.* 6-nm). Unfortunately it has been impossible to produce supracrystals with various sizes of Ag nanocrystals coated with C_{12}-NH_2 or C_{12}-SH. In a similar manner to what has been described above with C_{18}-NH_2 coated nanocrystals, those new Ag nanocrystals are deposited on a glass wafer and form thin films. Figure 6a and 6b show, as observed in Figure 2 for C_{18}-NH_2 coated Ag nanocrystals ordered on the substrates, that the films on glass are relatively inhomogeneous. Nevertheless the corresponding SAXRS patterns (Figure 6c, e and 6d, f) show that the ~6-nm nanocrystals coated with C_{12}-NH_2 and C_{12}-SH are ordered in *fcc* crystalline structure as observed with C_{18}-NH_2. Table 3 shows that the interparticle distance, δ_{pp}, remains similar (1.8-1.9 nm) for those specimens, those values being smaller than those obtained with C_{18}-NH_2 (3.1 nm).

The optical properties of these C_{12}-NH_2 and C_{12}-SH supracrystals (Figure 6e) differing by the nature of their coating agent show similar behavior as described above with C_{18}-NH_2 (Figure 2). Figure 6e shows a red shift of the SPR spectrum of supracrystals of ~6-nm Ag nanocrystals coated with C_{12}-NH_2 and C_{12}-SH compared to the same nanocrystals dispersed in toluene. Table 3 shows that the differences in the energies determined from the maximum of the SPR spectra between deposited and dispersed remain the same ($\Delta E \approx 0.40$ eV), when nanocrystals within the supracrystal keep similar interparticle distance (~1.8-nm) *i.e.* nanocrystals are coated with C_{12} derivatives. This difference is larger with supracrystals of 5.9-nm Ag nanocrystals coated with longer chain length of C_{18}-NH_2 ($\Delta E = 0.35$ eV). The interparticle distance of the latter is larger (3.1 nm) than that obtained with C_{12} derivatives (~1.8-nm). This clearly supports our claim that these differences in the maximum SPR positions between deposited and dispersed nanocrystals are due to dipolar interactions. Furthermore, the SPR spectrum of supracrystals coated with C_{12}-SH is red shifted compared to that of C_{12}-NH_2 with a difference in energy of 0.12 eV (Table 3 and Figure 6e). This difference can hardly be attributed to the slight variations in the average diameter between the two samples (6.3-nm and 6.0-nm, respectively) and is thought to stem from the decrease in the conductivity of the outer layer of the Ag-nanocrystals within the supracrystals compared to the inner core. That confirms the influence of the coating agent on the SPR spectra.

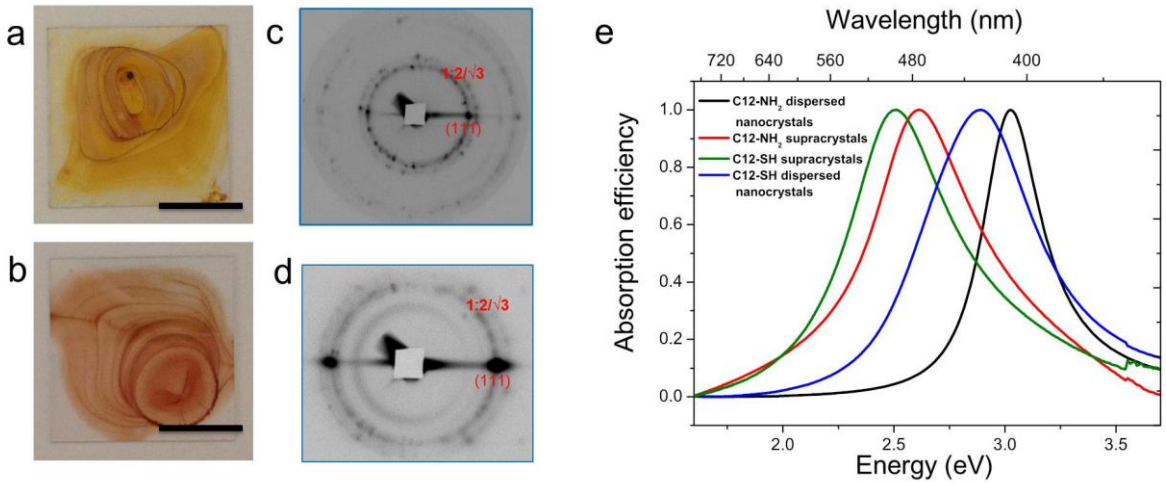

Figure 6. Optical images, X-ray diffraction patterns and SPR spectra of the thin supracrystalline films on glass made from 5.9-nm Ag nanocrystals with different coating agents: (a, c) dodecylamine (C_{12}-NH_2); (b, d) dodecanethiol (C_{12}-SH); (e) SPR spectra of the supracrystalline films coated with either C_{12}-NH_2 (red) or C_{12}-SH (green) and the SPR spectra of dispersed nanocrystals coated with either C_{12}-NH_2 (black) or C_{12}-SH (blue). The scale bar in the optical images is 1 cm.

Table 3. The interparticle distance (δ_{pp}) between Ag nanocrystals in the supracrystals differing by the coating agent C_{12}-NH_2 and C_{12}-SH. The maximum SPR wavelength and the corresponding energy of the SPR peak of Ag nanocrystals either dispersed in toluene or within the supracrystals recorded when the incident angle is 0 °

Ag nanocrystal	6.3-nm C_{12}-NH_2	6.0-nm C_{12}-SH
Size distribution	8%	9%
δ_{pp} / nm	1.8	1.9
Dispersed nanocrystal SPR peak value /eV	3.02	2.89
Supracrystal SPR peak value/eV	2.61	2.49
ΔE /eV	0.41	0.40

Table 4. SPR peak position of the longitudinal and transverse peaks with ~6-nm Ag-nanocrystal sizes coated with either dodecylamine (C_{12}-NH_2) or dodecanethiol (C_{12}-SH) when the incident angle is 60°

Ag nanocrystal	E (longitudinal peak/eV)	λ max (longitudinal/nm)	E (transverse peak/eV)	λ max (transverse/nm)
6.3-nm C_{12}-NH_2	2.61	475	3.41	364
6.0-nm C_{12}-SH	2.50	496	3.30	376

For an incident angle θ = 60° and by replacing C_{18}-NH_2 by C_{12}-NH_2 as coating agent, a rather good agreement is obtained between the data, whereas a marked discrepancy is observed when replacing C_{12}-NH_2 by C_{12}-SH (Figure 5). This is consistent with the fact that in the case of NH_2 when the coating agent keeps the same head polar group, the change in the conductivity of the outer layer of the nanocrystals is negligible. In the case of SH, when the strength of the interactions between Ag atoms at the surface and the head polar group is increased, the SPR resonance shifts to the lower energy. From these data it is concluded that dipolar interactions play the major role in the plasmonic properties of 3D thin supracrystals. However, the contribution of coating agents of nanocrystals embedded in supracrystals cannot be neglected. The high similitude between the DDA simulation of 2D superlattices [13] and the experimental data obtained with thin film supracrystals indicates that the substrate effect is negligible.

Here, we used another method to produce thin supracrystals film. A recent study shows that, by deposition of a colloidal solution at the diethylene glycol (DEG)/air interface, the nanocrystal ordering is markedly improved [36]. Hence, for comparison, the same amount of Ag nanocrystals coated with C_{18}-NH_2 colloidal solution, as used above was deposited on DEG liquid in a Teflon well. The supracrystalline film is formed at the interface of DEG/air and is transferred either on a TEM grid or on a glass substrate. The TEM images (Fig. S5) confirm a larger coherence length of Ag nanocrystal films as observed previously [36]. By deposition on glass a better homogeneity compared to drop deposition process (Fig. 2) is observed. However, some inhomogeneities can still be observed. The X-ray diffraction patterns (Fig. S6) is typical for a restricted number of well-ordered stacking monolayers. Spots become elongated perpendicular to the substrate compared to Figure 2. The interparticle distances (Table S1) deduced from the SAXRS patterns are almost the same for the supracrystalline films obtained by the two different methods. Optical measurements similar as those described

above were carried out on those supracrystalline films (Figure S7a). Similar trends are observed with a normal incident light to the substrate; that is, a red shift (low energy shift) occurs when increasing the nanocrystal sizes. However, Figure S7b shows a non-negligible decrease of the maximum energy of the SPR band that does not follow the same trend as that observed in Figure 3b. Similarly, by increasing θ from 0^O to 60^O, a splitting in the SPR spectrum takes place as observed in Figure S8. However, a careful analysis of these spectra shows that the evolution of the longitudinal and transverse SPR maximum energies with γ markedly change compared to what is shown on Figure 6 (Figure S9). These differences cannot be attributed to the changes in the interparticle distances that remain similar to those obtained by drop deposition (Table S1). Hence such differences are attributed to diffusion of DEG molecules inducing a change in the nanocrystal environments and consequently in the optical properties of nanocrystals within the supracrystals. This is also supported by the fact that it is impossible to image by STM the supracrystal film produced by using the DEG method and deposited on HOPG, whereas by simple solvent evaporation of same amount of colloidal solutions on HOPG, the film is very easily imaged with the appearance of well-defined Ag nanocrystals.

CONCLUSIONS

By comparing the SPR spectra of dispersed Ag nanocrystals and their assemblies of supracrystalline films, marked changes were discovered. Very surprisingly, data obtained here show a good agreement between simulated optical properties in 2D superlattices with 3D thin films self-assembled in fcc crystalline structure. The energy discrepancy (ΔE), determined from the difference in SPR band between dispersed nanocrystals and their assemblies was used to evaluate the collective optical properties due to nanocrystal ordering. It is found that ΔE is mainly determined by both the nanocrystals sizes and the interparticle distances inside the supracrystal. Upon increasing the nanocrystals sizes while keeping the interparticle distance constant, ΔE values showed a monotonic increase. Furthermore, it was shown that engineering the interparticle distance of nanocrystals of similar size within a supracrystal, can effectively modulate the optical properties of the Ag supracrystalline films.

REFERENCES

1. Pileni, M. P., Nanocrystal self-assemblies: Fabrication and collective properties. *J. Phys. Chem. B* **2001,** *105*, 3358-3371.
2. Pileni, M. P., Self organization of inorganic nanocrystals: Unexpected chemical and physical properties. *J. Colloid Interface Sci,* **2012,** *388*, 1-8.
3. Sun, S. H.; Murray, C. B.; Weller, D.; Folks, L.; Moser, A., Monodisperse FePt nanoparticles and ferromagnetic FePt nanocrystal superlattices. *Science* **2000,** *287*, 1989-1992.
4. Shevchenko, E. V.; Talapin, D. V.; Kotov, N. A.; O'Brien, S.; Murray, C. B., Structural diversity in binary nanoparticle superlattices. *Nature* **2006,** *439*, 55-59.
5. Murray, C. B.; Kagan, C. R.; Bawendi, M. G., Synthesis and characterization of monodisperse nanocrystals and close-packed nanocrystal assemblies. *Annu. Rev. Mater. Sci.* **2000,** *30*, 545-610.
6. Yang, Z.; Lisiecki, I.; Walls, M.; Pileni, M.-P., Nanocrystallinity and the Ordering of Nanoparticles in Two-Dimensional Superlattices: Controlled Formation of Either Core/Shell (Co/CoO) or Hollow CoO Nanocrystals. *ACS Nano* **2013,** *7*, 1342-1350.
7. Talgorn, E.; Abellon, R. D.; Kooyman, P. J.; Piris, J.; Savenije, T. J.; Goossens, A.; Houtepen, A. J.; Siebbeles, L. D. A., Supercrystals of CdSe Quantum Dots with High Charge Mobility and Efficient Electron Transfer to TiO2. *ACS Nano* **2010,** *4*, 1723-1731.
8. Goubet, N.; Yan, C.; Polli, D.; Portales, H.; Arfaoui, I.; Cerullo, G.; Pileni, M.-P., Modulating Physical Properties of Isolated and Self-Assembled Nanocrystals through Change in Nanocrystallinity. *Nano Lett.* **2013,** *13*, 504-508.
9. Goubet, N.; Pileni, M. P., Analogy Between Atoms in a Nanocrystal and Nanocrystals in a Supracrystal: Is It Real or Just a Highly Probable Speculation? *J. Phys. Chem. Lett.* **2011,** *2*, 1024-1031.
10. Courty, A.; Mermet, A.; Albouy, P. A.; Duval, E.; Pileni, M. P., Vibrational coherence of self-organized silver nanocrystals in f.c.c. supra-crystals. *Nat. Mater.* **2005,** *4*, 395-398.
11. Remacle, F.; Collier, C. P.; Markovich, G.; Heath, J. R.; Banin, U.; Levine, R. D., Networks of quantum nanodots: The role of disorder in modifying electronic and optical properties. *J. Phys. Chem. B* **1998,** *102*, 7727-7734.

12. Yang, P.; Arfaoui, I.; Cren, T.; Goubet, N.; Pileni, M.P.; Electronic properties probed by scanning tunneling spectroscopy: From isolated gold nanocrystal to well-defined supracrystals; *Phys. Rev. B,* **2012**, 86, 075409.
13. Yang, P.; Portalès, H.; Pileni, M.P.; Ability to discern the splitting between longitudinal and transverse plasmon resonances in Au compared to Ag Nanoparticles in close-packed planar arrays; *Phys. Rev. B,* **2010**, 81, 205405.
14. Parthasarathy, R.; Lin, X. M.; Jaeger, H. M., Electronic transport in metal nanocrystal arrays: The effect of structural disorder on scaling behavior. *Phys. Rev. Lett.* **2001,** *87*.
15. Shalaev, V. M., Transforming light. *Science* **2008,** *322*, 384-386.
16. Wertime, T. A., Begingins of Metallurgy-New *Science* **1973,** *182*, 875-887.
17. Rycenga, M.; Cobley, C. M.; Zeng, J.; Li, W.; Moran, C. H.; Zhang, Q.; Qin, D.; Xia, Y., Controlling the Synthesis and Assembly of Silver Nanostructures for Plasmonic Applications. *Chem. Rev.* **2011,** *111*, 3669-3712.
18. Lal, S.; Link, S.; Halas, N. J., Nano-optics from sensing to waveguiding. *Nat. Photonics* **2007,** *1*, 641-648.
19. Jain, P. K.; Lee, K. S.; El-Sayed, I. H.; El-Sayed, M. A., Calculated absorption and scattering properties of gold nanoparticles of different size, shape, and composition: Applications in biological imaging and biomedicine. *J. Phys. Chem. B* **2006,** *110*, 7238-7248.
20. Kelly, K. L.; Coronado, E.; Zhao, L. L.; Schatz, G. C., The optical properties of metal nanoparticles: The influence of size, shape, and dielectric environment. *J. Phys. Chem. B* **2003,** *107*, 668-677.
21. Wei, J. J.; Schaeffer N.; Pileni, M. P. *J. Phys. Chem. B* **2014,** *118*, 14070-14075.
22. Salzemann, C.; Brioude, A.; Pileni, M. P., Tuning of copper nanocrystals optical properties with their shapes. *J. Phys. Chem. B* **2006,** *110*, 7208-7212.
23. Lazarides, A. A.; Schatz, G. C., DNA-linked metal nanosphere materials: Structural basis for the optical properties. *J. Phys. Chem. B* **2000,** *104*, 460-467.
24. Peng, S.; McMahon, J. M.; Schatz, G. C.; Gray, S. K.; Sun, Y., Reversing the size-dependence of surface plasmon resonances. *Proc. Nat. Acad. Sci. U. S. A.* **2010,** *107*, 14530-14534.
25. Link, S.; El-Sayed, M. A., Spectral properties and relaxation dynamics of surface plasmon electronic oscillations in gold and silver nanodots and nanorods. *J. Phys. Chem. B* **1999,** *103*, 8410-8426.

26. Taleb, A.; Russier, V.; Courty, A.; Pileni, M. P., Collective optical properties of silver nanoparticles organized in two-dimensional superlattices. *Phys. Rev. B* **1999,** *59*, 13350-13358.
27. Nilius, N.; Ernst, N.; Freund, H. J., Photon Emission Spectroscopy of Individual Oxide-Supported Silver Clusters in a Scanning Tunneling Microscope. *Phys. Rev. Lett.* **2000,** *84* , 3994-3997.
28. Su, K. H.; Wei, Q. H.; Zhang, X.; Mock, J. J.; Smith, D. R.; Schultz, S., Interparticle coupling effects on plasmon resonances of nanogold particles. *Nano Lett.* **2003,** *3*, 1087-1090.
29. Ye, X.; Chen, J.; Diroll, B. T.; Murray, C. B., Tunable Plasmonic Coupling in Self-Assembled Binary Nanocrystal Super lattices Studied by Correlated Optical Microspectrophotometry and Electron Microscopy. *Nano Lett.* **2013,** *13*, 1291-1297.
30. Purcell, E. M.; Pennypac Cr, Scattering and Absorption of Light by Nonspherical Dielectric Grains. *Astrophysical J.* **1973,** *186*, 705-714.
31. Yang, S.-C.; Kobori, H.; He, C.-L.; Lin, M.-H.; Chen, H.-Y.; Li, C.; Kanehara, M.; Teranishi, T.; Gwo, S., Plasmon Hybridization in individual Gold Nanocrystal Dimers: Direct Observation of Bright and Dark Modes. *Nano Lett.* **2010,** *10*, 632-637.
32. Amendola, V.; Bakr, O. M.; Stellacci, F., A Study of the Surface Plasmon Resonance of Silver Nanoparticles by the Discrete Dipole Approximation Method: Effect of Shape, Size, Structure, and Assembly. *Plasmonics* **2010,** *5*, 85-97.
33. Henry, A. I.; Courty, A.; Pileni, M. P.; Albouy, P. A.; Israelachvili, J., Tuning of solid phase in supracrystals made of silver nanocrystals. *Nano Lett.* **2008,** *8*, 2000-2005.
34. Whetten, R. L.; Khoury, J. T.; Alvarez, M.M.; Murthy, S.; Vezmar, I.; Wang, Z.L.; Cleveland, C.C.; Luedtke, W.D.; Landman, U. *Adv. Mater*. **1996**, *8*, 428-433.
35. Alaeian, H.; Dionne, J. A., Plasmon nanoparticle superlattices as optical-frequency magnetic metamaterials. *Opt. Express* **2012,** *20*, 15781-15796.
36. Dong, A. G.; Chen, J.; Vora, P. M.; Kikkawa, J. M.; Murray, C. B., Binary nanocrystal superlattice membranes self-assembled at the liquid-air interface. *Nature* **2010,** *466*, 474-477.

4.3 Supporting Information

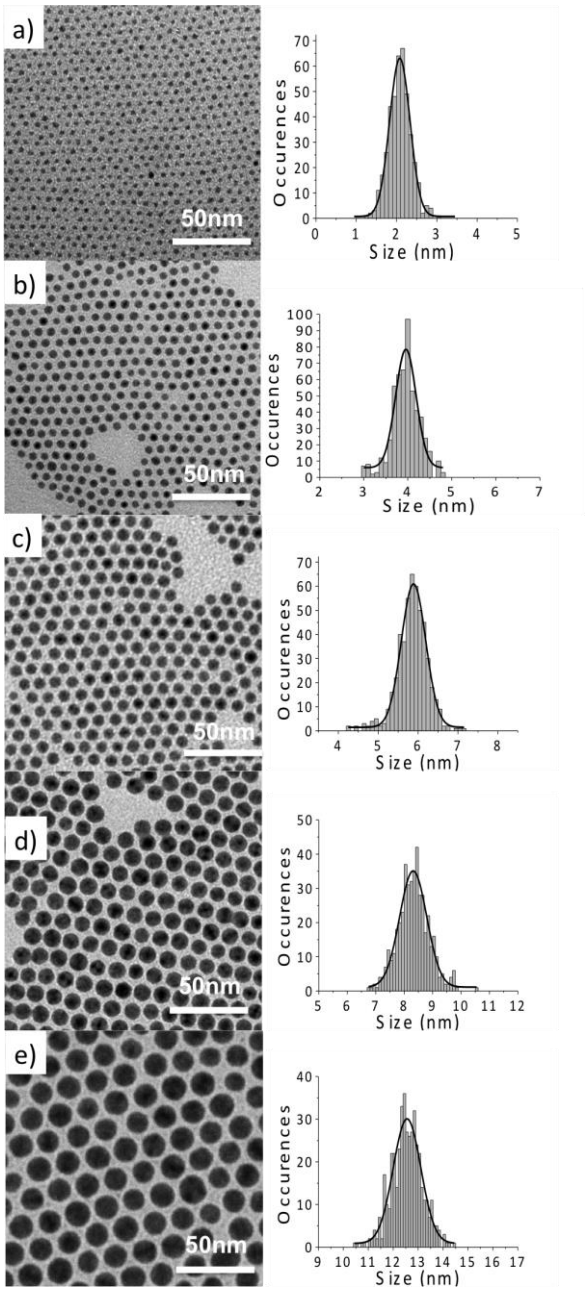

Figure S1: TEM images and size histograms of the silver nanocrystals coated with oleylamine with various diameters : (a) 2.2 nm (b) 4.1 nm (c) 5.9 nm (d) 8.7 nm (e) 12.9 nm.

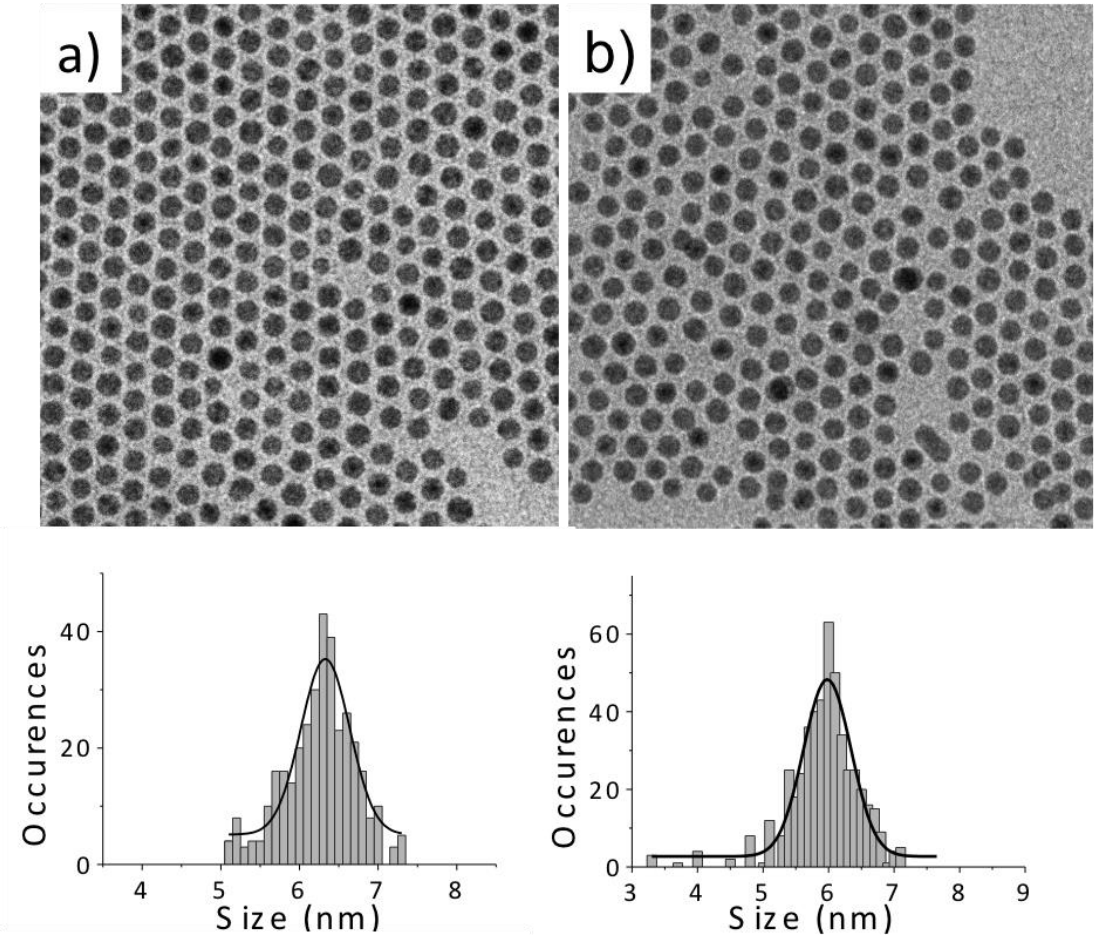

Figure S2: TEM images and size histograms of the ~6- nm nanocrystals coated with different coating agents: (a) nanocrystals coated with dodecylamine (b) nanocrystals coated with dodecanethiol.

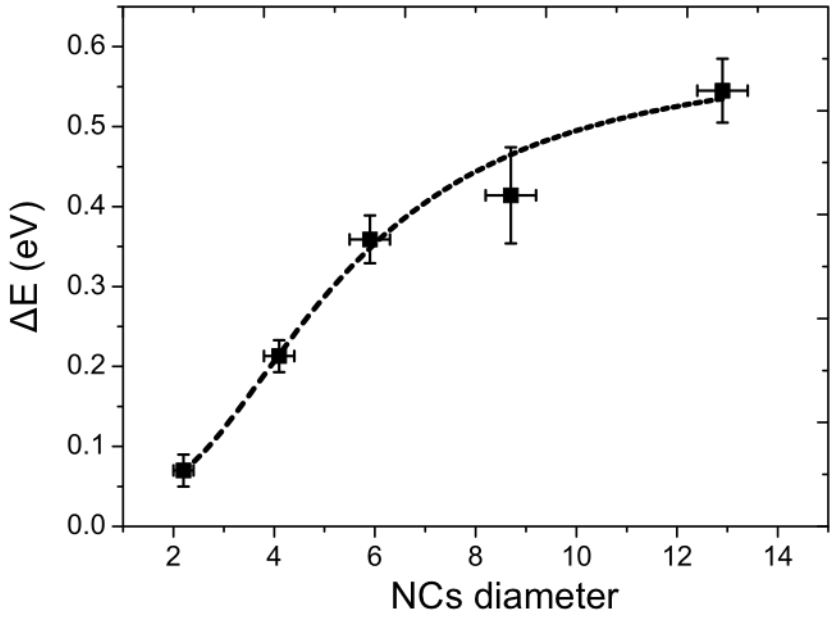

Figure S3: plot of the ΔE (the energy difference of the SPR peak position between the dispersed samples and the supracrystalline films) against nanocrystal diameter.

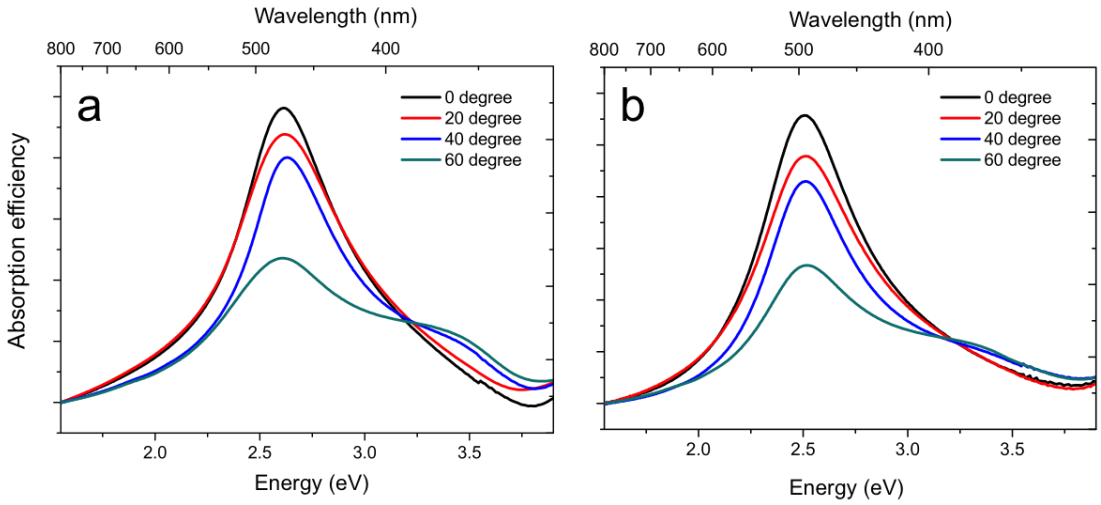

Figure S4. SPR spectra of the supracrystal films of nanocrystals coated with C12-NH_2 (a) or C12-SH (b) at various incident angles.

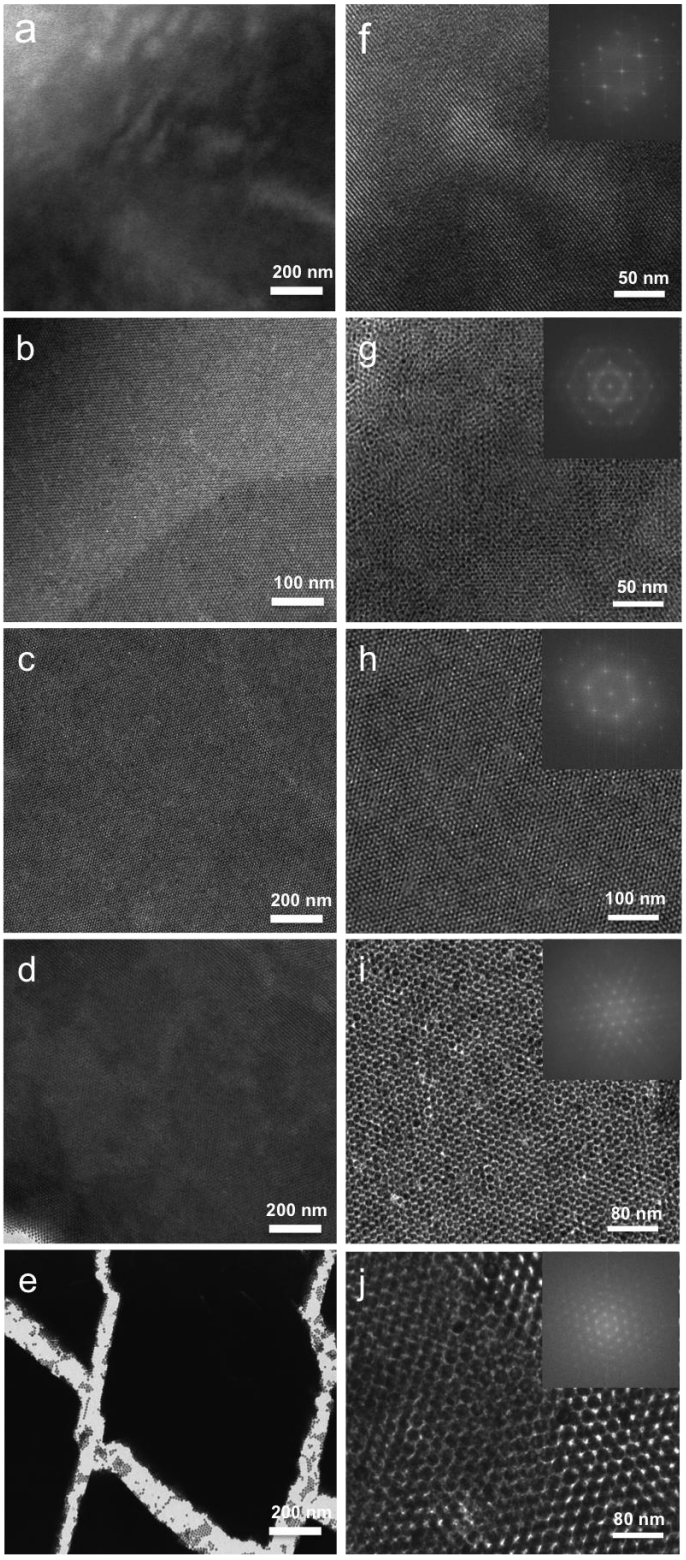

Figure S5. Large scale and magnified TEM images of thin supracrystalline films of oleyamine (C_{18}-NH_2) coated Ag nanocrystals differing by their diameters obtained from the DEG method: (a, f) 2.2 nm (b, g) 4.1 nm (c, h) 5.9 nm (d, i) 8.7 nm (e. j) 12.9 nm. Inset: FFT.

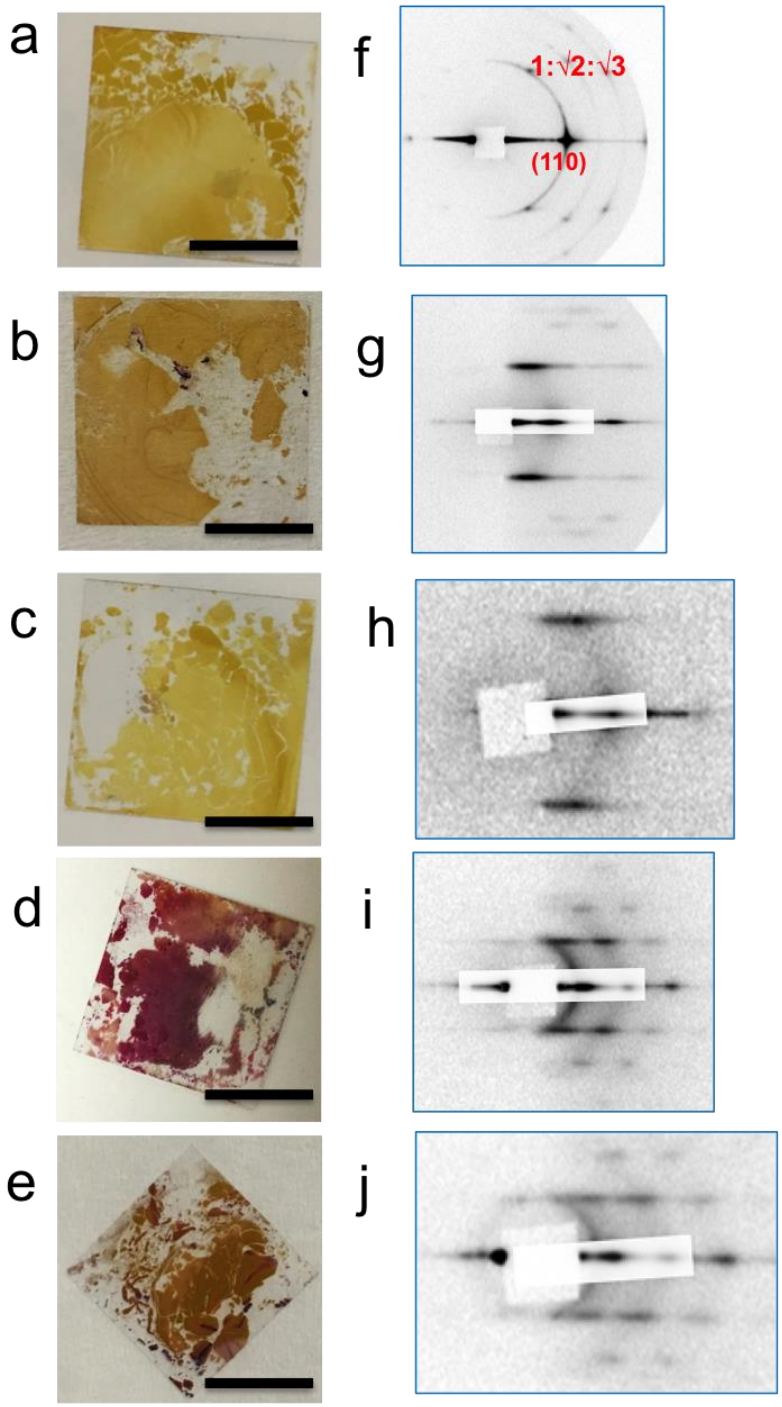

Figure S6. Optical images of the supracrystalline films on glass substrate obtained by DEG method and corresponding small angle X-ray scattering (SAXRS) of thin supracrystals of Ag nanocrystals coated with oleylamine (C_{18}-NH_2) and differed by their diameters: (a, f) 2.2 nm (b, g) 4.1 nm (c, h) 5.9 nm (d, i) 8.7 nm (e, j) 12.9 nm. The scale bars in the optical images all are 1cm.

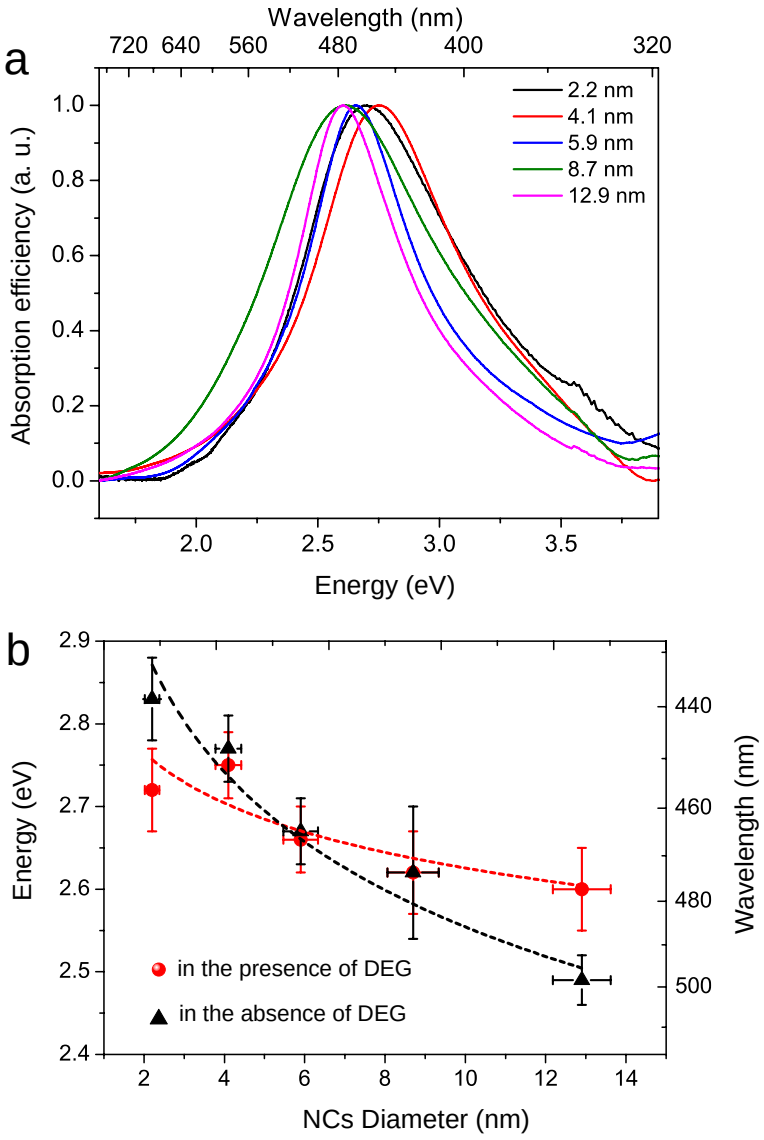

Figure S7. (a) Normalized SPR spectra of Ag supracrystalline films coated with C18-NH_2 differing by nanocrystal sizes obtained from the DEG method at incident angle of 0^O. (b) Plots of the SPR peak positions with various Ag nanocrytal sizes: (red sphere) supracrystals produced in the presence of DEG; (black triangle) supracrystals produced in the absence of DEG.

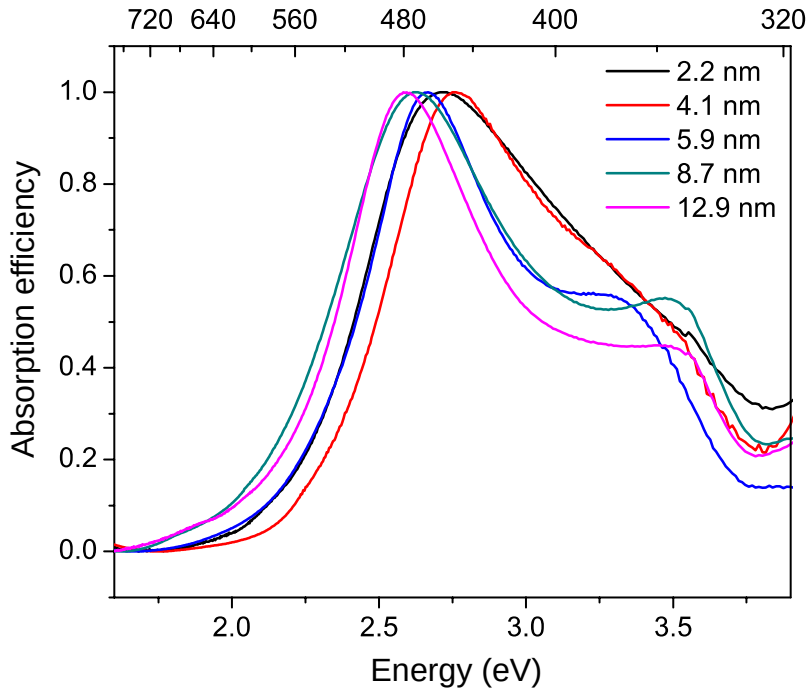

Figure S8. SPR spectra of the supracrystal films of nanocrystals coated with C18-NH_2 differing by nanocrystal sizes obtained from DEG method at incidence angles of 60 °

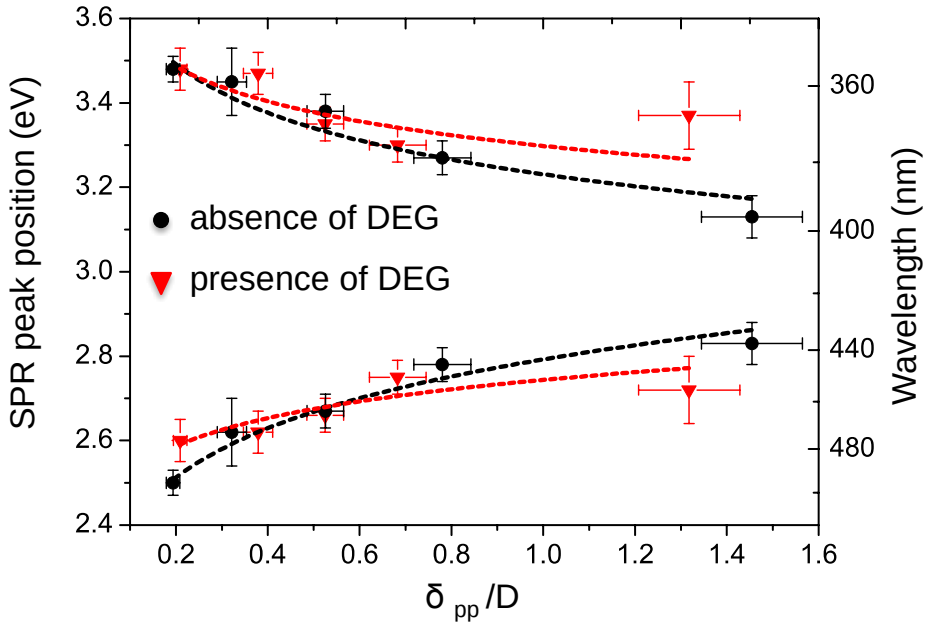

Figure S9. Plot of the longitudinal and transverse SPR peak position value against δ_{pp}/D in the absence (black) and presence of DEG (red).

Table S1. Interparticle distance (δ pp) between Ag nanocrystal coated with C18-NH2 within the supracrystals obtained by DEG method, deduced from small angle X-ray scattering (SAXRS) measurements; Longitudinal and transverse SPR peak position of the supracrystals obtained from DEG method with various Ag-nanocrystal sizes coated with oleylamine (C18-NH_2).

Incident angle	Nanocrystal size/nm	2.2	4.1	5.9	8.7	12.9
	δpp /nm	2.9	2.8	3.1	3.3	2.7
0^o	E/eV	2.72	2.75	2.66	2.62	2.60
	λ_{max} /nm	456	451	466	473	477
60^O	E/eV longitudinal	2.71	2.75	2.67	2.62	2.60
	λ_{max} /nm	457	451	464	473	477
	E/eV transverse	3.37	3.30	3.35	3.47	3.48
	λ_{max} /nm	367	376	370	357	356

Chapter 5
Surface Chemistry Controls the Crystal Structures in Binary Nanocrystal Superlattices

5.1 Abstract

Surface chemistry is of particular importance for nanocrystals in modulating their chemistry and physical properties. In this chapter, we demonstrate that the hydrophobic coating agent of nanocrystals can play a role in the formation of binary nanocrystal superlattices where two distinct nanocrystals, coated with either the same or two different coating agents. First we consider Ag nanorystals differing by their average diameters with the same coating agent: oleylamine (OAM). Crystalline structures of the binary nanocrystal superlattices, such as NaCl, AlB_2, $NaZn_{13}$ and $MgZn_2$, are obtained and are in good agreement with the hard sphere model predicted from the space-filling curves.

However, when the binary nancrystals differing by their diameters are coated with two different ligands oleylamine (OAM) and dodecanethiol (DDT), the supercrystal structures produced cannot be simple predicted from the space-filling curves and various structures such as Cu_3Au, CaB_6, quasicrystalline ordering are produced. This ligands effect is also extended to other binary system, such as Ag-Au and $CoFe_2O_4$-Ag. In the case of $CoFe_2O_4$-Ag, packing motif of the periodic (3^2.4.3.4) Archimedean tiling can also be observed. For binary nanocrystal mixtures containing two or more kinds of coating agents, rich crystal phases can be produced, while the phase purity of the binary superlattices is much more difficult to control despite the crystal domain size can also be up to micrometer scale in some cases. These data implies that the ability to control the surface chemistry (ligand exchange process) in binary system may provide another fruitful way to modify the crystal phases in binary nanocrystal superlattices.

Ligand exchange mechanism is proposed in the binary system with multiple ligands, which may affect the thermodynamics in the system. Hence the formation of a binary superlattice with lower packing density may be favored kinetically because the required energetic penalty is smaller than that for a denser structure.

5.2 Article : Surface Chemistry Controls the Crystal Structures in Binary Nanocrystal Superlattices

Surface Chemistry Controls the Crystal Structures in Binary Nanocrystal Superlattices

Jingjing Wei,[a,b] Nicolas Schaeffer,[a,b] Marie-Paule Pileni[a, b, c]*

[a] Sorbonne Universités, UPMC Univ Paris 06, UMR 8233, MONARIS, F-75005, Paris, France

[b] CNRS, UMR 8233, MONARIS, F-75005, Paris, France

[c] CEA/IRAMIS, CEA Saclay, 91191, Gif-sur-Yvette, France

INDRODUCTION

Self-assembly of micrometer-sized colloids have been intensively studied, and the phase behavior of those colloids is determined by minimizing the free energy F = U – TS or, since those colloids are forbidden to interpenetrate and the thermal energy U is a constant, by maximizing the entropy S.[1-5] Coming to the nanoscale, owing to the surface coat of flexible organic molecules, the assembly process is accompanied by effective control over the interactions between the nanocrystals and all entropic forces.[6-8] The interaction between nanocrystals can be described by a soft model, which assumes isotropic nanocrystal interaction potentials and, thus predicts the formation of close-packed arrays.[9,10] However, the electrical charge induced by ligand and the surface coverage of the ligand introduces important perturbations that can lead to the formation of superlattices with lower packing density.[11,12] Although advances have been made using a variety of electrostatic forces, covalent and noncovalent molecular interactions, to control the crystal structure, it remains a challenge to use spontaneous self-assembly to predict the phase structures comprised of two different types of building blocks, namely binary nanocrystal superlattices.[13]

A variety of crystal phases in binary nanocrystal superlattices have been fabricated from nanocrystals of semiconductors, metals and oxides, and the prediction of crystal

structures is mainly replies on the space-filling principles. In addition to the well-known crystal structures analogous to NaCl, AlB_2, $NaZn_{13}$ and laves phases that observed in binary microcolloids,[14-16] other phases such as CuAu-type, Cu_3Au-type, Fe_4C-type, CaB_6-type as well as quasicrystalline ordering are also discovered in binary nanocrystal superlattices.[17-20] The emergence of these binary nanocrystal superlattices that cannot be simply predicted from the hard-sphere models needs to be further studied.

In the present paper, colloidal binary nanocrystal mixtures containing two distinct nanocrystals with either the same surface coating, or the different surface coating, are used to grow binary nanocrystal superlattices, respectively. We describe a systematic study on binary nanocrystal superlattices from Ag-Ag binary mixtures with two distinct nanocrystal sizes, aiming to shed light on the effect of surface capping on the structure control of binary nanocrystal superlattices. Furthermore, this effect can be extended to the other binary systems, such as Ag-Au, and $CoFe_2O_4$-Ag.

EXPERIMENTAL SECTIONS

Materials. Silver nitrate (99.9%), methanol (99.8%), *o*-dichlorobenzene (99%), oleylamine (70%), dodecanediol (99%), dodecanethiol (99%) and *tert*-butylamine (97%) were purchased from Sigma, Chloro(triphenylphosphine)gold (98%) was purchased from STREM, toluene (98%) from Riedel de Haen, ethanol (99.8%) from Prolabo,. All reagents were used as received without further purification.

Apparatus. Transmission electron microscopy (TEM) images were obtained with a JEOL JEM 1011(100 kV). High-resolution scanning electron microscopy (HRSEM) images were obtained with Hitachi Su-70 instrument. The optical spectra Measurements have been performed on a conventional Varian Cary 5000 spectrophotometer in the energy interval 1.9-4.9 eV.

Synthesis of nanocrystals. Ag Nanocrystals with diameter of 3.7-nm and 5.5-nm were synthesized with hot injection method and the coating agent used is oleylamine [21]. For the synthesis of smaller 2.9-nm Ag nanocrystals, 100 μL of oleic acid and 1 mL of oleylamine were added. While the oleic acid was washed five times with ethanol-toluene cycle, and additional 50 μL of oleylamine was added during the washing cycle. The 7.5, 8.2, 9.6 and 11.9 nm Ag nanocrystals were synthesized with one-pot method and the coating agent is also oleylamine.[22] Thiol coated 4-nm Ag nanocrystals were prepared by

the reverse micelles method.[23] All the nanocrystals can be seen in the TEM images in Figure S1. All the nanocrystals were dispersed in toluene and exhibited a size distribution below 10% (Table 1). Synthesis of 4.0-nm Au nanocrystals coated with dodecanethiol was according to Stucky's method.[24] In addition, 12-nm $CoFe_2O_4$ nanocrystals coated with oleic acid were produced from thermal decomposition of a mixture of Co-oleate and Fe-oleate as published elsewhere.[25] The synthesis details and the TEM images of Au nanocrystals and $CoFe_2O_4$ are shown in supporting information (Figure S2).

Superlattices Formation. Self-assembly of binary colloidal solution is carried out in an experimental setup shown in elsewhere published before,[26] and the temperature can be controlled (*i.e.* 35ºC in the present study). Carbon-coated copper TEM grids were used as the substrate for self-assembly experiments. The grids were placed inside a glass vial with inner diameter of ~4 mm. Then 40 μL of solution containing a binary mixture of nanocrystals with the desired particle ratios, keeping the overall particle concentration constant ~1×10^{-6} M, was injected into the glass vial. Concentrations of the Ag nanocrystals were estimated by weighing the mass of the product. The mixed colloidal solution was evaporated under N_2 atmosphere.

RESULTS AND DISCUSSION

Here, nanocrystals differing by their composition, coating agents, diameters and characterized by low size distribution are used to engineer various binary nanocrystal superlattices. The coating agents used are either oleylamine (OAM), oleic acid (OA) or dodecanethiol (DDT). The nanocrystals differ by their composition include Ag, Au and $CoFe_2O_4$. Their sizes range from 2.9- to 12-nm for Ag nanocrystals and are 4-nm and 12-nm for Au and $CoFe_2O_4$, respectively. The various diameters (D) and their corresponding size distribution (δ) of these nanocrystals are shown in Table 1.

Two colloidal solutions containing either small (S) or large nanocrystals (L) are dispersed in toluene. The total nanocrystal concentration is fixed to $[Nanocrystals]_S = [Nanocrystals]_L = 1 \times 10^{-6}$ M. The relative ratio between small and large nanocrystals is determined by changing the relative volume of the two colloidal solutions. 40 μl of the mixed colloidal solution was injected into a beaker containing a carbon coated TEM grid. The deposition of colloidal mixture of nanocrystals differing by their diameters was carried out at 35ºC with the evaporation of the carrier solvent under N_2 flow.

Table 1. Various parameters of nanocrystals used as building blocks for the growth binary nanocrystal superlattices in the present work.

Nanocrystal@coating agent	Diameter/nm	Diameter distribution δ	D_{eff}/nm	D_{eff} distribution
Ag@OAM[#]	2.9	8%	5.9	7%
	3.7	6%	6.3	6%
	5.5	7%	8.0	6%
	7.5	8%	9.9	7%
	8.2	7%	10.8	5%
	9.6	7%	12.1	6%
	11.9	6%	14.3	5%
Ag@DDT[*]	4.0	9%	6.0	9%
Au@DDT[*]	4.0	8%	5.9	6%
$CoFe_2O_4$@OA[&]	12.0	5%	14.0	6%

OAM[#]: oleylamine; DDT[*]: dodecanethiol; OA[&]: oleic acid

The effective nanocrystal diameter, D_{eff}, is defined as the center-to-center distance between nanocrystals self-ordered in a compact hexagonal network, *i.e.,* as the sum of metal core diameter and twice the thickness of the organic ligand. The D_{eff} of the nanocrystals in this study are shown in Table 1. The effective diameter ratio, $\gamma_{eff,}$ is defined as $\gamma_{eff} = D_{eff\text{-}small}/D_{eff\text{-}large}$, plays a determining role during the assembly of binary mixtures.[28] By mixing the two colloidal solutions and by depositing the mixture on the TEM grid, during the evaporation process, the system is expected to adopt the crystal structure corresponding to the most efficient space filling system and reach the maximum packing density ρ for a given ratio of the sphere radii γ.[29]

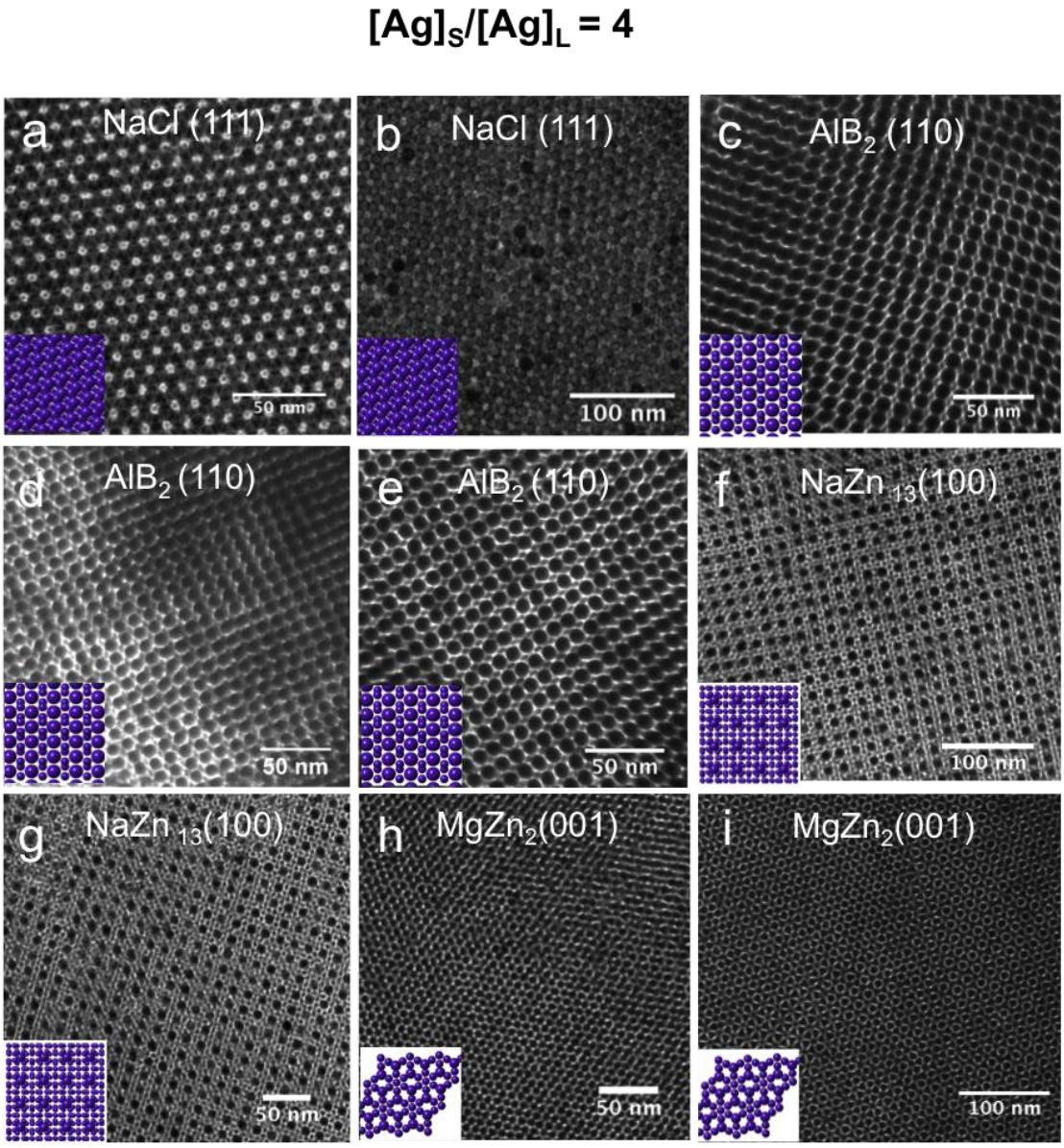

Figure 1. Binary nanocrystal superlattices formed from Ag@OAM single ligand system with $[Ag]_S/[Ag]_L$ =4: (a) 11.9 nm Ag@OAM and 2.9 nm Ag@OAM, γ_{eff} = 0.42; (b) 11.9 nm Ag@OAM and 3.7 nm Ag@OAM, γ_{eff} = 0.44; (c) 9.6 nm Ag@OAM and 3.7 nm Ag@OAM, γ_{eff} = 0.52; (d) 8.2 nm Ag@OAM and 2.9 nm Ag@OAM, γ_{eff} = 0.55; (e) 8.2 nm Ag@OAM and 3.7 nm Ag@OAM, γ_{eff} = 0.58; (f) 8.2 nm Ag@OAM and 3.7 nm, γ_{eff} = 0.58; (g) 7.5 nm Ag@OAM and 3.7 nm Ag@OAM, γ_{eff} = 0.64; (h) 5.5 nm Ag@OAM and 3.7 nm, γ_{eff} = 0.79; (i) 7.5 nm Ag@OAM and 5.5 nm Ag@OAM, γ_{eff} = 0.81.

Binary mixtures of Ag nanocrystals differing by their diameters and coated with oleylamine (OAM) called for simplicity Ag@OAM are first considered. The concentration ratio $[Ag]_S/[Ag]_L$ is fixed to 4. The large nanocrystals is characterized by an average diameter of 11.9-nm with a size distribution of 6% whereas the diameter and size distribution of small nanocrystals are 2.9 nm and 8% respectively with γ_{eff} = 0.42. In these conditions, AB-type binary superlattices were produced as shown in Figure 1a, where the small Ag@OAM nanocrystals are located into the vacancies between large Ag nanocrystals, isostructural with NaCl (Space Group *Fm3m*).[30] The TEM images show typical (111) crystal planes of NaCl-type binary superlattices with the corresponding crystal model in the insets. The size of crystal domains of this NaCl-type binary structures is up to ~10 micrometers (Figure S3, Supporting Information). Note that in addition to the binary system, in some part of the TEM grid, single-component superlattices self-assembled from 2.9-nm Ag nanocrystals can also be found. Although we mainly focused on the formation of binary structures, the formation of single component nanocrystal superlattices are also mentioned when observed and summarized in Tables 2. By keeping the large nanocrystals as 11.9-nm while replacing the smaller ones with 3.7-nm that induces the γ_{eff} increasing to 0.44, similar features are obtained with the formation of NaCl-type binary structures (Figure 1b and Figure S4). To increase the γ_{eff} value to 0.52, the average size of larger nanocrystals used was set to be 9.6-nm and the same small nanocrystals (3.7nm) were kept. In those conditions, the TEM images show the appearance of AlB_2-type structures (Figure 1c). A further increase of γ_{eff} to 0.55 and 0.58 by using large (8.2-nm) and small (2.9-nm and 3.7-nm) nanocrystals, respectively, long-range ordered AlB_2-type superlattices (Figure 1d) without any detectable single-component superlattices were produced. Yet another increase of γ_{eff} to 0.58 (8.2-nm and 3.7-nm) and 0.64 (7.5-nm and 3.7-nm) induces the formation of $NaZn_{13}$- (Figure 1f and 1g) binary structures. Finally, increasing the γ_{eff} value to 0.79 (5.5-nm and 3.7-nm) and 0.81 (7.5-nm and 5.5-nm) led to the formation of long-range ordered $MgZn_2$-type binary structures (Figure 1h and1i).

The data presented above are obtained for $[Ag]_S/[Ag]_L$ = 4. Previous studies showed that the change of the relative volume of colloidal solutions can induce the phase transformation in binary nanocrystal superlattices.[31] Here, the relative volume of colloidal solutions containing either small or large Ag@OAM nanocrystals were modulated, and the results in Table 2 show that similar data were produced with $[Ag]_S/[Ag]_L$= 2 and 10 (See

figures S5 and S6 for TEM images). In some cases, it appears amorphous phases and single-component Ag superlattices.

Table 2. The influence of the nanocrystal concentration ratios $[Ag]_S/[Ag]_L$ and effective diameter ratios γ_{eff} on the crystal structures of binary superlattices assembled from bidisperse Ag@OAM nanocrystals.

Nanocrystal ratios $[Ag]_S/[Ag]_L$			2:1	4:1	10:1
Ag_{large} size	Ag_{small} size	Effective size ratio γ_{eff}			
11.9 nm	2.9 nm	~0.42	NaCl	NaCl+ SCS*	NaCl + SCS*
11.9 nm	3.7 nm	~0.44	NaCl	NaCl + SCS*	NaCl + SCS*
9.6 nm	3.7 nm	~0.52	AlB_2	SCS* + AlB_2	SCS* + AlB_2
8.2 nm	2.9 nm	~0.55	AlB_2	AlB_2	AlB_2 + SCS*
8.2 nm	3.7 nm	~0.58	AlB_2	AlB_2 + $NaZn_{13}$	$NaZn_{13}$
7.5 nm	3.7 nm	~0.64	$NaZn_{13}$ + Am⌘	$NaZn_{13}$+ Am⌘	$NaZn_{13}$ + Am⌘
5.5 nm	3.7 nm	~0.79	$MgZn_2$ + Am⌘	$MgZn_2$ +SCS* + Am⌘	SCS*+ Am⌘
7.5 nm	5.5 nm	~0.81	$MgZn_2$	$MgZn_2$ +SCS*	$MgZn_2$+SCS*+ Am⌘

SCS*: single component nanocrystal superlattices

Am⌘: amorphous films

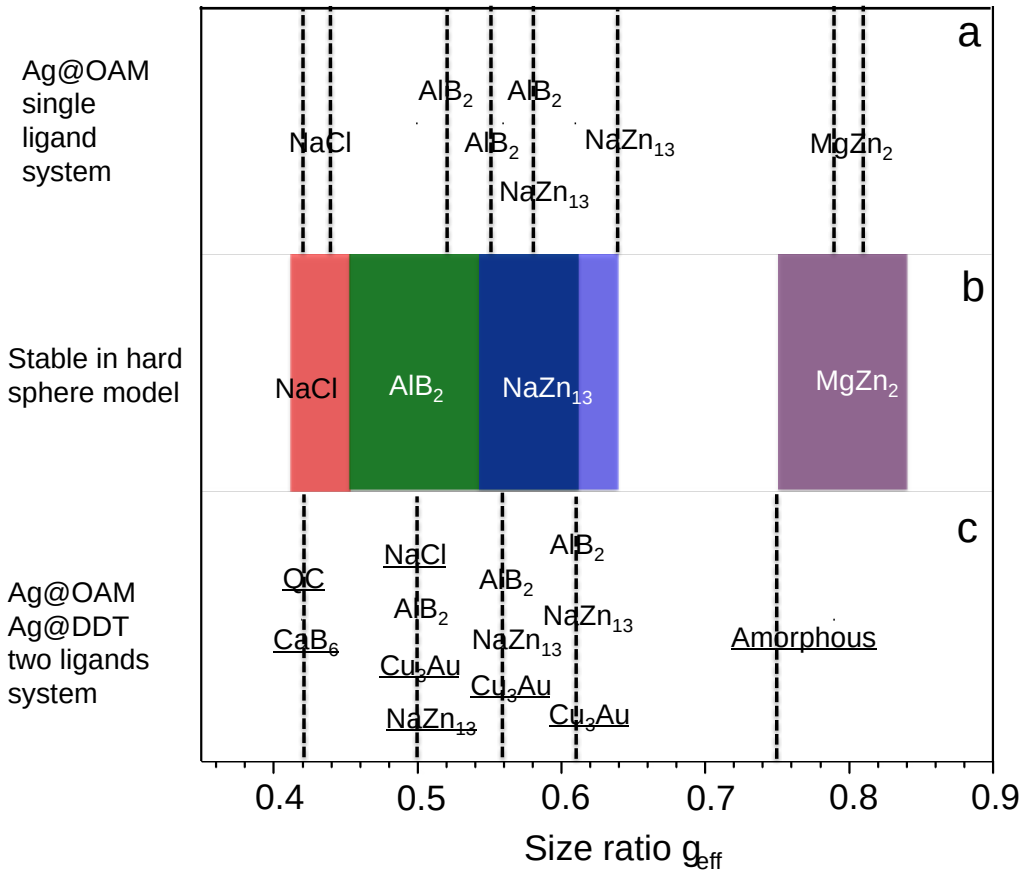

Figure 2. Various binary structures formed: (a) single ligand system (Ag@OAM); (b) hard sphere theoretical predictions; (c) two ligands (Ag@OAM) and (Ag@DDT) system.

Figures 2a and 2b clearly show a sequential structural evolution with the increase of γ going from NaCl, AlB_2, $NaZn_{13}$, to $MgZn_2$. All these crystal phases can also be observed in the microsized colloidal systems without the "soft" surface layer coating, called hard-sphere phases.[16] In the hard sphere system, the self-organization of micrometer-sized colloidal balls into binary structures was generally driven by pure entropic forces. During the condensation of the colloidal balls, the entropic change is positive and reaches maximum when the ordering has the highest packing density. To date, available theoretical predictions can be made based on the calculation of free energy of entropy contribution, and it was pointed out that NaCl, AlB_2 and $NaZn_{13}$ are stable in the range of $0.414 \leq \gamma \leq 0.45$, $0.45 \leq \gamma \leq 0.61$ and $0.54 \leq \gamma \leq 0.625$ respectively. Laves phases ($MgZn_2$, $MgCu_2$, $MgNi_2$) is stable in the range of $0.76 \leq \gamma \leq 0.84$.[14] Our results are highly consistent with the theoretical calculation for hard spheres models. These data confirm that the hard sphere model produced with microcolloids is also valid for nanocrystals with the same coating

agent. Consequently the space filing curves can be applied to predict the crystal phases of binary nanocrystal superlattices for the single ligand system.

The influence of the coating agent on the formation of binary structures was then investigated in order to verify if the hard sphere model is still responsible for the crystal phases of binary nanocrystal superlattices in the case of colloidal binary mixtures contain two kinds of nanocrystals differing by their coatings agents. Thus, 11.9-nm Ag@OAM nanocrystals were used as large nanocrystals, whereas small nanocrystals was replaced by 4.0-nm Ag nanocrystals coated with dodecanethiol (Ag@DDT). This corresponds to γ_{eff} value of ~0.42. The other experimental conditions remained the same and $[Ag]_S/[Ag]_L$ was kept equal to 4. Remarkable changes occur with this replacement. Figure 3b shows long-range ordered crystal domains up to micrometer scale of CaB_6-type superlattices, where six small Ag nanocrystals forming the octahedron, and this octahedron is surrounded by the simple cubic packed large Ag nanocrystal and matched well with the corresponding crystal model (inset in Figure 3b). This corresponds to the (100) plane of the CaB_6 phase. Note that this is opposite to what was observed with Ag@OAM binary systems, where neither the NaCl structure nor the single component superlattices could be observed. In some regions of the TEM grid, it was observed that the octahedral shape with six small Ag nanocrystals and single small Ag nanocrystals are separated by the large Ag nanocrystals in a random manner (Figure. 3d). While the fast Fourier transform (FFT) pattern shows the 12-fold symmetry for those structures, revealing its dodecagonal quasicrystalline (QC) order, which well agrees with the result of previous observation of such aperiodic structure.[32] Figure 3g shows that the layer-by-layer growth process of such QC superlattices is detected. The domain size of such QC order is very large and reaches several micrometers shown in Figure 4. It is of importance to note that the crystal domain boundaries between CaB_6 phase and QC phase are observed, as shown in Figure 3f, and agree with the reported growth mechanism based on entropic force.[31] It is also worth noting that this is the first demonstration on the QC order in the silver/silver binary materials. Similar experiments were carried out by changing the relative concentration $[Ag]_S/[Ag]_L$ from 2 to 10 and keeping the γ_{eff} =0.42, QC ordered superlattices were obtained for $2<[Ag]_S/[Ag]_L<4$. For $[Ag]_S/[Ag]_L=10$, only CaB_6 and single component superlattices were produced (Table 3).

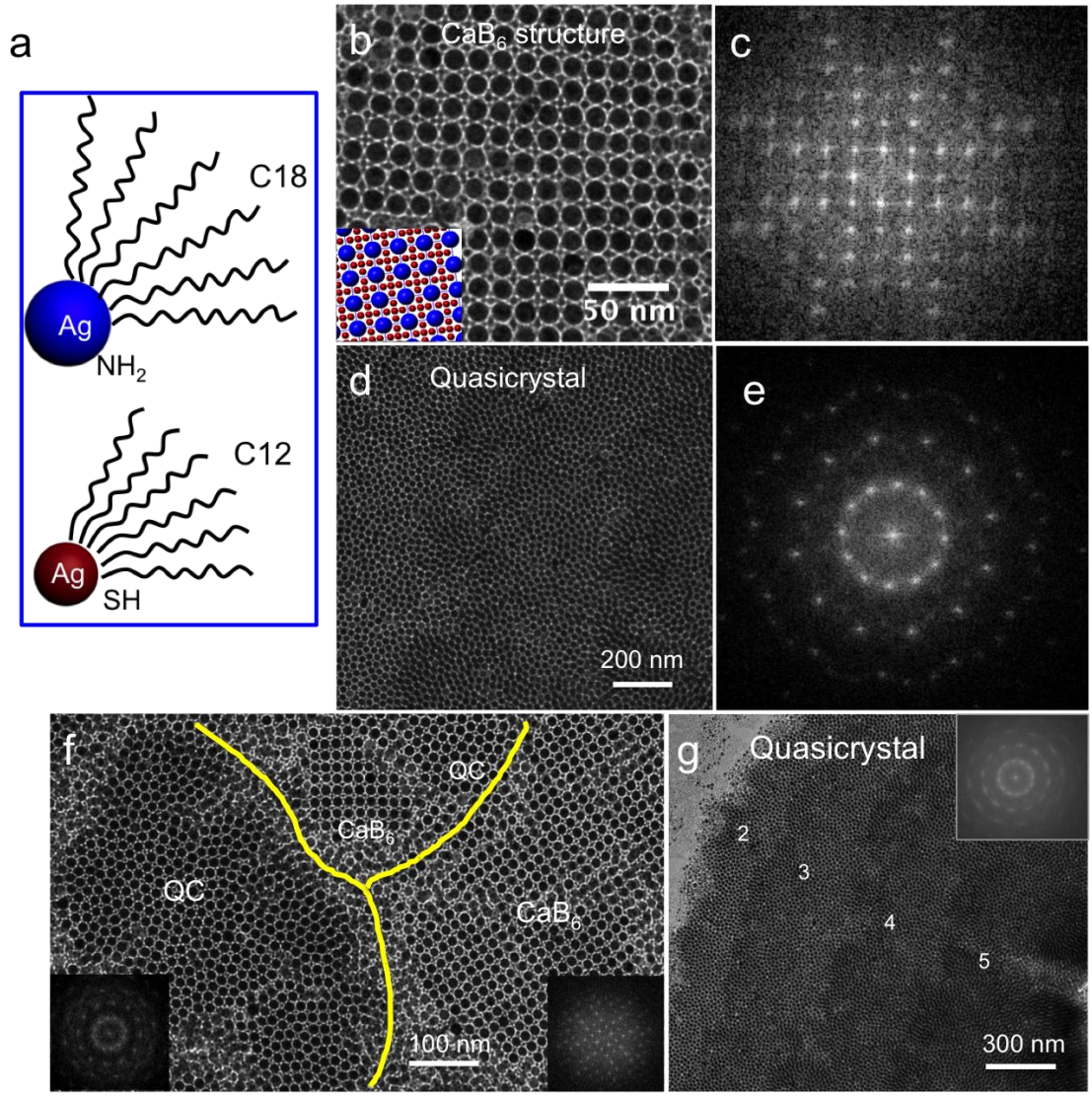

Figure 3. TEM images of binary superlattices formed with 11.9-nm Ag@OAM and 4.0-nm Ag@DDT binary mixtures: (a) schematic information of multiple ligand system; (b) TEM images of CaB_6-type binary nanocrystal superlattices with (100) planes parallel to the substrate; (c) corresponding FFT pattern to panel (b); (d) TEM images of QC order; (e) corresponding FFT pattern to panel (d); (f) mixture of the QC order in binary nanocrystal superlattices and CaB_6-type binary nanocrystal superlattices; (g) TEM images of large-scale QC with layer by layer structures (the numbers correspond to the different layers of QC order).

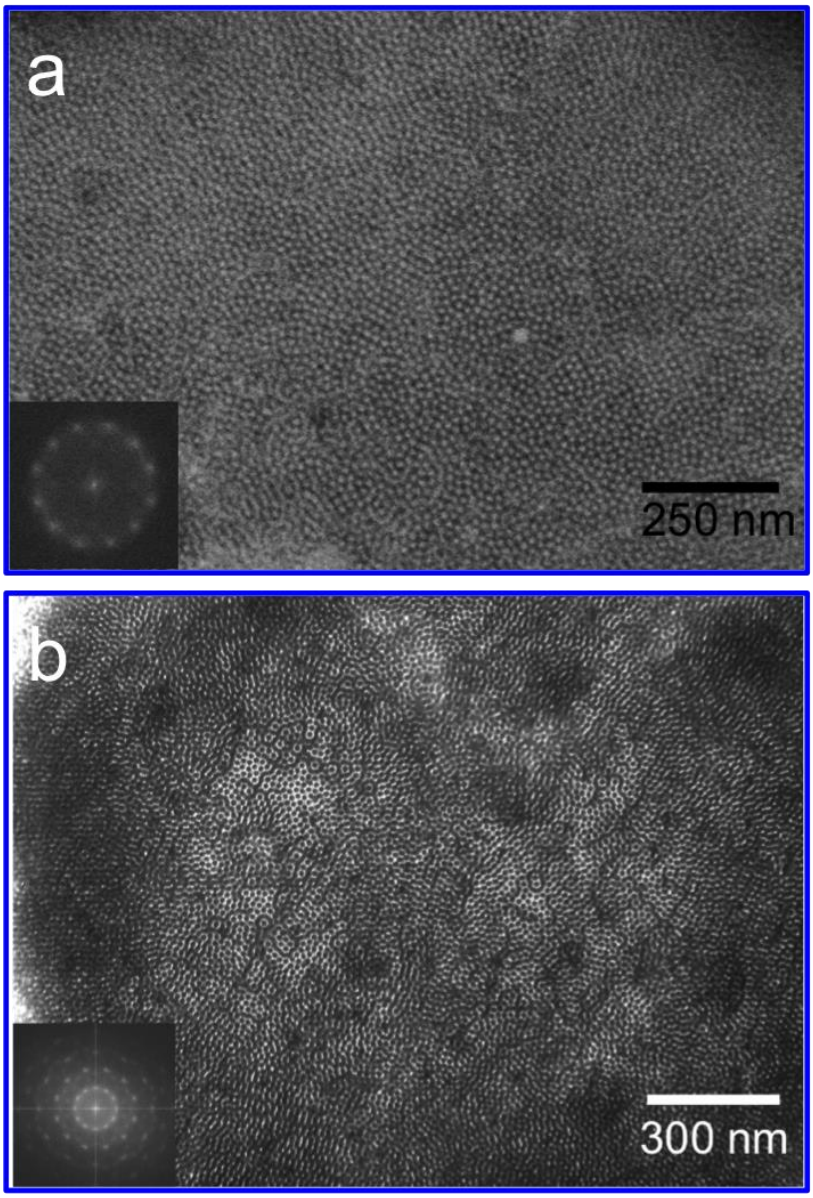

Figure 4. (a) HRSEM (High-Resolution Scanning Electron Microscopy) images of QC ordered superlattices formed with 11.9-nm Ag@OAM and 4.0-nm Ag@DDT binary mixtures; (b) low magnified TEM images of QC ordered superlattices formed with 11.9-nm Ag@OAM and 4.0-nm Ag@DDT binary mixtures.

Building on these data, we studied the influence on the overall binary system phase diagram when the large and small nanocrystals are stabilized by two distinct coating agent, respectively. Hence, experiments similar to those described above were carried out with Ag@OAM as the larger nanocrystals (5.5-nm $\leq$ D $\leq$ 11.9-nm) and Ag@DDT as the smaller one (D = 4-nm). By changing these parameters the γ_{eff} values evolve from 0.42 to

0.75. The total Ag concentration remained unchanged (1×10^{-6} M) and the relative concentration $[Ag]_S/[Ag]_L$ evolved from 2 to 10. On increasing γ_{eff} to 0.50, various phases, including NaCl, AlB_2, Cu_3Au and $NaZn_{13}$ structures appear, as depicted in Table 3 and TEM images in Figure 5. It is worth noting that AlB_2, NaCl and $NaZn_{13}$ phases are still present in these conditions. According to hard sphere theoretical predictions, AlB_2 is the predictable product, whereas the other structures, such as NaCl, Cu_3Au and $NaZn_{13}$, are not expected to be the outcome at this size ratio (γ_{eff} = 0.50) (Figure 2c). Furthermore, when γ_{eff} is increased to 0.56 and 0.61, unstable phase, such as Cu_3Au structure with a rather low packing efficiency was formed, and is not expected (see Figure S7, Supporting Information). Furthermore, $MgZn_2$ structure that is a highly stable phase in hard sphere model, but is not produced at a large γ_{eff} (~0.75), instead is the amorphous film without any ordering.

Table 3. The influence of the nanocrystal concentration ratios $[Ag]_S/[Ag]_L$ and effective diameter ratios γ_{eff} on the crystal structures of binary superlattices assembled of Ag nanocrystals differing by their sizes and coating agents (Ag@OAM and Ag@DDT)

Nanocrystal ratios $[Ag_{small}]/[Ag_{large}]$		2:1	4:1	10:1
Ag_{large} size	effective size ratio γ			
11.9 nm	~0.42	quasicrystal + CaB_6+ Am⌘	CaB_6+quasicrystal	CaB_6+SCS*
9.6 nm	~0.50	NaCl + AlB_2 + Cu_3Au	AlB_2 + Cu_3Au	AlB_2 + Cu_3Au + $NaZn_{13}$
8.2 nm	~0.56	AlB_2 + $NaZn_{13}$	AlB_2 + $NaZn_{13}$+ Cu_3Au	$NaZn_{13}$
7.4 nm	~0.61	AlB_2 + $NaZn_{13}$	AlB_2 + Cu_3Au	Am + SCS*
5.5 nm	~0.75	Am⌘	Am⌘	Am⌘

SCS*: single-component nanocrystal superlattices

Am⌘: amorphous film

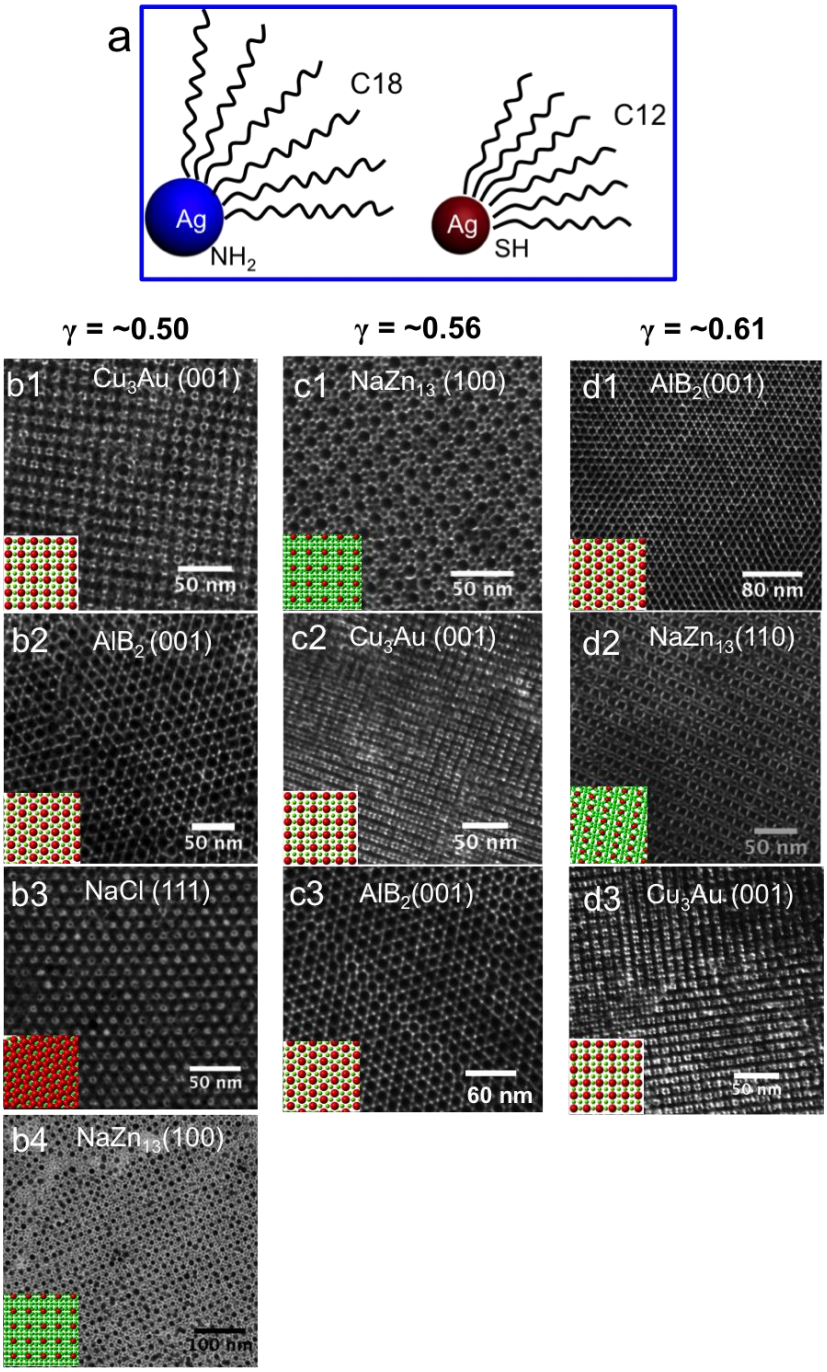

Figure 5. TEM images of binary superlattices formed with Ag@OAM and Ag@DDT binary mixtures: (a) schematic information of multiple ligand system; (b1-b4) TEM images of Cu_3Au, AlB_2, NaCl and $NaZn_{13}$ phases with $\gamma_{eff} \approx 0.50$; (c1-c3) TEM images of $NaZn_{13}$, Cu_3Au and AlB_2 phases with $\gamma_{eff} \approx 0.56$; (d1-d3) TEM images of $NaZn_{13}$, AlB_2 and Cu_3Au phases with $\gamma_{eff} \approx 0.61$. Insets in all figures are the corresponding crystal models, respectively.

From these data it is clearly shown that the binary structures produced with two different coating agents cannot be simply predicted from the hard sphere model. Furthermore, the phase diagram in Figure 2b and 2c show marked changes compared to what was obtained with same coating agents for both small and large nanocrystals.

At this stage we have to raise the following question: is the use of two different ligands to coat the nanocrystals one of the key parameters to produce binary superlattices with lower packing density, such as QC and CaB_6 structure? To answer this question, Ag@DDT was replaced by Au@DDT while keeping the same average diameter of 4.0-nm for Au nanocrystals. Hence we can consider a binary mixture of 11.9-nm Ag@OAM and 4.0-nm Au@DDT with an effective size ratio of γ_{eff} = 0.41. The overall Ag and Au nanocrystals concentration remains the same (10^{-6} M) and the nanocrystal concentration ratio, $[Au]_S/[Ag]_L$ = 4. In those conditions, CaB_6 and dodecahedral QC structures are clearly observed (Figure 6), which is consistent with the result obtained from Ag@OAM + Ag@DDT binary system with a similar γ_{eff} value. Note that the size of the crystal domains of either CaB_6 or dodecahedral QC structures produced are smaller than that of Ag@OAM + Ag@DDT binary system.

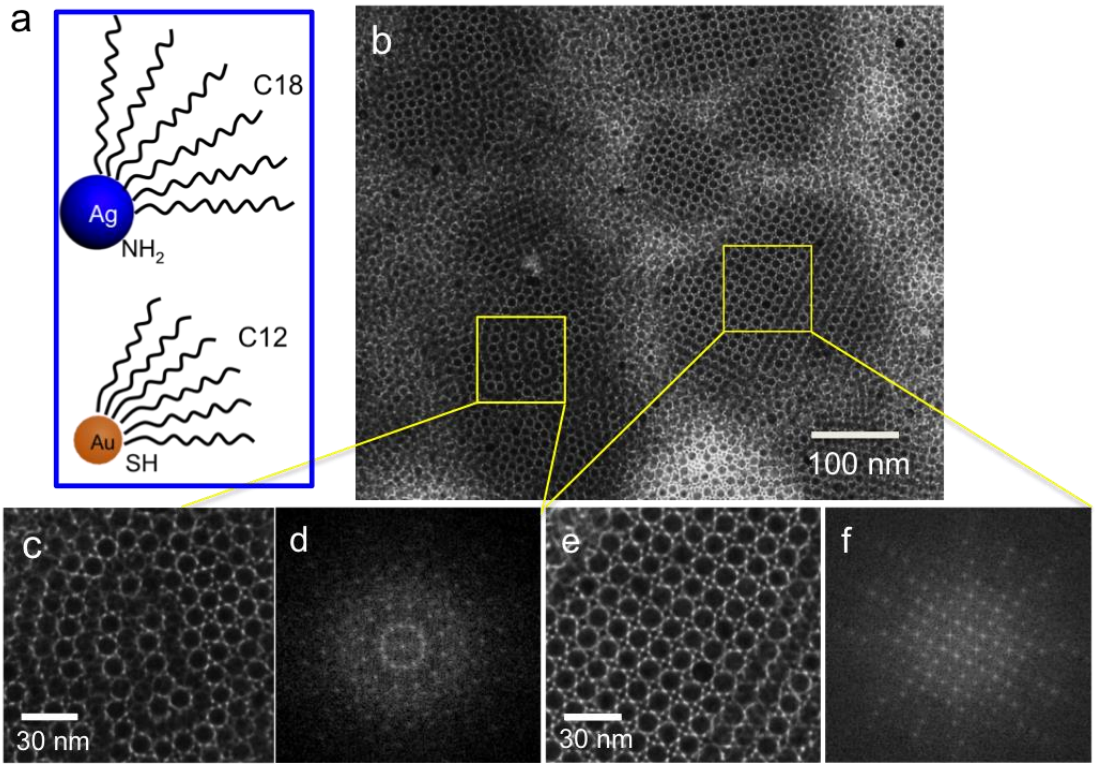

Figure 6. TEM images of binary nanocrystal superlattices from Au-Ag binary mixtures produced with $[Au]_S/[Ag]_L$ = 4: (a) schematic information of multiple ligands system: 11.9-nm Ag@OAM and 4-nm Au@DDT; (b) low magnification of TEM images of QC superlattices and CaB_6-type superlattices; (c) and (e) magnification of the area of panel (b); (d) and (f) corresponding FFT pattern of panel (c) and (e).

From these data it is reasonable to assume that a way to produce QC order in binary superlattices is related to the fact that small and large nanocrystals involved in the binary systems need to be coated by two different ligands. To support this claim we consider other types of nanocrystals differing by sizes and coating agents: 12-nm $CoFe_2O_4$ nanocrystals coated with oleic aid (OA) and either Ag nanocrystals coated either with oleylamine (Ag@OAM) or with dodecanethiol (Ag@DDT) having an average diameter of 3.7nm and 4-nm, respectively. Figure 7 shows binary systems of $CoFe_2O_4$@OA + Ag@OAM (Figures 7a, 7b and 7c) and of $CoFe_2O_4$@OA + Ag@DDT (Figures 7d, 7e and 7f). TEM image in Figure 7b shows the packing motif of the periodic (3^2.4.3.4) Archimedean tiling, and the corresponding FFT pattern inset indicates its 4-fold rotational symmetry in the case of $CoFe_2O_4$@OA and 3.7-nm Ag@OAM binary mixture.[32,33] In addition, dodecagonal QC structures and AlB_2-type structures can also be observed in Figure 7c. With $CoFe_2O_4$@OA

+ Ag@DDT binary system, CaB_6-type and dodecagonal QC structures are observed (Figure 7e and 7f). Hence, in both cases CaB_6-type and dodecagonal QC structures are observed instead of that expected from the hard sphere model (NaCl). This clearly demonstrates that the use of two different coating agents for small and large nanocrystals induces the formation of both CaB_6-type and dodecagonal QC structures.

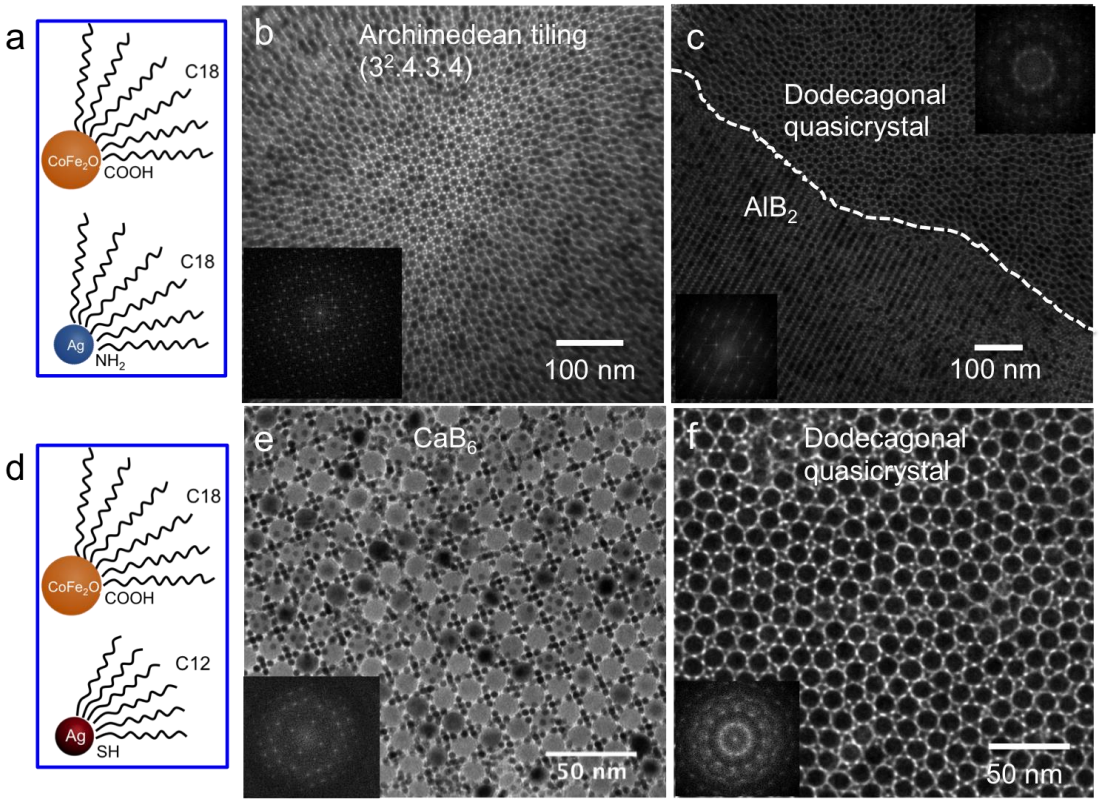

Figure 7. (a) Schematic information of multiple ligands system: $CoFe_2O_4$@OA and Ag@OAM; (b) and (c) TEM image of the binary nanocrystal superlattices formed with 12.0-nm $CoFe_2O_4$@OA and 3.7-nm@ Ag@OAM binary mixtures with $[Ag]_S/[CoFe_2O_4]_L$ = 4; (d) schematic information of multiple ligands system: $CoFe_2O_4$@OA and Ag@DDT; (e) and (f) TEM image of the binary nanocrystal superlattices formed with 12.0-nm $CoFe_2O_4$@OA and 3.7-nm@ Ag@DDT binary mixtures with $[Ag]_S/[CoFe_2O_4]_L$ = 4.

A careful survey on the literature shows that the formation of either CaB_6 or QC structure in binary superlattices is obtained with nanocrystals having two different coating agents. This is observed for Fe_2O_3@oleic acid (OA) + Au@DDT, Fe_3O_4@OA + Au@DDT and PbS@OA + Pd@DDT binary systems (Summarized in Table S1).[32-34] These data highly support our claim saying that, in order to produce either CaB_6 and QC structures in

binary superlattices, the small and large nanocrystals need to be coated by two different coating agents.

To explain this effect, the first attempt could be to consider the *van der Waals* interactions. A recent simulation has shown that these interactions between metal nanocrystals are strong and the pair potential that exceeds the thermal energy (k_BT) could play a major role during the assembly of binary nanocrystal superlattices.[14] The Hamaker constant for the various nanocrystals used (Ag, Au or $CoFe_2O_4$) changes with the material used, the nanocrystal size and the coating agents differ from one binary system to another. This indicates that the *van der Waals* interactions evolve from one system to another and such parameter cannot be the unique one. The similarity of the data indicates that even though the *van der Waals* interactions play a role, other forces have to be taken into account. Previous studies pointed out that the additional surfactant could induce the electrical charges on nanocrystals even in non-polar solvent, and this surface electrical charge may play a role in the binary assemblies in terms of electrostatic interactions.[13] As mentioned above, the nanocrystals were washed several times to get rid of residual surfactant molecules such as either OAM or DDT. Hence the electrostatic interaction or Coulombic interaction is not account for the forces involved in the binary system. Besides, our recent studies demonstrated that the magnetic force could play a role during the evaporation-induced-binary-assembly process, but it is a unique example where ferromagnetic nanocrystals are involved.[35]

Then we have to take into account the procedure used to grow nanocrystal superlattices: the deposition process takes place at 35ºC and the solvent evaporation time is close to 4h. During the continuous drying process, dynamic ligand adsorption/desorption on nanocrystal surface will take place in the colloidal solution even though the bonding between the nanocrystal cores and the coating agents differ from one system to another. The bonding between nanocrystal core and coating agent can be described by its adsorption and desorption equilibrium constant, K, and the adsorption and desorption kinetic constants, k_a and k_d, respectively.

For single ligand system, where QC structure are not detected, we can assume that the adsorption and desorption kinetic constants, k_a and k_d, are kept constant and are independent on the nanocrystals' sizes.[36] Then the thermodynamic term K in binary system remains the same. Hence the assembly of binary nanocrystal mixture with the same coating agents is mainly determined by their effective size ratios. Pure entropic force is responsible

for the formation of binary nanocrystal superlattices regardless of the other forces. As a result, the binary nanocrystal superlattices can be well predicted from the space-filling curves at a certain size ratio. As is known, for the single-component nanocrystal system, the solvent-evaporation induced *fcc* superlattices with the highest packing density of ~0.74 are frequently observed,[37,38] which agrees well with the hard sphere model purely driven by the entropic force.

While for binary system with two different kinds of coating agents, the thermodynamic constant K differs from one kind of nanocrystal to another. During the continuous evaporation of the carrier solvent, we can assume that ligand exchange processes take place as illustrated by the Scheme S1 (Supporting Information). This can be inferred from our previous study where we used a ligand exchange procedure to change the coating agents of Ag nanocrystals.[21] The complete evaporation of the carrier solvent provides sufficient time for the ligand exchange process in the colloidal solution. During the formation of nanocrystal superlattices, the system must pay a large energetic penalty to take the ligand exchange process, which may affect the thermodynamics of the assembly of binary nanocrystal superlattices during the solvent evaporation. Thus the formation of a superlattice with lower packing density may be favored kinetically because the required energetic penalty is smaller than that for a denser structure. In other words, a binary structure is probably in a kinetically trapped state at a local free energy minimum despite the lower packing density. As a result, binary superlattices, such as CaB_6, QC, and Cu_3Au phases with lower packing density that are known not to be found in hard sphere systems can be produced in the nanoscale binary system. These data implies that the ability to control the surface chemistry in binary system may provide another fruitful way to control the crystal structures in binary nanocrystal superlattices.

CONCLUSIONS

Here it is shown that by using one given coating agent, the binary superlattices are predicted by using the model set up for atoms that takes into account the space-filling principle. Four types of binary structures, NaCl, AlB_2 and $NaZn_{13}$, $MgZn_2$ can be produced driven by entropy. When two different coating agents are used to coat either the small or large nanocrystals the phase diagram observed previously markedly changes with appearance of various phases as quasicrystals, CaB_6 and Cu_3Au. The ligand exchange process is responsible for the interparticle interactions between neighboring nanocrystals,

resulting in diversity in binary nanocrystal superlattices including some structures with lower packing density. These structures are formed probably due to the fact that it is in a kinetically trapped state at a local free energy minimum. Our findings are of particular importance for the design of novel 3D metamaterials from the numerous high-quality colloidal nanocrystals available now.

REFERENCES

1. Sanders, J. V., *Nature* **1964,** *204*, 1151-1153.
2. Allpress, J. G.; Sanders, J. V., *Surf. Sci.* **1967,** *7*, 1-25.
3. Bartlett, P.; Ottewill, R. H.; Pusey, P. N., *Phys. Rev. Lett.* **1992,** *68*, 3801-3804.
4. Eldridge, M. D.; Madden, P. A.; Frenkel, D., *Nature* **1993,** *365*, 35-37.
5. Ohara, P. C.; Leff, D. V.; Heath, J. R.; Gelbart, W. M., *Phys. Rev. Lett.* **1995,** *75* , 3466-3469.
6. Korgel, B. A.; Fullam, S.; Connolly, S.; Fitzmaurice, D., *J. Phys. Chem. B* **1998,** *102*, 8379-8388.
7. Murray, C. B.; Kagan, C. R.; Bawendi, M. G., *Annu. Rev. Mater. Sci.* **2000,** *30*, 545-610.
8. Henry, A. I.; Courty, A.; Pileni, M. P.; Albouy, P. A.; Israelachvili, J., *Nano Lett.* **2008,** *8*, 2000-2005.
9. Murray, C. B.; Kagan, C. R.; Bawendi, M. G., *Science* **1995,** *270*, 1335-1338.
10. Pileni, M. P., *Acc. Chem. Res.* **2007,** *40*, 685-693.
11. Choi, J. J.; Bealing, C. R.; Bian, K.; Hughes, K. J.; Zhang, W.; Smilgies, D.-M.; Hennig, R. G.; Engstrom, J. R.; Hanrath, T., *J. Am. Chem. Soc.* **2011,** *133*, 3131-3138.
12. Chan, H.; Demortiere, A.; Vukovic, L.; Kral, P.; Petit, C., *ACS Nano* **2012,** *6*, 4203-4213.
13. Shevchenko, E. V.; Talapin, D. V.; Kotov, N. A.; O'brien, S.; Murray, C. B., *Nature* **2006,** *439*, 55-59;
14. Evers, W. H.; Nijs, B. D.; Filion, L.; Castillo, S.; Dijkstra, M.; Vanmaekelbergh, D., *Nano Lett.* **2010,** *10*, 4235-4241.
15. Bodnarchuk, M. I.; Kovalenko, M. V.; Heiss, W.; Talapin, D. V., *J. Am. Chem. Soc.* **2010,** *132*, 11967-11977.
16. Filion, L.; Dijkstra, M., *Phys. Rev. E* **2009,** *79*.
17. Vanmaekelbergh, D., *Nano Today* **2011,** *6*, 419-437.

18. Bodnarchuk, M. I.; Shevchenko, E. V.; Talapin, D. V., *J. Am. Chem. Soc.* **2011,** *133*, 20837-20849.

19. Shevchenko, E. V.; Talapin, D. V.; Murray, C. B.; O'brien, S., *J. Am. Chem. Soc.* **2006,** *128*, 3620-3637.

20. Bodnarchuk, M. I.; Erni, R.; Krumeich, F.; Kovalenko, M. V., *Nano Lett.* **2013,** *13*, 1699-1705.

21. Wei, J.; Schaeffer, N.; Pileni, M.-P., *J. Phys. Chem. B* **2014,** *118*, 14070-14075.

22. Peng, S.; Mcmahon, J. M.; Schatz, G. C.; Gray, S. K.; Sun, Y., *Proc. Natl. Acad. Sci. U. S. A.* **2010,** *107*, 14530-14534.

23. Courty, A.; Richardi, J.; Albouy, P.-A.; Pileni, M.-P., *Chem. Mater.* **2011,** *23*, 4186-4192.

24. Zheng, N.; Fan, J.; Stucky, G. D. *J. Am. Chem. Soc.* **2006,** *128***,** 6550-6551.

25. Goubet, N.; Portales, H.; Yan, C.; Arfaoui, I.; Albouy, P. A.; Mermet, A.; Pileni, M. P., *J. Am. Chem. Soc.* **2012,** *134*, 3714-3719.

26. Bodnarchuk, M. I.; Kovalenko, M. V.; Groiss, H.; Resel, R.; Reissner, M.; Hesser, G.; Lechner, R. T.; Steiner, W.; Schaeffler, F.; Heiss, W., *Small* **2009,** *5*, 2247-2252.

27. Wan, Y. F.; Goubet, N.; Albouy, P. A.; Pileni, M. P., *Langmuir* **2013,** *29*, 7456-7463.

28. Chen, Z.; O'Brien, S., *ACS Nano* **2008,** *2*, 1219-1229.

29. Parthe E., *Z. Kristallogr.* **1961**, *115*, 52-79.

30. Saunders, A. E.; Korgel, B. A., *ChemPhysChem* **2005,** *6*, 61-65.

31. Yang, Z.; Wei, J.; Pileni, M. P., *Chem. Mater.* **2015,** *27*,2152.

32. Talapin, D. V.; Shevchenko, E. V.; Bodnarchuk, M. I.; Ye, X.; Chen, J.; Murray, C. B., *Nature* **2009,** *461*, 964-967.

33. Ye, X.; Chen, J.; Murray, C. B., *J. Am. Chem. Soc.* **2011,** *133*, 2613-2620.

34. Bodnarchuk, M.I.; Erni, R.; Krumeich, F.; Kovalenko, M.V. *Nano Lett.* **2013**, *13*, 1699–1705.

35. Yang, Z.; Wei, J.; Bonville, P.; Pileni, M.-P., *J. Am. Chem. Soc.* **2015,** *137*, 4487-4493.

36. Ji, X.; Copenhaver, D.; Sichmeller, C.; Peng, X., *J. Am. Chem. Soc.* **2008,** *130*, 5726-5735.

37. Nagaoka, Y.; Chen, O.; Wang, Z.; Cao, Y. C., *J. Am. Chem. Soc.* **2012,** *134*, 2868-2871.

38. Wan, Y.; Goubet, N.; Albouy, P.-A.; Schaeffer, N.; Pileni, M.-P., *Langmuir* **2013,** *29*, 13576-13581.

5.3 Supporting Information

EXPERIMENTAL DETAILS

Synthesis of 4.0-nm Au@DDT nanocrystals

Au nanocrystals with 4.0 nm in diameter are synthesized by revisiting the Stucky method.[S1] Typically, two solutions are used. One consists of 0.20 mmol of Chlorotriphenylphosphine Au (I) dissolved in 25 mL of toluene to which 500 μL of dodecanethiol (DDT) is added. While the other one contains 5 mmol of *tert*-butylamine borane dissolved in 2 mL of toluene. The two solutions are placed in a silicone oil bath at 100 ^{o}C and are stirred for 10 min. Subsequently *tert*-butylamine borane solution is injected into the solution with gold salt swiftly. The colorless and clear mixture turns to brown and reaches a dark purple red solution in 1 min, and this solution is kept at 100 ^{o}C for another 4 min followed by the remove of the oil bath. The Au nanocrystals are precipitated from the colloidal solution by adding 10 mL of methanol. The supernatant is removed. The black precipitate is dried in a nitrogen flow in order to eliminate the remaining solvent. The Au nanocrystals are weighted and redispersed in toluene with desired nanocrystal concentration.

Synthesis of 12.0-nm $CoFe_2O_4$@OA nanocrystals

12 nm $CoFe_2O_4$ nanocrsytals with an oleic acid capping are synthesized by revisiting the method described by Bodnarchuk et al.[S2] using octadecene and octyl ether as the solvent. (Co,Fe) oleate mixture is prepared by combing 4.33 g $FeCl_3$•$6H_2O$ in 40 mL methanol are mixed with 2.00 g $Co(Ac)_2$•$4H_2O$ in 20 mL methanol and with 20.1 g oleic acid. 2.56 g NaOH in 160 mL methanol are added dropwise to the above solution under vigorous stirring. A dark viscous product is separated and washed by 100 mL methol and dissolved in 100 mL of hexane. The hexane solution is further washed 3 times by warm water (~50 ^{o}C) and separated in a separatory funnel. The viscous product is obtained by evaporating the hexane in a rotary evaporator. A stock precursor solution with a concentration of 0.5 mol/kg is prepared by adding 1.48 g of octadecene to each gram of mixed oleate.

In a typical synthesis of 12 nm $CoFe_2O_4$ nanocrsytals, 4.8 g of precursor solution is mixed with 0.38 g oleic acid and with 6.0 g oecadecene and 0.9 g octylether. The mixture is heated to 110 ^oC and maintained at this temperature for 60 min under N_2 protection. Then the solution is heated to the boiling point of the solution (~308 ^oC) and is kept at this temperature for 30 min followed by removal of the heater. The colloidal solution is washed 5 times using ethanol/hexane (1:1 v/v) by sedimenting and redispersing using centrifugation. Finally, the $CoFe_2O_4$ nanocrsytals are weighted and redispersed in toluene with desired nanocrystal concentration.

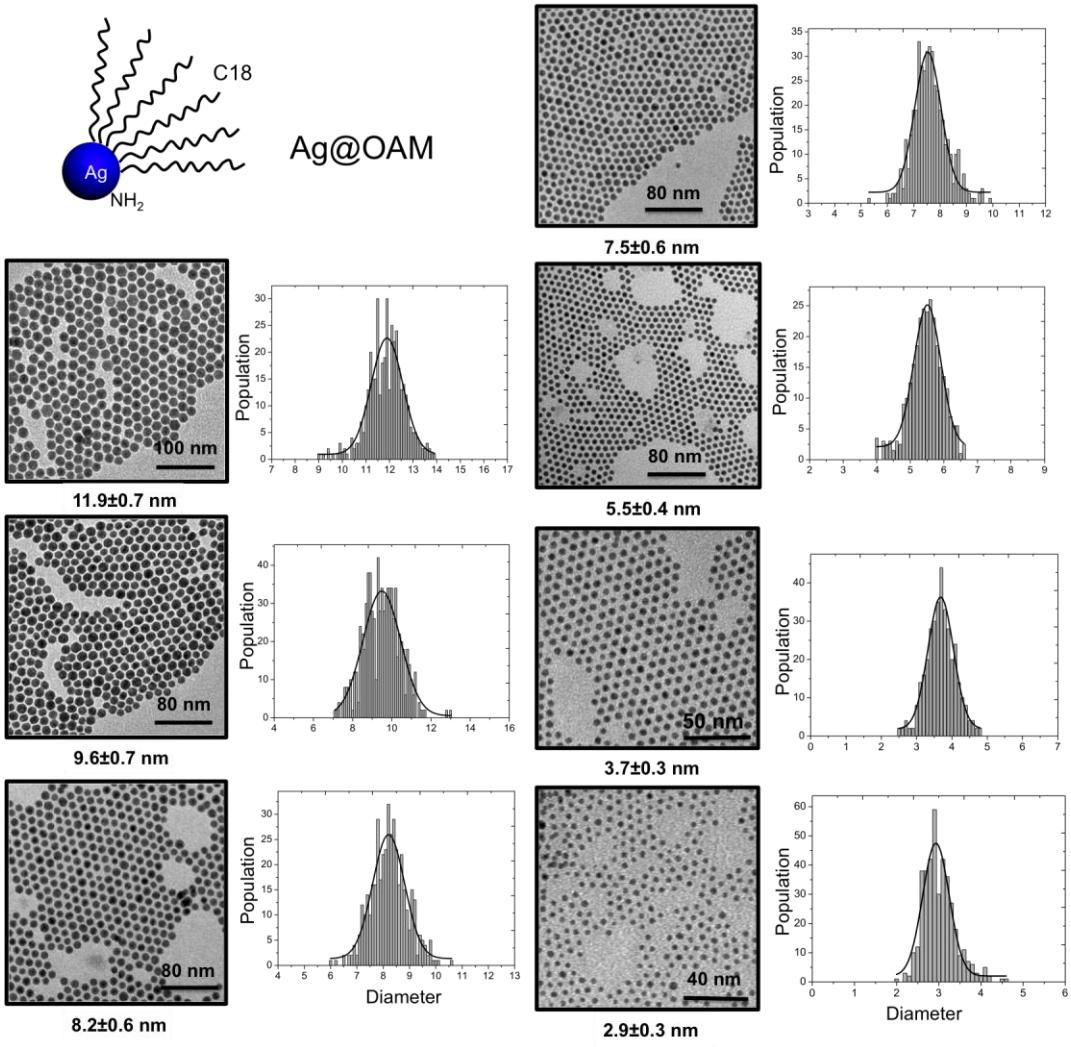

Figure S1. TEM images and corresponding histogram of the Ag nanocrystals with various diameters coated with oleylamine that used for the growth of binary nanocrystal superlattices.

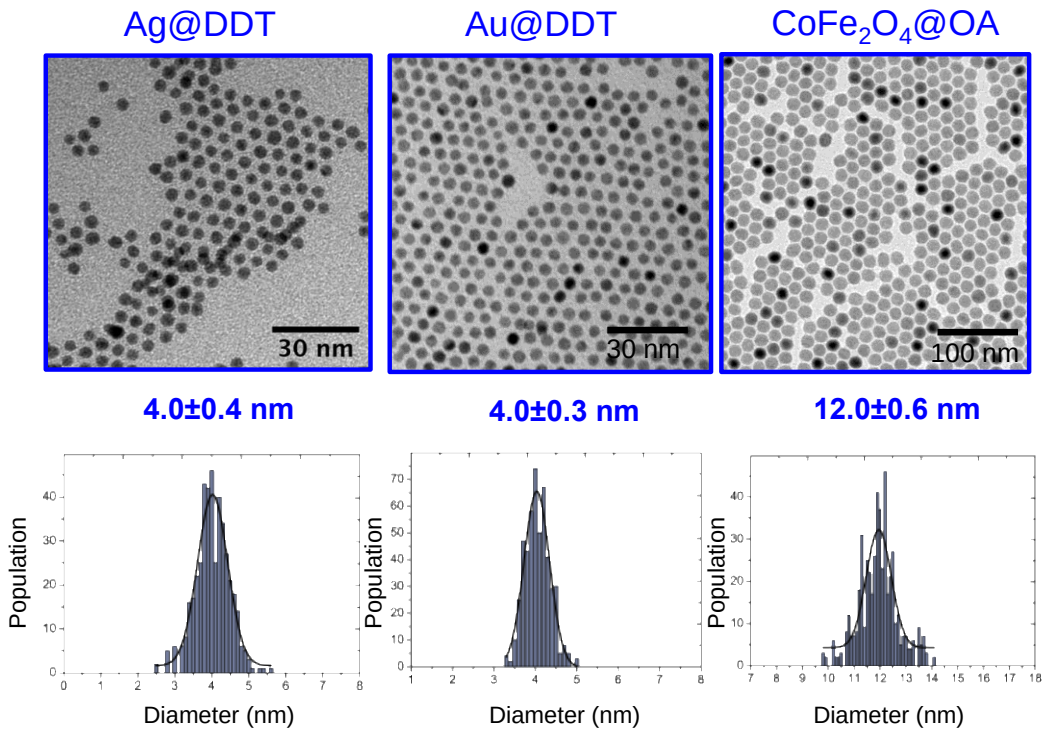

Figure S2. TEM images and corresponding histogram of the nanocrystals with various diameters coated with different ligands that used for the growth of binary nanocrystal superlattices.

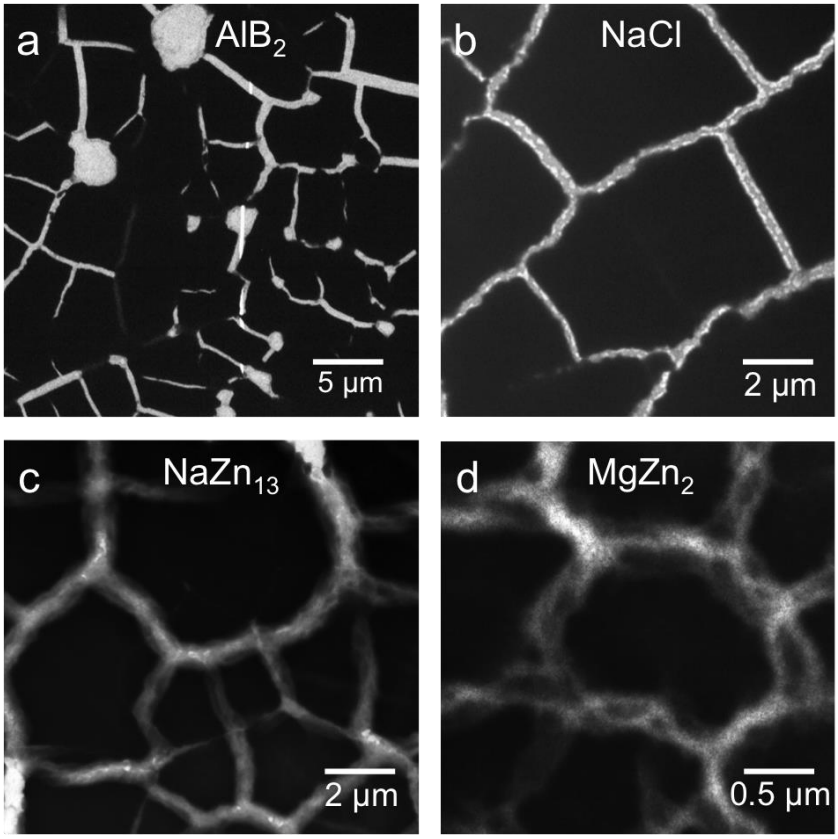

Figure S3. Low magnification of TEM images of the binary nanocrystals superlattices : (a) Binary nanocrystal superlattices formed from 8.2 nm Ag@OAM and 2.9 nm Ag@OAM nanocrystals with $[Ag]_S/[Ag]_L$ =4; (b) Binary nanocrystal superlattices formed from 11.9 nm Ag@OAM and 2.9 nm Ag@OAM nanocrystals with $[Ag]_S/[Ag]_L$ =4; (c) Binary nanocrystal superlattices formed from 8.2 nm Ag@OAM and 3.7 nm Ag@OAM nanocrystals with $[Ag]_S/[Ag]_L$ =4; (d) Binary nanocrystal superlattices formed from 7.5 nm Ag@OAM and 5.5 nm Ag@OAM nanocrystals with $[Ag]_S/[Ag]_L$ =4. The high contrast is due to the low electron dosage in low magnification mode.

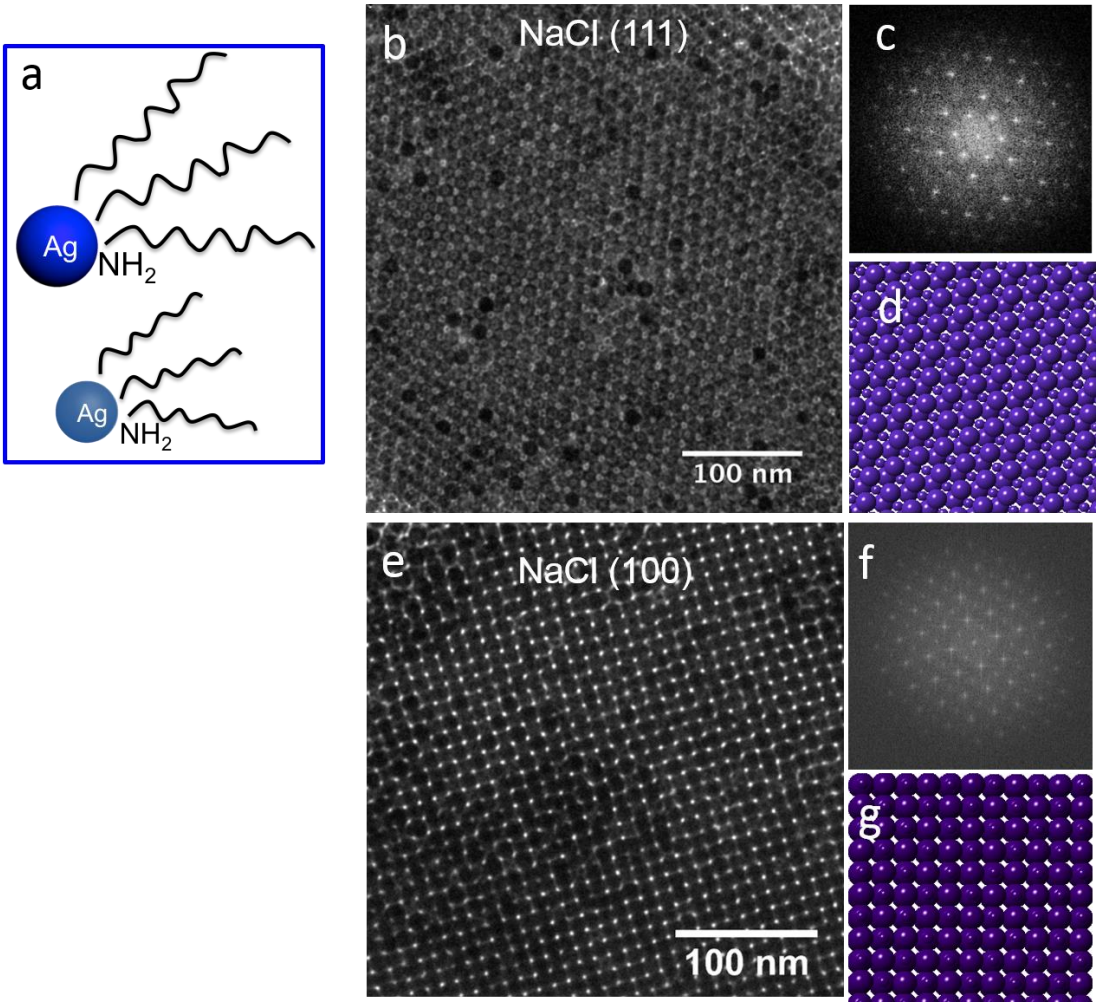

Figure S4. TEM images of binary superlattices formed with 11.9-nm Ag@OAM and 3.7-nm Ag@OAM binary mixtures: (a) schematic information of same ligand system; (b) TEM images of NaCl-type binary nanocrystal superlattices with (111) planes parallel to the substrate; (c) corresponding FFT pattern to panel (b); (d) corresponding crystal model of (111) crystal plane of NaCl-type binary structures. (e) TEM images of NaCl-type binary nanocrystal superlattices with (100) planes parallel to the substrate; (f) corresponding FFT pattern to panel (e); (g) corresponding crystal model of (100) crystal plane of NaCl-type binary structures.

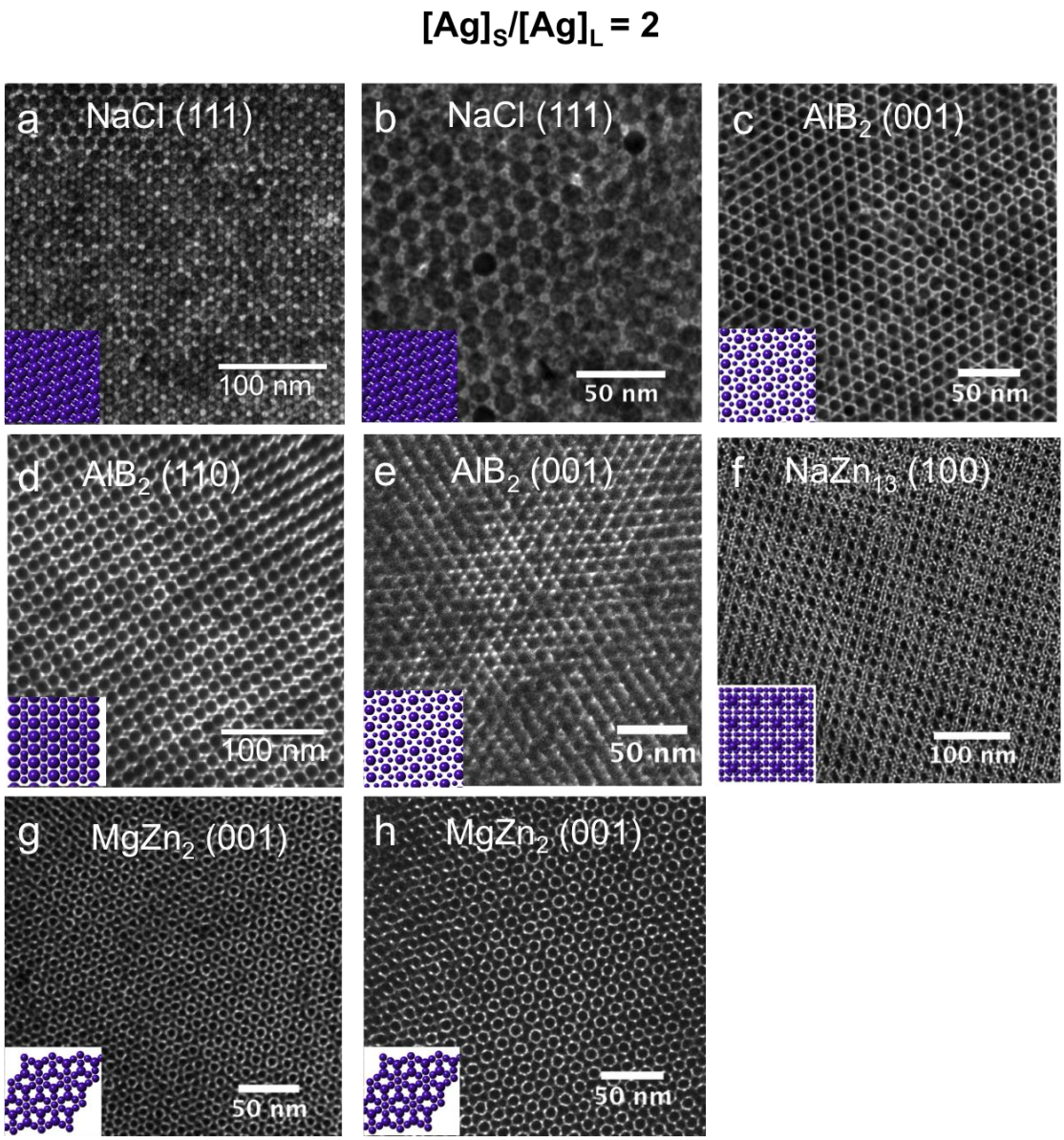

Figure S5. Binary nanocrystal superlattices formed from Ag@OAM single ligand system with $[Ag]_S/[Ag]_L$=2: (a) 11.9 nm Ag@OAM and 2.9 nm Ag@OAM, γ_{eff} = 0.42; (b) 11.9 nm Ag@OAM and 3.7 nm Ag@OAM, γ_{eff} = 0.44; (c) 9.6 nm Ag@OAM and 3.7 nm Ag@OAM, γ_{eff} = 0.52; (d) 8.2 nm Ag@OAM and 2.9 nm Ag@OAM, γ_{eff} = 0.55; (e) 8.2 nm Ag@OAM and 3.7 nm Ag@OAM, γ_{eff} = 0.58; (f) 7.5 nm Ag@OAM and 3.7 nm Ag@OAM, γ_{eff} = 0.64; (g) 5.5 nm Ag@OAM and 3.7 nm, γ_{eff} = 0.79; (h) 7.5 nm Ag@OAM and 5.5 nm Ag@OAM, γ_{eff} = 0.81.

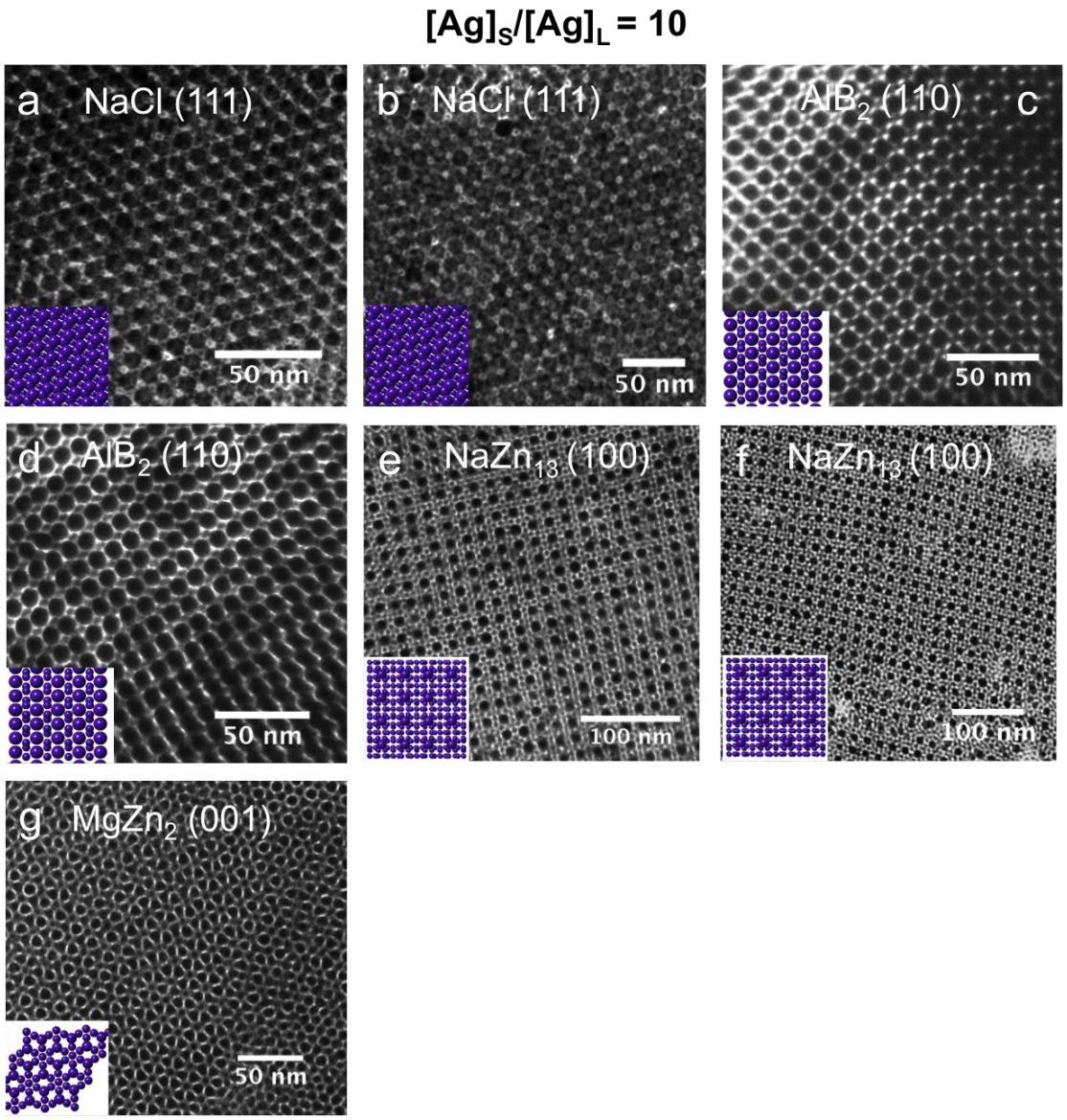

Figure S6. Binary nanocrystal superlattices formed from Ag@OAM single ligand system with $[Ag]_S/[Ag]_L$=10: (a) 11.9 nm Ag@OAM and 2.9 nm Ag@OAM, γ_{eff} = 0.42; (b) 11.9 nm Ag@OAM and 3.7 nm Ag@OAM, γ_{eff} = 0.44; (c) 9.6 nm Ag@OAM and 3.7 nm Ag@OAM, γ_{eff} = 0.52; (d) 8.2 nm Ag@OAM and 2.9 nm Ag@OAM, γ_{eff} = 0.55; (e) 8.2 nm Ag@OAM and 3.7 nm Ag@OAM, γ_{eff} = 0.58; (f) 7.5 nm Ag@OAM and 3.7 nm, γ_{eff} = 0.79; (g) 7.5 nm Ag@OAM and 5.5 nm Ag@OAM, γ_{eff} = 0.81.

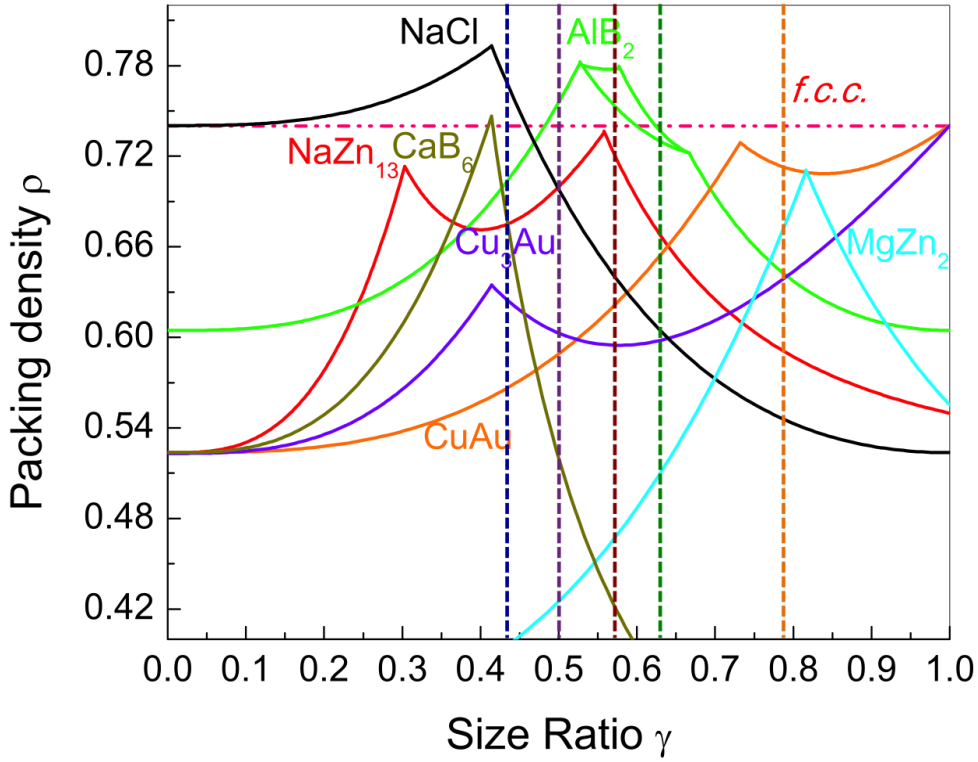

Figure S7. Calculated space-filling curves for NaCl, CuAu, AlB_2, $MgZn_2$, Cu_3Au, CaB_6 and $NaZn_{13}$ binary structures. Dashed red line is the space-filling of single-component fcc structure. The Dashed vertical lines show γ for nanocrystals studied in this work.

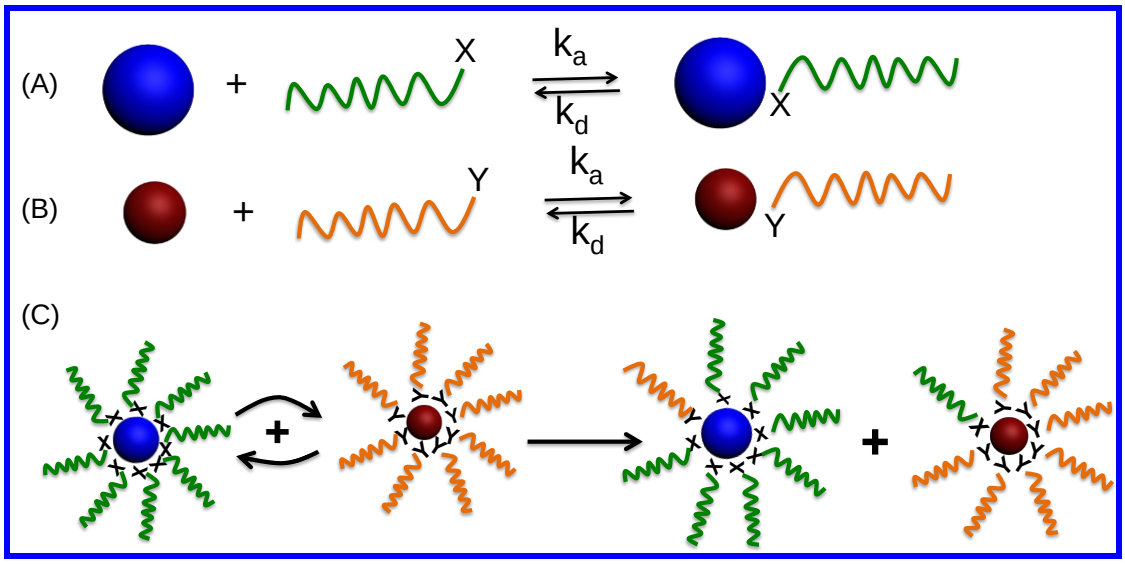

Scheme S1. (A) and (B) are the equilibrium of the bonding of nanocrystal-ligand with different size and different coating agents by adsorption and desorption kinetic constants, k_a and $k_{d;}$ (C) Ligand exchange takes places between the nanocrsytals with different surface coatings.

Table S1. Summarized structures of binary nanoparticle superlattices that cannot be observed from hard sphere binary systems.

'A' site	'A' ligand	'B' site	'B' ligand	Binary	References
14nm-Fe_3O_4	OA	4.6nm-Au	C12-SH	CaB_6,QC,	S3
14nm-Fe_3O_4	OA	5.8nm-Au	C12-SH	BCC-AB_6	S3
8.1nm-PbS	OA	2.9nm-POM	C12-SH	QC	S4
5.8nm-PbSe	OA	3.4nm-Ag	C12-SH	Cu_3Au	S5
5.8nm-PbSe	OA	3.0nm-Pd	C12-SH	Fe_4C	S5
6.3nm-PbSe	OA	3.6nm-Ag	C12-SH	$CaCu_5$	S5
7.2nm-PbSe	OA	5.0nm-Au	C12-SH	$CaCu_5$	S5
6.2nm-PbSe	OA	5.0nm-Au	C12-SH	$CaCu_5$	S5
13.4nm-Fe_2O_3	OA	5.0nm-Au	C12-SH	CaB_6, QC	S6
12.6nm-Fe_3O_4	OA	4.7nm-Au	C12-SH	CaB_6 QC	S6
9nm-PbS	OA	3.0nm-Pd	C12-SH	QC	S6
7.7nm-PbSe	OA	3.4nm-Pd	C12-SH	CuAu,Cu_3Au, AB_4	S7
7.7nm-PbSe	OA	4.9nm-Pd	C12-SH	CuAu,Cu_3Au,	S7
PbSe	OA	CdSe	OA	A_6B_{19}	S8

REFERENCES

S1. Zheng, N.; Fan, J.; Stucky, G. D. *J. Am. Chem. Soc.* **2006,** *128***,** 6550-6551.

S2. Bodnarchuk, M. I.; Kovalenko, M. V.; Groiss, H.; Resel, R.; Reissner, M.; Hesser, G.; Lechner, R. T.; Steiner, W.; Schaeffler, F.; Heiss, W., *Small* **2009,** *5*, 2247-2252.

S3. Ye, X.; Chen, J.; Murray, C. B., *J. Am. Chem. Soc.* **2011,** *133*, 2613-2620.

S4. Bodnarchuk, M. I.; Erni, R.; Krumeich, F.; Kovalenko, M. V., *Nano Lett.* **2013,** *13*, 1699-1705.

S5. Shevchenko, E. V.; Talapin, D. V.; Murray, C. B.; O'Brien, S., *J. Am. Chem. Soc.* **2006,** *128*, 3620-3637.

S6. Talapin, D. V.; Shevchenko, E. V.; Bodnarchuk, M. I.; Ye, X.; Chen, J.; Murray, C. B., *Nature* **2009,** *461*, 964-967.

S7. Bodnarchuk, M. I.; Kovalenko, M. V.; Heiss, W.; Talapin, D. V., *J. Am. Chem. Soc.* **2010,** *132*, 11967-11977.

S8. Boneschanscher, M. P.; Evers, W. H.; Qi, W.; Meeldijk, J. D.; Dijkstra, M.; Vanmaekelbergh, D., *Nano Lett.* **2013,** *13*, 1312-1316.

Conclusions and Perspectives

Nanocrystals, which are of importance artificial materials, have been synthesized with purposive design and show their potential application in many different fields. Silver nanocrystals, which are famous for its optical properties, are highly investigated recent years. Commonly silver nanocrystals are composed of inorganic nanocrystal cores and surrounding organic molecule coatings. These molecule coatings can on one hand protect the nanocrystals from aggregates and bring new properties on the other. For example, by changing the parameters of silver nanocrystals, i.e. the diameter of nanocrystals or the coating agtens, the surface plamon resonance which is arised from the oscillations of nanocrystals electrons and the incident light can be rational tuned. Furthermore, the assemblies of nanocrystals can also influence the properties of the nanocrystals by inducing the collective effect. In this thesis, we focused on silver nanocrystals, and investigate the nanaocrystals size, coating agents, and the ordering on the optical properties of silver nanocrystals.

In the first part, silver nanocrystals ranging from 4 nm to 7 nm that are coated by dodecanethiol are synthesized with reverse micelleds method and same sized gold nanocrystals are produced from modified Stuky's method. After deposition onto a glass wafer, these nanocrystals self-organize in thin layer films where interparticle spacing is short enough to promote near-field coupling between nanocrystals and the emergence of collective optical properties. The UV-visible absorption spectra of 2D assemblies of Ag and Au NCs are recorded at various incidence angles. In 2D assemblies of Ag NCs, due to the optical anisotropy of the system, the SPR absorption band splits in two contributions, namely, the longitudinal and transverse SPR modes. For Ag NCs, these features are satisfactorily reproduced in the absorption spectra calculated using the DDA method. At variance, in similar assemblies of Au NCs, only one SPR band is observed whatever the incidence angle and NC size. The transverse SPR mode is difficult to observe experimentally, partially due to the strong ligands-metal interactions that lower the electron conductivity in the outermost metal atomic layer of the nanocrystals.

In the second part, we develop a new method to synthesize silver nanocrysals with narrow distribution based on hot-injection methods. The sizes of nanocrystals are ranging 2-12 nm and nanocrystals are coated with oleylamine. With this method, nanocrystals coated with dodecylamine with varying diameters can also be produced. By using ligand exchange

method, the coating layer of these nanocrystals is replaced by thiol-terminated coating agent. The optical properties of these different speciments reveal that SPR band position is not only dependent on the nanocrystals size, but also on the nature of the coating agents; would it be through the influence of the head-group (amine or thiol) or the chain length.

In the third part, we use the silver nanocrystals obtained above to grow thin layers superlattices (2-7 layers), then study the optical properties of these superlattices. By comparing the SPR spectra of dispersed Ag nanocrystals and their assemblies of supracrystalline films, marked changes are discovered. Very surprisingly, data obtained here show a good agreement between simulated optical properties in 2D superlattices with 3D thin films self-assembled in fcc crystalline structure. The energy discrepancy (ΔE), determined from the difference in SPR band between dispersed nanocrystals and their assemblies was used to evaluate the collective optical properties due to nanocrystal ordering. It is found that ΔE is mainly determined by both the nanocrystals sizes and the interparticle distances inside the supracrystal. Upon increasing the nanocrystals sizes while keeping the interparticle distance constant, ΔE values showed a monotonic increase. Furthermore, it was shown that engineering the interparticle distance of nanocrystals of similar size within a supracrystal, can effectively modulate the optical properties of the Ag supracrystalline films.

In the last part, we use the nanocrystals produced in the second part to assemble to binary nanocrystals superlattices. By studying the structure of the binary superlattices we obtained, we find that by using one given coating agent, the binary superlattices are predicted by using the model set up for atoms that takes into account the space-filling principle. Four types of binary structures, NaCl, AlB_2 and $NaZn_{13}$, $MgZn_2$ can be produced driven by entropy. When two different coating agents are used to coat either the small or large nanocrystals the phase diagram observed previously markedly changes with appearance of various phases as quasicrystals, CaB_6 and Cu_3Au. The ligand exchange process is responsible for the interparticle interactions between neighboring nanocrystals, resulting in diversity in binary nanocrystal superlattices including some structures with lower packing density. These structures are formed probably due to the fact that it is in a kinetically trapped state at a local free energy minimum. Our findings are of particular importance for the design of novel 3D metamaterials from the numerous high-quality colloidal nanocrystals available now.

As presented above, the optical properties of silver nanocrystals are highly dependent on the silver nanocrystal size, the coating agent, especially the ordering of the nanocrystals.

Furthermore, the coating agenes with different kinds can also influent the chemical properties of assemblies of nanocrystals. These findings allow further designing the optical properties on more complex system, especially binary nanocrystals superlattices.

Bibliography

1. Wu, Y.; Wang, D.; Li, Y., Nanocrystals from solutions: catalysts. *Chemical Society Review* **2014,** *43* (7), 2112-24.

2. Cushing, B. L.; Kolesnichenko, V. L.; O'Connor, C. J., Recent Advances in the Liquid-Phase Syntheses of Inorganic Nanoparticles. *Chemical Reviews* **2004,** *104* (9), 3893-3946.

3. Gao, J.; Gu, H.; Xu, B., Multifunctional Magnetic Nanoparticles: Design, Synthesis, and Biomedical Applications. *Accounts of Chemical Research* **2009,** *42* (8), 1097-1107.

4. Shenhar, R.; Rotello, V. M., Nanoparticles: Scaffolds and building blocks. *Accounts of Chemical Research* **2003,** *36* (7), 549-561.

5. Belloni, J., Photography: enhancing sensitivity by silver-halide crystal doping. *Radiation Physics and Chemistry* **2003,** *67* (3), 291-296.

6. Gramotnev, D. K.; Bozhevolnyi, S. I., Plasmonics beyond the diffraction limit. *Nature Photonics.* **2010,** *4* (2), 83-91.

7. Rycenga, M.; Cobley, C. M.; Zeng, J.; Li, W.; Moran, C. H.; Zhang, Q.; Qin, D.; Xia, Y., Controlling the Synthesis and Assembly of Silver Nanostructures for Plasmonic Applications. *Chemical Reviews* **2011,** *111* (6), 3669-3712.

8. Tao, A. R., Nanocrystal assembly for bottom-up plasmonic materials and surface-enhanced Raman spectroscopy (SERS) sensing. *Pure and Applied Chemistry* **2009,** *81* (1), 61-71.

9. Michaels, A. M.; Nirmal, M.; Brus, L. E., Surface enhanced Raman spectroscopy of individual rhodamine 6G molecules on large Ag nanocrystals. *Journal of the American Chemical Society* **1999,** *121* (43), 9932-9939.

10. Tian, Z. Q.; Ren, B.; Wu, D. Y., Surface-enhanced Raman scattering: From noble to transition metals and from rough surfaces to ordered nanostructures. *The Journal of Physical Chemistry B* **2002,** *106* (37), 9463-9483.

11. Mulvihill, M. J.; Ling, X. Y.; Henzie, J.; Yang, P. D., Anisotropic Etching of Silver Nanoparticles for Plasmonic Strutures Capable of Single-Particle SERS. *Journal of the American Chemical Society* **2010,** *132* (1), 269-274.

12. Sun, Y., Silver nanowires--unique templates for functional nanostructures. *Nanoscale* **2010,** *2* (9), 1626-42.

13. Jia, C.-J.; Schüth, F., Colloidal metal nanoparticles as a component of designed catalyst. *Physical Chemistry Chemical Physics* **2011,** *13* (7), 2457-2487.

14. Christopher, P.; Xin, H. L.; Linic, S., Visible-light-enhanced Catalystic Oxidation Reaction on Plasmonic Silver Nanostructures. *Nature Chemistry* **2011**, *3*, 467-472.

15. Huang, X.; Neretina, S.; El-Sayed, M. A., Gold nanorods: from synthesis and properties to biological and biomedical applications. *Advanced Materials* **2009,** *21* (48), 4880-910.

16. Kwon, S. G.; Hyeon, T., Colloidal Chemical Synthesis and Formation Kinetics of Uniformly Sized Nanocrystals of Metals, Oxides, and Chalcogenides. *Accounts of Chemical Research* **2008,** *41* (12), 1696-1709.

17. Shenhar, R.; Rotello, V. M., Nanoparticles: Scaffolds and Building Blocks. *Accounts of Chemical Research* **2003,** *36* (7), 549-561.

18. Jones, M. R.; Osberg, K. D.; Macfarlane, R. J.; Langille, M. R.; Mirkin, C. A., Templated Techniques for the Synthesis and Assembly of Plasmonic Nanostructures. *Chemical Reviews* **2011,** *111* (6), 3736-3827.

19. Jia, C. J.; Sun, L. D.; Yan, Z. G.; You, L. P.; Luo, F.; Han, X. D.; Pang, Y. C.; Zhang, Z.; Yan, C. H., Single-Crystalline Iron Oxide Nanotubes. *Angewandte Chemie* **2005,** *117*, 4402-4407.

20. Burda, C.; Chen, X.; Narayanan, R.; El-Sayed, M. A., Chemistry and Properties of Nanocrystals of Different Shapes. *Chemical Reviews* **2005,** *105* (4), 1025-1102.

21. Noguez, C., Surface Plasmons on Metal Nanoparticles: The Influence of Shape and Physical Environment. *The Journal of Physical Chemistry C* **2007,** *111* (10), 3806-3819.

22. Chen, Z.; Moore, J.; Radtke, G.; Sirringhaus, H.; O'Brien, S., Binary Nanoparticle Superlattices in the Semiconductor−Semiconductor System: CdTe and CdSe. *Journal of the American Chemical Society* **2007,** *129* (50), 15702-15709.

23. Sun, Y., Controlled synthesis of colloidal silver nanoparticles in organic solutions: empirical rules for nucleation engineering. *Chemical Society Review* **2013,** *42* (7), 2497-511.

24. Thanh, N. T.; Maclean, N.; Mahiddine, S., Mechanisms of nucleation and growth of nanoparticles in solution. *Chemical Reviews* **2014,** *114* (15), 7610-30.

25. Pileni, M. P., Supracrystals of Inorganic Nanocrystals: An Open Challenge for New Physical Properties. *Accounts of Chemical Research* **2008,** *41* (12), 1799-1809.

26. Pileni, M. P., Self-Assembly of Inorganic Nanocrystals: Fabrication and Collective Intrinsic Properties. *Accounts of Chemical Research* **2007,** *40* (8), 685-693.

27. Faraday, M., *Philos. Trans. R. Soc. London* **1857,** *147*, 145.

28. Brust, M.; Kiely, C. J., Some recent advances in nanostructure preparation from gold and silver particles: a short topical review. *Colloids and Surfaces A: Physicochemical and Engineering Aspects* **2002,** *202* (2–3), 175-186.

29. Enustun, B. V.; Turkevich, J., Coagulation of Colloidal Gold. *Journal of the American Chemical Society* **1963,** *85* (21), 3317-3328.

30. Turkevich, J., Colloidal gold. Part II. *Gold Bulletin* **1985,** *18* (4), 125-131.

31. Petit, C.; Lixon, P.; Pileni, M. P., Structural study of divalent metal bis(2-ethylhexyl) sulfosuccinate aggregates. *Langmuir* **1991,** *7* (11), 2620-2625.

32. Lisiecki, I.; Lixon, P.; Pileni, M. P., Synthesis in Situ in Reverse Micelle of Copper Metallic Clusters. In *Trends in Colloid and Interface Science V*, Corti, M.; Mallamace, F., Eds. Steinkopff: **1991**, *84*, 342-344.

33. Lisiecki, I.; Boulanger, L.; Lixon, P.; Pileni, M. P., Synthesis of copper metallic particles using functionalized surfactants in w/o and o/w microemulsions. In *Trends in Colloid and Interface Science VI*, Helm, C.; Lösche, M.; Möhwald, H., Eds. Steinkopff: **1992**, *89*, 103-105.

34. Brust, M.; Fink, J.; Bethell, D.; Schiffrin, D. J.; Kiely, C., Synthesis and Reactions of Functionalised Gold Nanoparticles. *Journal of the Chemical Society, Chemical Communications* **1995,** 1655-1656.

35. Peng, X.; Manna, L.; Yang, W.; Wickham, J.; Scher, E.; Kadavanich, A.; Alivisatos, A. P., Shape control of CdSe nanocrystals. *Nature* **2000,** *404* (6773), 59-61.

36. William, W., Synthesis of monodisperse iron oxide nanocrystals by thermal decomposition of iron carboxylate salts. *Chemical Communications* **2004,** (20), 2306-2307.

37. Sun, S.; Murray, C.; Weller, D.; Folks, L.; Moser, A., Monodisperse FePt nanoparticles and ferromagnetic FePt nanocrystal superlattices. *Science* **2000,** *287* (5460), 1989-1992.

38. Murray, C. B.; Norris, D. J.; Bawendi, M. G., Synthesis and characterization of nearly monodisperse CdE (E = sulfur, selenium, tellurium) semiconductor nanocrystallites. *Journal of the American Chemical Society* **1993,** *115* (19), 8706-8715.

39. Park, J.; Joo, J.; Kwon, S. G.; Jang, Y.; Hyeon, T., Synthesis of Monodisperse Spherical Nanocrystals. *Angewandte Chemie International Edition* **2007,** *46* (25), 4630-4660.

40. Kwon, S. G.; Hyeon, T., Formation Mechanisms of Uniform Nanocrystals via Hot‐Injection and Heat‐Up Methods. *Small* **2011,** *7* (19), 2685-2702.

41. Xia, X. H.; Zeng, J.; Zhang, Q.; Moran, C. H.; Xia, Y. N., Recent Development in Shape-Controlled Synthesis of Silver Nanocrystals. *Journal of Physical Chemistry C* **2012,** *116*, 21647-21656.

42. Sellers, H.; Ulman, A.; Shnidman, Y.; Eilers, J. E., Structure and Binding of Alkanethiolates on Gold and Silver Surfaces - Implications for Self-Assembled Monolayers. *Journal of the American Chemical Society* **1993,** *115* (21), 9389-9401.

43. Peng, S.; McMahon, J. M.; Schatz, G. C.; Gray, S. K.; Sun, Y., Reversing the size-dependence of surface plasmon resonances. *Proceedings of the National Academy of Sciences of the United States of America* **2010,** *107* (33), 14530-14534.

44. Pradhan, N.; Reifsnyder, D.; Xie, R.; Aldana, J.; Peng, X., Surface Ligand Dynamics in Growth of Nanocrystals. *Journal of the American Chemical Society* **2007,** *129* (30), 9500-9509.

45. Templeton, A. C.; Pietron, J. J.; Murray, R. W.; Mulvaney, P., Solvent refractive index and core charge influences on the surface plasmon absorbance of alkanethiolate monolayer-protected gold clusters. *Journal of Physical Chemistry B* **2000,** *104* (3), 564-570.

46. Seoudi, R.; Shabaka, A.; El Sayed, Z. A.; Anis, B., Effect of stabilizing agent on the morphology and optical properties of silver nanoparticles. *Physica E-Low-Dimensional Systems & Nanostructures* **2011,** *44* (2), 440-447.

47. Wan, Y.; Portalès, H.; Goubet, N.; Mermet, A.; Pileni, M.-P., Impact of nanocrystallinity segregation on the growth and morphology of nanocrystal superlattices. *Nano Research* **2013,** *6* (8), 611-618.

48. Lee, P.; Meisel, D., Adsorption and surface-enhanced Raman of dyes on silver and gold sols. *The Journal of Physical Chemistry* **1982,** *86* (17), 3391-3395.

49. Deng, Z.; Mansuipur, M.; Muscat, A. J., New Method to Single-Crystal Micrometer-Sized Ultra-Thin Silver Nanosheets: Synthesis and Characterization. *The Journal of Physical Chemistry C* **2008,** *113* (3), 867-873.

50. Lim, P. Y.; Liu, R. S.; She, P. L.; Hung, C. F.; Shih, H. C., Synthesis of Ag nanospheres particles in ethylene glycol by electrochemical-assisted polyol process. *Chemical Physics Letters* **2006,** *420* (4-6), 304-308.

51. Courty, A.; Richardi, J.; Albouy, P.-A.; Pileni, M.-P., How To Control the Crystalline Structure of Supracrystals of 5-nm Silver Nanocrystals. *Chemistry of Materials* **2011,** *23* (18), 4186-4192.

52. Stoeva, S. I.; Huo, F.; Lee, J.-S.; Mirkin, C. A., Three-Layer Composite Magnetic Nanoparticle Probes for DNA. *Journal of the American Chemical Society* **2005,** *127* (44), 15362-15363.

53. Zhang, Q.; Li, W.; Moran, C.; Zeng, J.; Chen, J.; Wen, L.-P.; Xia, Y., Seed-Mediated Synthesis of Ag Nanocubes with Controllable Edge Lengths in the Range of 30−200 nm and Comparison of Their Optical Properties. *Journal of the American Chemical Society* **2010,** *132* (32), 11372-11378.

54. Jana, N. R.; Gearheart, L.; Murphy, C. J., Seed-Mediated Growth Approach for Shape-Controlled Synthesis of Spheroidal and Rod-like Gold Nanoparticles Using a Surfactant Template. *Advanced Materials* **2001,** *13* (18), 1389-1393.

55. Pietrobon, B.; McEachran, M.; Kitaev, V., Synthesis of Size-Controlled Faceted Pentagonal Silver Nanorods with Tunable Plasmonic Properties and Self-Assembly of These Nanorods. *ACS Nano* **2008,** *3* (1), 21-26.

56. Wiley, B.; Sun, Y. G.; Xia, Y. N., Polyol Synthesis of Silver Nanostructures- Control of Product Morphology with Fe(II) or Fe(III) species. *Langmuir* **2005,** *21* (18), 8077-8080.

57. Nadagouda, M. N.; Varma, R. S., Microwave-Assisted Shape-Controlled Bulk Synthesis of Ag and Fe Nanorods in Poly(ethylene glycol) Solutions. *Crystal Growth & Design* **2007,** *8* (1), 291-295.

58. Peng, S.; Sun, Y., Synthesis of Silver Nanocubes in a Hydrophobic Binary Organic Solvent. *Chemistry of Materials* **2010,** *22* (23), 6272-6279.

59. Chen, S.; Fan, Z.; Carroll, D. L., Silver Nanodisks: Synthesis, Characterization, and Self-Assembly. *The Journal of Physical Chemistry B* **2002,** *106* (42), 10777-10781.

60. Maillard, M.; Giorgio, S.; Pileni, M.-P., Silver nanodisks. *Advance Materials* **2002,** *14* (15), 1084.

61. Schuller, J. A.; Barnard, E. S.; Cai, W.; Jun, Y. C.; White, J. S.; Brongersma, M. L., Plasmonics for extreme light concentration and manipulation. *Nature Materials* **2010,** *9* (4), 368-368.

62. Shalaev, V. M., Transforming Light. *Science* **2008,** *322* (5900), 384-386.

63. Lazarides, A. A.; Schatz, G. C., DNA-linked metal nanosphere materials: Structural basis for the optical properties. *Journal of Physical Chemistry B* **2000,** *104* (3), 460-467.

64. Kelly, K. L.; Coronado, E.; Zhao, L. L.; Schatz, G. C., The optical properties of metal nanoparticles: The influence of size, shape, and dielectric environment. *Journal of Physical Chemistry B* **2003,** *107* (3), 668-677.

65. Hao, E.; Li, S. Y.; Bailey, R. C.; Zou, S. L.; Schatz, G. C.; Hupp, J. T., Optical properties of metal nanoshells. *Journal of Physical Chemistry B* **2004,** *108* (4), 1224-1229.

66. Haes, A. J.; Van Duyne, R. P., A nanoscale optical blosensor: Sensitivity and selectivity of an approach based on the localized surface plasmon resonance spectroscopy of triangular silver nanoparticles. *Journal of the American Chemical Society* **2002,** *124* (35), 10596-10604.

67. Portales, H.; Pinna, N.; Pileni, M.-P., Optical Response of Ultrafine Spherical Silver Nanoparticles Arranged in Hexagonal Planar Arrays Studied by the DDA Method. *Journal of Physical Chemistry A* **2009,** *113* (16), 4094-4099.

68. Salzemann, C.; Brioude, A.; Pileni, M. P., Tuning of copper nanocrystals optical properties with their shapes. *Journal of Physical Chemistry B* **2006,** *110* (14), 7208-7212.

69. Liang, H.; Rossouw, D.; Zhao, H.; Cushing, S. K.; Shi, H.; Korinek, A.; Xu, H.; Rosei, F.; Wang, W.; Wu, N.; Botton, G. A.; Ma, D., Asymmetric Silver "Nanocarrot" Structures: Solution Synthesis and Their Asymmetric Plasmonic Resonances. *Journal of the American Chemical Society* **2013,** *135* (26), 9616-9619.

70. Yang, S.-C.; Kobori, H.; He, C.-L.; Lin, M.-H.; Chen, H.-Y.; Li, C.; Kanehara, M.; Teranishi, T.; Gwo, S., Plasmon Hybridization in individual Gold Nanocrystal Dimers: Direct Observation of Bright and Dark Modes. *Nano Letters* **2010,** *10* (2), 632-637.

71. Bakr, O. M.; Amendola, V.; Aikens, C. M.; Wenseleers, W.; Li, R.; Dal Negro, L.; Schatz, G. C.; Stellacci, F., Silver Nanoparticles with Broad Multiband Linear Optical Absorption. *Angewandte Chemie* **2009,** *121* (32), 6035-6040.

72. Gunnarsson, L.; Rindzevicius, T.; Prikulis, J.; Kasemo, B.; Kall, M.; Zou, S. L.; Schatz, G. C., Confined plasmons in nanofabricated single silver particle pairs: Experimental observations of strong interparticle interactions. *Journal of Physical Chemistry B* **2005,** *109* (3), 1079-1087.

73. Mie, G., *ANN. Phys. (Weinheim. Ger.)* **1908,** *25*, 377.

74. Bohren, C. F.; Huffman, D. R., *Absorption and scattering of light by small particles*. John Wiley & Sons: 2008.

75. Liu, M.; Guyot-Sionnest, P., Synthesis and optical characterization of Au/Ag core/shell nanorods. *The Journal of Physical Chemistry B* **2004,** *108* (19), 5882-5888.

76. Wang, H.; Tam, F.; Grady, N. K.; Halas, N. J., Cu Nanoshells: Effects of Interband Transitions on the Nanoparticle Plasmon Resonance. *The Journal of Physical Chemistry B* **2005,** *109* (39), 18218-18222.

77. Mulvaney, P., Surface plasmon spectroscopy of nanosized metal particles. *Langmuir* **1996,** *12* (3), 788-800.

78. Wiley, B.; Sun, Y.; Mayers, B.; Xia, Y., Shape‐Controlled Synthesis of Metal Nanostructures: The Case of Silver. *Chemistry-A European Journal* **2005,** *11* (2), 454-463.

79. Hutter, E.; Fendler, J. H., Exploitation of localized surface plasmon resonance. *Advanced Materials* **2004,** *16* (19), 1685-1706.

80. Wiley, B. J.; Im, S. H.; Li, Z.-Y.; McLellan, J.; Siekkinen, A.; Xia, Y., Maneuvering the Surface Plasmon Resonance of Silver Nanostructures through Shape-Controlled Synthesis. *The Journal of Physical Chemistry B* **2006,** *110* (32), 15666-15675.

81. Xia, Y.; Halas, N. J., Shape-controlled synthesis and surface plasmonic properties of metallic nanostructures. *MRS bulletin* **2005,** *30* (05), 338-348.

82. Wei, J.; Schaeffer, N.; Pileni, M.-P., Ag Nanocrystals: 1. Effect of Ligands on Plasmonic Properties. *The Journal of Physical Chemistry B* **2014,** *118* (49), 14070-14075.

83. Redl, F. X.; Cho, K. S.; Murray, C. B.; O'Brien, S., Three-dimensional binary superlattices of magnetic nanocrystals and semiconductor quantum dots. *Nature* **2003,** *423* (6943), 968-971.

84. Sun, S. H., Recent advances in chemical synthesis, self-assembly, and applications of FePt nanoparticles. *Advanced Materials* **2006,** *18* (4), 393-403.

85. Chen, Z. Y.; Moore, J.; Radtke, G.; Sirringhaus, H.; O'Brien, S., Binary nanoparticle superlattices in the semiconductor-semiconductor system: CdTe and CdSe. *Journal of the American Chemical Society* **2007,** *129* (50), 15702-15709.

86. Yang, Z.; Lisiecki, I.; Walls, M.; Pileni, M.-P., Nanocrystallinity and the Ordering of Nanoparticles in Two-Dimensional Superlattices: Controlled Formation of Either Core/Shell (Co/CoO) or Hollow CoO Nanocrystals. *ACS Nano* **2013,** *7* (2), 1342-1350.

87. Taleb, A.; Russier, V.; Courty, A.; Pileni, M. P., Collective optical properties of silver nanoparticles organized in two-dimensional superlattices. *Physcial Review B* **1999,** *59* (20), 13350-13358.

88. Yang, P.; Arfaoui, I.; Cren, T.; Goubet, N.; Pileni, M.-P., Unexpected Electronic Properties of Micrometer-Thick Supracrystals of Au Nanocrystals. *Nano Letters* **2012,** *12* (4), 2051-2055.

89. Ye, X.; Chen, J.; Diroll, B. T.; Murray, C. B., Tunable Plasmonic Coupling in Self-Assembled Binary Nanocrystal Super lattices Studied by Correlated Optical Microspectrophotometry and Electron Microscopy. *Nano Letters* **2013,** *13* (3), 1291-1297.

90. Urban, J. J.; Talapin, D. V.; Shevchenko, E. V.; Kagan, C. R.; Murray, C. B., Synergism in binary nanocrystal superlattices leads to enhanced p-type conductivity in self-assembled PbTe/Ag2Te thin films. *Nature Materials* **2007,** *6* (2), 115-121.

91. Taleb, A.; Petit, C.; Pileni, M. P., Optical properties of self-assembled 2D and 3D superlattices of silver nanoparticles. *Journal of Physical Chemistry B* **1998,** *102* (12), 2214-2220.

92. Pileni, M. P., Inorganic nanocrystals self ordered in 2D superlattices: how versatile are the physical and chemical properties? *Physical Chemistry Chemical Physics* **2010,** *12* (38), 11821-11835.

93. Dong, A.; Ye, X.; Chen, J.; Murray, C. B., Two-dimensional binary and ternary nanocrystal superlattices: the case of monolayers and bilayers. *Nano Lett* **2011,** *11* (4), 1804-9.

94. Yockell-Lelievre, H.; Gingras, D.; Lamarre, S.; Vallee, R.; Ritcey, A. M., In Situ Monitoring of the 2D Aggregation Process of Thiol-Coated Gold Nanoparticles Using Interparticle Plasmon Coupling. *Plasmonics* **2013,** *8* (3), 1369-1377.

95. Paul, S.; Pearson, C.; Molloy, A.; Cousins, M. A.; Green, M.; Kolliopoulou, S.; Dimitrakis, P.; Normand, P.; Tsoukalas, D.; Petty, M. C., Langmuir−Blodgett Film Deposition of Metallic Nanoparticles and Their Application to Electronic Memory Structures. *Nano Letters* **2003,** *3* (4), 533-536.

96. Tao, A.; Kim, F.; Hess, C.; Goldberger, J.; He, R.; Sun, Y.; Xia, Y.; Yang, P., Langmuir−Blodgett Silver Nanowire Monolayers for Molecular Sensing Using Surface-Enhanced Raman Spectroscopy. *Nano Letters* **2003,** *3* (9), 1229-1233.

97. Dong, A. G.; Chen, J.; Vora, P. M.; Kikkawa, J. M.; Murray, C. B., Binary nanocrystal superlattice membranes self-assembled at the liquid-air interface. *Nature* **2010,** *466* (7305), 474-477.

98. Gong, J.; Li, G.; Tang, Z., Self-assembly of noble metal nanocrystals: Fabrication, optical property, and application. *Nano Today* **2012,** *7* (6), 564-585.

99. Talapin, D. V.; Shevchenko, E. V.; Murray, C. B.; Titov, A. V.; Kr á l, P., Dipole−Dipole Interactions in Nanoparticle Superlattices. *Nano Letters* **2007,** *7* (5), 1213-1219.

100. Sun, Z.; Luo, Z.; Fang, J., Assembling Nonspherical 2D Binary Nanoparticle Superlattices by Opposite Electrical Charges: The Role of Coulomb Forces. *ACS Nano* **2010,** *4* (4), 1821-1828.

101. Bodnarchuk, M. I.; Kovalenko, M. V.; Heiss, W.; Talapin, D. V., Energetic and Entropic Contributions to Self-Assembly of Binary Nanocrystal Superlattices: Temperature as

the Structure-Directing Factor. *Journal of the American Chemical Society* **2010,** *132* (34), 11967-11977.

102. Talapin, D. V.; Shevchenko, E. V.; Murray, C. B.; Titov, A. V.; Kral, P., Dipole-dipole interactions in nanoparticle superlattices. *Nano Letters* **2007,** *7* (5), 1213-1219.

103. Talapin, D. V.; Shevchenko, E. V.; Kornowski, A.; Gaponik, N.; Haase, M.; Rogach, A. L.; Weller, H., A new approach to crystallization of CdSe nanoparticles into ordered three-dimensional superlattices. *Advanced Materials* **2001,** *13* (24), 1868.

104. Quan, Z.; Fang, J., Superlattices with non-spherical building blocks. *Nano Today* **2010,** *5* (5), 390-411.

105. Rupich, S. M.; Shevchenko, E. V.; Bodnarchuk, M. I.; Lee, B.; Talapin, D. V., Size-dependent multiple twinning in nanocrystal superlattices. *Journal of the American Chemical Society* **2009,** *132* (1), 289-296.

106. Lisiecki, I.; Albouy, P. A.; Pileni, M. P., Face-Centered-Cubic "Supracrystals" of Cobalt Nanocrystals. *Advanced Materials* **2003,** *15* (9), 712-716.

107. Talapin, D. V.; Lee, J. S.; Kovalenko, M. V.; Shevchenko, E. V., Prospects of Colloidal Nanocrystals for Electronic and Optoelectronic Applications. *Chemical Reviews* **2010,** *110* (1), 389-458.

108. Wan, Y. F.; Goubet, N.; Albouy, P. A.; Pileni, M. P., Hierarchy in Au nanocrystal ordering in supracrystals: a potential approach to detect new physical properties. *Langmuir* **2013,** *29* (24), 7456-63.

109. Shevchenko, E. V.; Talapin, D. V.; Kotov, N. A.; O'Brien, S.; Murray, C. B., Structural diversity in binary nanoparticle superlattices. *Nature* **2006,** *439* (7072), 55-59.

110. Urban, J. J.; Talapin, D. V.; Shevchenko, E. V.; Kagan, C. R.; Murray, C. B., Synergismin binary nanocrystal superlattices leads to enhanced p-type conductivity in self-assembled PbTe/Ag-2 Te thin films. *Nature Materials* **2007,** *6* (2), 115-121.

111. Chen, Z.; O'Brien, S., Structure Direction of II−VI Semiconductor Quantum Dot Binary Nanoparticle Superlattices by Tuning Radius Ratio. *ACS Nano* **2008,** *2* (6), 1219-1229.

112. Shevchenko, E. V.; Ringler, M.; Schwemer, A.; Talapin, D. V.; Klar, T. A.; Rogach, A. L.; Feldmann, J.; Alivisatos, A. P., Self-Assembled Binary Superlattices of CdSe and Au Nanocrystals and Their Fluorescence Properties. *Journal of the American Chemical Society* **2008,** *130* (11), 3274-3275.

113. Shevchenko, E. V.; Talapin, D. V.; Murray, C. B.; O'Brien, S., Structural characterization of self-assembled multifunctional binary nanoparticle superlattices. *Journal of the American Chemical Society* **2006,** *128* (11), 3620-3637.

114. Parthe, E. Z., *Kirstallogr* **1961,** *115*, 52-79.

115. Sanders, J., Close-packed structures of spheres of two different sizes I. Observations on natural opal. *Philosophical Magazine A* **1980,** *42* (6), 705-720.

116. Murray, M.; Sanders, J., Close-packed structures of spheres of two different sizes II. The packing densities of likely arrangements. *Philosophical Magazine A* **1980,** *42* (6), 721-740.

117. Shevchenko, E. V.; Talapin, D. V.; O'Brien, S.; Murray, C. B., Polymorphism in AB13 Nanoparticle Superlattices: An Example of Semiconductor−Metal Metamaterials. *Journal of the American Chemical Society* **2005,** *127* (24), 8741-8747.

118. Chen, J.; Ye, X.; Murray, C. B., Systematic Electron Crystallographic Studies of Self-Assembled Binary Nanocrystal Superlattices. *ACS Nano* **2010,** *4* (4), 2374-2381.

119. Evers, W. H.; Nijs, B. D.; Filion, L.; Castillo, S.; Dijkstra, M.; Vanmaekelbergh, D., Entropy-driven formation of binary semiconductor-nanocrystal superlattices. *Nano letters* **2010,** *10* (10), 4235-4241.

120. Kalsin, A. M.; Fialkowski, M.; Paszewski, M.; Smoukov, S. K.; Bishop, K. J. M.; Grzybowski, B. A., Electrostatic Self-Assembly of Binary Nanoparticle Crystals with a Diamond-Like Lattice. *Science* **2006,** *312* (5772), 420-424.

121. Gwo, S.; Lin, M.-H.; He, C.-L.; Chen, H.-Y.; Teranishi, T., Bottom-Up Assembly of Colloidal Gold and Silver Nanostructures for Designable Plasmonic Structures and Metamaterials. *Langmuir* **2012,** *28* (24), 8902-8908.

122. Chen, C.-F.; Tzeng, S.-D.; Chen, H.-Y.; Lin, K.-J.; Gwo, S., Tunable Plasmonic Response from Alkanethiolate-Stabilized Gold Nanoparticle Superlattices: Evidence of Near-Field Coupling. *Journal of the American Chemical Society* **2007,** *130* (3), 824-826.

123. Yang, P.; Portalès, H.; Pileni, M.-P., Ability to discern the splitting between longitudinal and transverse plasmon resonances in Au compared to Ag nanoparticles in close-packed planar arrays. *Physical Review B* **2010,** *81* (20), 205405.

List of publications

1. “Ag Nanocrystals: 1. Effect of Ligands on Plasmonic Properties. ”, Wei, J. J.; Schaeffer, N.; Pileni, M.-P., *J. Phys. Chem. B* **2014,** *118*, 14070-14075.
2. “Surface Plasmon Resonance of Silver Nanocrystals Differing by Sizes and Coating Agents Ordered In 3D.”, Wei, J. J.; Schaeffer, N.; Albouy, P.-A.; Pileni, M.-P., submitted.
3. “Surface Chemstry Controls the Crystal Structures in Binary”, Wei, J. J.; Schaeffer, N.; Pileni, M.-P., in preparation.
4. “Collective surface plasmon resonances in two-dimensional assemblies of Au and Ag nanocrystals: Experiments and DDA simulation”, Wei, J. J.; Yang, P.; Portalès, H.; M.-P. Pileni, in preparation.